THE ROLE OF NEURONAL CALCIUM SENSOR PROTEIN VILIP-1 IN Aβ-INDUCED NEURONAL DEATH IN ALZHEIMER DISEASE

by

Caitlin Marie Kirkwood

Bachelor of Science, Bioengineering, University of Pittsburgh, 2009

Submitted to the Graduate Faculty of

University of Pittsburgh School of Medicine in partial fulfillment

of the requirements for the degree of

Doctor of Philosophy

University of Pittsburgh

2015

UNIVERSITY OF PITTSBURGH

SCHOOL OF MEDICINE

This dissertation was presented

by

Caitlin Marie Kirkwood

It was defended on

April 29, 2015

and approved by

Kenneth N. Fish, PhD, Dept. of Psychiatry

Kathryn M. Albers, PhD, Dept. of Medicine and Neurobiology

William E. Klunk, MD, PhD, Dept. of Psychiatry and Neurology

Steven E. Arnold, MD, Dept. Psychiatry, University of Pennsylvania

Committee Chair: Etienne L. Sibille, PhD, Dept. of Psychiatry, Pharmacology and Toxicology, University of Toronto

Dissertation Advisor: Robert A. Sweet, MD, Dept. of Psychiatry and Neurology

THE ROLE OF NEURONAL CALCIUM SENSOR PROTEIN VILIP-1 IN Aβ-INDUCED NEURONAL DEATH IN ALZHEIMER DISEASE

Caitlin Marie Kirkwood, PhD

University of Pittsburgh, 2015

Alzheimer disease (AD) is the most prevalent form of dementia in the United States affecting an estimated 5.3 million individuals in 2015. Clinically, AD presents with progressive memory loss, decline in cognitive abilities, and behavioral changes. Neuropathologically, increased synaptic pathology and neuronal loss correlate with cognitive impairment in AD. While the specific neurobiological mechanisms underlying AD neuronal loss are not fully understood, a growing pool of evidence implicates soluble amyloid-β (Aβ) oligomers as a primary neurotoxic agent. Previous work has demonstrated that Aβ disrupts neuronal Ca^{2+} homeostasis, initiating a cascade of pathological events that ultimately culminate in widespread neuronal death. Recently, neuronal calcium sensor protein visinin-like protein 1 (Vilip-1) has been identified an AD-specific peripheral biomarker, however little is known about Vilip-1 in the AD brain. Previous work has alluded to associations between Vilip-1, Aβ, and neuronal death. VSNL1, the gene that encodes Vilip-1, coexpresses with genes related to AD throughout normal aging, notably amyloid precursor protein (APP), which is cleaved in the pathogenesis of AD to form Aβ. Vilip-1 immunoreactivity also associates with neuritic plaques in the neocortex of the human AD brain. Finally, overexpression of Vilip-1 in a cell line increased death rates following a Ca^{2+} challenge, suggesting Vilip-1 may play a functional role in neuronal loss. To determine if Vilip-1 plays a causal role in AD, first we investigated Vilip-1 levels in two regions of the human AD brain. Then we used model systems to evaluate the impact of Aβ on Vilip-1 expression and

determined whether manipulation of Vilip-1 expression affected Aβ-induced neuronal death. We demonstrated that Vilip-1 is reduced within brain regions characterized by prominent neuronal loss in both AD and frontotemporal lobar degeneration (FTLD). We reported that Vilip-1 expression is not driven by Aβ. Finally, we found that Aβ-initiated neuron death was unaffected by the extent of Vilip-1 expression. Together, these data suggest that Vilip-1 is a general marker for neuronal loss in brain tissue rather than participant in an AD-specific neuronal death process. In addition, Vilip-1 may have value as a novel marker for neuronal integrity and loss in human brain tissue.

TABLE OF CONTENTS

LIST OF TABLES

LIST OF FIGURES

LIST OF ABBREVIATIONS

Aβ: Amyloid-β

AD: Alzheimer disease

AD+P: Alzheimer disease with psychosis

ADRC: Alzheimer Disease Research Center

APP: Amyloid precursor protein

CERAD: Consortium to Establish a Registry for Alzheimer Disease

CSF: Cerebrospinal fluid

ERC: Entorhinal cortex

FTLD: Frontotemporal lobar degeneration

LC-SRM/MS: Liquid Chromatography-Selected Reaction Monitoring/Mass Spectrometry

MAP2: Microtubule-associated protein 2

MCI: Mild cognitive impairment

MMSE: Mini-Mental State Examination

nAChR: Nicotinic acetylcholine receptor

NFT: neurofibrillary tangle

PMI: Postmortem interval

SF: Superior frontal gyrus

Vilip-1/VSNL: visinin-like protein 1

PREFACE

Graduate school has been a tremendous experience and there are a number of people I would like to thank for their support, both professionally and personally, throughout my graduate training. First, I would like to thank my advisor and mentor, Dr. Robert Sweet. Rob is an exceptional scientist who has always made my training a priority and I feel incredibly fortunate for having conducted my graduate training under his guidance. I have grown immensely, both as a scientist and as a person, with his support and I cannot thank him enough. I am grateful to my wonderful and supportive committee members Dr. Ken Fish, Dr. Etienne Sibille, Dr. Kathy Albers, and Dr. William Klunk for their guidance and insights that have shaped and enriched my dissertation project.

I was fortunate to conduct research in a wonderful environment full of encouragement, support, and friendship thanks to my labmates: Micah Shelton, Caitlin Moyer, Patrick Murray, Matt MacDonald, Brad Rocco, Michelle Richard, Darius Becker-Krail, Anthony Deo, and Isaac Goldszer. I was privileged to mentor a fantastic undergraduate student, Tadhg Schempf, and I am grateful for his contributions to data collection and analysis in studies presented in ***Chapters 2.0*** and ***3.0***. I am grateful to Dr. Susan Erickson for her guidance, advice, and support in maintaining the mice required for these studies. I would like to give special thanks to Tracey Capotosto for all of her encouragement throughout my graduate training.

Most importantly, I would like to thank my friends and family. Michelle Failla for being

an incredible friend and support system that has on countless occasions provided invaluable scientific and life advice. Allison Marin for not only helping edit the discussion of this dissertation but for being a wonderful mentor in the world of freelance writing. Jamey Maniscalco for all of the epic study sessions first year and continued support and friendship. And last but not least I would like to thank my parents, Don and Jan Kirkwood; my grandparents, Raymond and Anna Riedl; my aunt, Joyce Riedl, and my sister, Kerrie Kirkwood for their constant and unwavering love, support, and encouragement throughout graduate school and in life.

1.0 INTRODUCTION

1.1 OVERVIEW OF ALZHEIMER DISEASE

1.1.1 Disease Prevalence, Cost, and Projections

Alzheimer disease (AD) is the most prevalent form of dementia, accounting for 60-80% of all dementia cases (2014). According to the Centers for Disease Control and Prevention, AD ranks as the sixth leading cause of death in the United States, while some estimates indicate it could be as high as third, right after heart disease and cancer, resulting in the loss of more than half a million lives each year (James et al., 2014). Excluding rare genetic mutations that only occur in one percent of AD cases, advanced age is the strongest risk factor for AD, with most diagnoses occurring at age 65 or older. One in nine people (11 percent) age 65 or older have AD. This number jumps to one in three people (32 percent) age 85 and over. As the “baby boomer” generation continues to age and reach unprecedented life expectancies, the proportion of the population meeting the advanced age criteria continues to rise and the number of Americans living with AD is slated to dramatically escalate in coming years. In 2014, an estimated 5.2 million people in the United States were living with AD. Barring medical breakthroughs that effectively prevent, delay onset, or halt the progression of the disease, this number of existing AD cases is projected to reach as high as 16 million by some estimates in the year 2050.

As AD numbers are poised to rise and death rates for other major diseases like HIV, stroke, heart disease, and cancer are in decline, AD remains the only top 10 cause of death without a cure or even a way to slow disease progression. Lack of effective intervention is creating an enormous economic burden on society. In 2014, the direct costs to society for providing AD care were projected to total $214 billion, and are expected to rise to an astronomical $1.2 trillion in 2050 (not accounting for inflation). These figures only touch on direct costs and do not account for the estimated 17.7 billion hours of care provided by family and other unpaid caregivers in 2013 that would account for more than $220.2 billion in economic value. By some estimates, if the onset of AD could be delayed by 5 years through the development of a successful intervention, the number of patients affected by AD would be reduced by 57 percent and the annual Medicare costs could be cut by almost 50 percent (Fagan, 2014).

1.1.2 Clinical Presentation and Neuropathological Hallmarks

In the early 1900s, Auguste D., a woman in her early 50s, was admitted to the hospital after exhibiting increasingly peculiar behavior; she was experiencing memory impairment, sleep disturbances, increased aggression, hallucinations, and delusions. German psychiatrist, Alois Alzheimer, chronicled Auguste's case. He detailed her symptomatology, progression, and disease course, which would later be recognized as the first documentation of a patient with AD. After her death in 1906, Alzheimer was able to study the brain of Auguste D. and describe the organ both morphologically and histologically, correlating her cognitive and behavioral changes

with neuropathological elements he observed in her cerebral cortex (Alzheimer et al., 1995, Holtzman et al., 2011).

The clinical expression of AD is defined by declining memory, progressive loss of cognitive ability, and behavioral impairments that worsen over time. Progression of the disease tracks from an asymptomatic preclinical stage to the prodromal symptomatic stage known as mild cognitive impairment (MCI), before reaching the fully expressed symptomatic stage characterized by dementia. The time course of this continuous decline in mental faculties averages between 7 to 10 years and ultimately culminates in death (Holtzman et al., 2011). AD is clinically diagnosed based on the established National Institute of Neurological and Communicative Disorders and Stroke and the Alzheimer's Disease and Related Disorders Association (NINCDS-ADRDA) criteria (McKhann et al., 1984).

AD can only be definitively diagnosed postmortem after histological examination of the brain through identification of the two characteristic pathological hallmarks originally described by Alzheimer: extracellular amyloid plaques comprised of aggregations of the amyloid-β (Aβ) peptide and intracellular neurofibrillary tangles (NFTs) composed of hyperphosphorylated microtubule-associated tau protein (Selkoe, 2004, Ballatore et al., 2007). Three sets of diagnostic histological criteria currently exist that describe the quantification and regional distribution of these classic AD pathological features: Consortium to Establish a Registry for Alzheimer Disease (CERAD), National Institute on Aging-Reagan (NIA-Reagan), and Khachaturian (Mirra et al., 1991, Hyman and Trojanowski, 1997).

In the AD brain, NFTs form in a predictable spatiotemporal pattern (Serrano-Pozo et al., 2011). As described in the clinicopathological study by Braak and Braak, NFTs initially present in the perirhinal region, followed by the entorhinal cortex and hippocampus before proceeding to

develop in the further limbic structures and finally all neocortical regions (Braak and Braak, 1991). Notably, until very end stage disease the primary sensory, motor, and visual cortices are largely spared. Distribution of amyloid plaques is less predictable than NFTs and the majority of accumulation occurs in the neocortex, with entorhinal cortex and hippocampus being effected to a lesser extent (Serrano-Pozo et al., 2011).

1.1.3 Neuronal Loss in AD

In addition to accumulating protein aggregates, AD also exhibits gross atrophy of the brain and enlargement of the ventricles that results from prominent neuronal death, synapse loss, and reactive gliosis (Gomez-Isla et al., 1996, Ingelsson et al., 2004). Atrophy primarily occurs in the medial temporal and parietal lobes and is limited in the primary motor, sensory, and visual corticies (Serrano-Pozo et al., 2011). The primary source of cortical atrophy is often attributed to neuronal loss (Serrano-Pozo et al., 2011). A number of stereological studies have investigated neuronal loss in varying brain regions in AD.

In particular, the entorhinal cortex is highly vulnerable in AD, being one of the first regions affected by neurofibrillary tangles (Braak and Braak, 1991). In a study using an unbiased stereological approach, neuron counts in the ERC were compared between AD subjects with early and late stage disease (n =10) and cognitively normal control subjects (n =10). Neuron numbers in normal control subjects remained consistent across aging, with no detectible loss from age 60 to 90. In contrast, neuron numbers in AD individuals were significantly reduced compared to normal controls with an observed 48% decrease in total number of ERC neurons (Gomez-Isla et al., 1996). This reduction was significant even at early stages of AD. All ERC layers had significantly fewer neurons than normal control subjects, with layer II displaying the

greatest deficit. Additionally, in AD subjects, cognitive function correlated with degree of neuron loss in all ERC layers, with the most impaired individuals exhibiting the most severe neuron deficits (Gomez-Isla et al., 1996).

Another brain region that is primarily affected by neuronal loss in AD is the hippocampus. Several studies have documented severe loss of neurons within several hippocampal areas including CA1, hilus, and subiculum in end stage disease (West et al., 1994, Simic et al., 1997, Rossler et al., 2002, West et al., 2004).

Unlike the consistently documented dramatic neuron loss in the ERC and hippocampus, the degree of neuron loss in the neocortex of AD subjects is more widely debated. Regeur and colleagues used an unbiased, uniform sampling stereological approach to estimate total neuron population in the neocortex of late stage Alzheimer disease. Brains from 11 severely demented females from a chronic psychogeriatric ward in Copenhagen, Denmark and 10 age-matched controls were evaluated. They found that neocortical neuron numbers generated from frontal, temporal, parietal, and occipital brain regions in AD were decreased by 6% compared to normal controls, however the reduction was not statistically significant (Regeur et al., 1994). In another larger stereological study investigating the superior temporal sulcus in 34 individuals with AD and 17 cognitively normal control subjects saw a significant 53% decrease in neuron number, with loss increasing to 75% in subjects with more advanced disease (Gomez-Isla et al., 1997). Importantly, no significant difference in neuron number was observed with increasing age in normal subjects (Gomez-Isla et al., 1997). An additional study investigated neuron number in prefrontal cortex deep layer III and superficial layer V within 10 AD cases of varying degrees of cognitive impairment and 9 elderly controls. Neuron counts were dramatically decreased in AD subjects compared to controls in both layers, with numbers in layer V demonstrating the greatest

reduction. In addition, neuron loss again correlated with severity of disease, with more than 90% loss at end stages of AD (Bussiere et al., 2003). These differences are likely attributed to differences in the brain regions investigated, stage of disease, small subject cohort sizes, and technical variations, however it does appear that ERC is a primarily effected region even at early stages of AD, while other regions like the prefrontal cortex are more greatly impacted later as the disease progresses.

Neuronal loss not only positively correlates with the temporal-regional and laminar distribution of NFT pathology, but it far exceeds the number of NFTs formed within a region, and thus serves as a better correlate of cognitive impairment than NFTs (Gomez-Isla et al., 1996, Gomez-Isla et al., 1997). However, synapse loss also follows the same spatiotemporal pattern as neuronal loss and is widely considered to be the best correlate of cognitive decline in AD (Serrano-Pozo et al., 2011). This is likely because synapse loss not only precedes neuronal loss but is also caused by neuronal loss. Neurons with synaptic connections in regions of widespread neuron death become less well connected leading to cognitive impairments (DeKosky and Scheff, 1990, Terry et al., 1991, Scheff and Price, 1993, Scheff et al., 2007).

1.1.4 Soluble Aβ Toxicity

Aβ peptides aggregate in the extracellular space of the brain and comprise the principle proteinaceous component in amyloid plaques. Produced from the cleavage of transmembrane amyloid precursor protein (APP) by β-secretase and γ-secretase enzyme complexes, Aβ peptides can vary in length, ranging from 36- to 43- amino acids long (Thal et al., 2015). In the human brain, the $A\beta_{1\text{-}40}$ is the most abundantly produced peptide isoform (Esbjorner et al., 2014). Different lengths of Aβ exhibit varying degrees of toxicity, with $A\beta_{1\text{-}42}$ widely considered to be

the most toxic species in humans. Its toxicity may be in part due to the $A\beta_{1-42}$ isoform having a higher propensity for self-aggregation and oligomerization in vivo than other species like $A\beta_{1-40}$ (Haass and Selkoe, 2007, Murray et al., 2012). In fact, many of the known familial mutations in APP and presenilin-1, the enzymatic element of the γ-secretase complex, result in increased production of $A\beta_{1-42}$ (Haass and Selkoe, 2007). During the process of self-aggregation Aβ peptides form several different transient immediate species between monomers and fibrils including dimers, trimers, dodecamers, higher molecular weight oligomers and protofibrils (Mucke and Selkoe, 2012, Thal et al., 2015). Currently, Aβ dimers are the most studied oligomeric species, likely because they are elevated in overexpressing transgenic mouse brains and following extraction from human AD brain tissue dimers have been shown to impair long term potentiation (Larson and Lesne, 2012). Additionally, dimers have been shown to induce dendritic spine loss (Shankar et al., 2007), increase tau phosphorylation, and produce cytoskeletal abnormalities in culture (Jin et al., 2011). Amyloid plaques may actually serve as reservoirs of soluble Aβ oligomers (Koffie et al., 2009), as a halo of nonfibrillar Aβ exists in the plaque surround (***Appendix A***).

Recently soluble Aβ oligomers have emerged as the leading neurotoxic agent in AD, however the precise mechanism(s) behind the peptide's actions remain elusive. The amyloid or Aβ cascade hypothesis posits that the deposition of Aβ protein is a central event in AD pathogenesis initiating numerous damaging pathways involving synaptic dysfunction, oxidative stress, microglia activation, and disruption of Ca^{2+} homeostasis, which ultimately culminate in neuron loss and cognitive impairment.

The particular manner by which Aβ oligomers perturb neuronal Ca^{2+} homeostasis and increase neurotoxicity is complex and still a matter of debate, however a number of potential

mechanisms have been identified. One theory is that Aβ oligomers fuse with lipid bilayers creating annular structures that function as artificial pores or channels in the membrane, allowing for increased cation flux into the cell (Arispe et al., 1993). Other studies have demonstrated that Aβ interacts with endogenous highly Ca^{2+}-permeable channels including voltage-gated calcium channels, glutamate receptors (N-methyl D-aspartate-receptors (NMDARs) and α-amino-3-hydroxy-5-methylisoxazole-4-propionic acid receptors (AMPARs)), and nicotinic acetylcholine receptors (nAChRs), increasing Ca^{2+} influx through these channels (Li et al., 2009, Demuro et al., 2010). Additional studies have shown that Aβ can cause the release of Ca^{2+} from internal stores through altering the sensitivity of inositol triphosphate receptor (IP3R) and ryanodine receptor (RyR) channels in the endoplasmic reticulum (Stutzmann et al., 2004, Bezprozvanny and Mattson, 2008).

While a clear sequence of events following Aβ-induced Ca^{2+} dysregulation have yet to be established, both Aβ and increases in intracellular Ca^{2+} have been demonstrated to increase tau phosphorylation (Busciglio et al., 1995, Hartigan and Johnson, 1999, Zheng et al., 2002, Oliveira et al., 2015) and initiate neuronal apoptosis cascades (Loo et al., 1993, Mark et al., 1995). Identifying more of the key players in the Aβ cascade hypothesis will enhance our understanding of the disease process and shed light on possible therapeutic targets for intervention prior to cognitive impairment.

1.2 VILIP-1

1.2.1 Structure and Function

Neuronal calcium sensor (NCS) proteins are a large family of calcium-dependent molecular switches that modulate many intracellular signaling cascades involving neuronal functions like neurotransmitter release, receptor trafficking, and apoptosis. Visinin-like protein 1 (Vilip-1, gene name VSNL1) is an NCS protein that is highly and widely expressed throughout the brain. In the central and peripheral nervous systems, Vilip-1 expression is neuron specific (Bernstein et al., 1999). One comprehensive study investigating Vilip-1 mRNA expression in the rat brain found robust VILIP-1 expression throughout all brain regions except in the caudate and putamen (Paterlini et al., 2000). Outside of the brain, Vilip-1 is present in the heart, liver, lungs, pancreas, skin, colon, and testis of the human and rat (Gierke et al., 2004). Vilip-1 expression in the adult brain is higher compared to embryonic development (Gierke et al., 2004). In mice, knocking out the VSNL1 gene is embryonic lethal.

Vilip-1 belongs to the Vilip subfamily of NCS proteins. Members of the Vilip NCS subfamily share between 67 – 94 percent identical amino acids and include: Vilip-1, Vilip-2, Vilip-3, hippocalcin, and neurocalcin-δ (Braunewell and Klein-Szanto, 2009). The amino acid sequence for Vilip-1 is evolutionarily highly conserved, sharing 100% homology in mouse, rat, chicken, bovine, and human. Vilip-1 is 191 amino acids residues long. Like all NCS proteins in the Vilip subfamily, it contains 4 EF-hand binding domains: EF1 – EF4. Each EF-hand motif consists of a standard core of amino acids (D-X-D/N-X-D/N-X-Y-X4-E, where X is any amino acid) (Braunewell and Klein-Szanto, 2009). The first EF-hand contains the sequence CPXG, which eliminates its ability to bind Ca^{2+} (Li et al., 2011). EF-1 is also the most variable part of

the sequence in NCS proteins and is thought to be a point of interaction with other target proteins. At the N-terminus, Vilip-1 has an M-G-X3-S consensus sequence for myristoylation. Independent of Ca^{2+} and myristoylation, Vilip-1 forms a dimeric structure in solution (Li et al., 2011). Upon binding two Ca2+ at EF-2 and EF-3, Vilip-1 undergoes a conformational change that exposes a hydrophobic myristoylated side chain region. The extrusion of the myristoyl group allows the protein to translocate and interact with cellular membrane compartments or target proteins (Spilker and Braunewell, 2003, Li et al., 2011). Vilip-1 has a higher binding affinity for Ca^{2+} than calmodulin (Burgoyne and Weiss, 2001) and myristoylation lowers the binding affinity of Vilip-1 (Li et al., 2011). In culture after an increase in intracellular Ca^{2+} levels, Vilip-1 has been shown to reversibly translocate to subcellular membrane compartments, like the trans-Golgi membranes in hippocampal neurons (Spilker and Braunewell, 2003), and associate with cell surface membranes, including in dendrites and axons (Lin et al., 2002). This localization of Vilip-1 to the cell surface membrane is Ca^{2+} binding dependent (Spilker et al., 2002).

Consistent with other subfamily members, Vilip-1 appears to modulate membrane trafficking, surface expression, and function of various ion channels and receptors including nicotinic acetylcholine receptors (nAChRs) (Lin et al., 2002, Zhao et al., 2009), receptor guanylyl cyclases (GC-B) (Brackmann et al., 2005), and adenosine triphosphate (ATP) receptor P2X2 (Chaumont et al., 2008). Vilip-1 interacts with the cytoplasmic loop of the α4-subunit of the α4β2 nAChR, the most abundant nAChR subtype in the brain (Hogg et al., 2003, Zhao et al., 2009). Coexpression of Vilip-1 with recombinant α4β2 nAChR in cell lines resulted in significant increases in receptor surface expression and sensitivity to acetylcholine. Additionally, mutating Vilip-1 in a way that renders the protein incapable of being myristoylated or binding Ca^{2+}, thus losing its ability to associate with the cell membrane, attenuated Vilip-1's ability to

interact and modulate α4β2 nAChRs (Lin et al., 2002). Overexpression of Vilip-1 in hippocampal neurons also leads to enhanced surface expression of nAChRs and increased responsiveness to acetylcholine. In contrast, siRNA knockdown of Vilip-1 leads to reduced α4β2 nAChR currents (Zhao et al., 2009). Additionally, in at least some cases, such as with GC-B receptors Vilip-1 receptor modulation has been linked to clathrin-dependent receptor recycling (Brackmann et al., 2005). However, whether Vilip-1 impacts synaptic plasticity, particularly in the setting of neurodegenerative disease is not known.

Previous work has also suggested a role for Vilip-1 in cell death. Overexpression of Vilip-1 in PC12 cells increased death rates following a Ca^{2+} challenge (Schnurra et al., 2001). Hippocalcin, a highly homologous Vilip subfamily member has been shown to be neuroprotective against Ca^{2+}-mediated death in neural cell lines, further connecting NCS proteins to neuronal death processes (Mercer et al., 2000).

1.2.2 Vilip-1 and Alzheimer Disease

Originally pioneered as an indicator of neuronal integrity for stroke, several studies have since identified Vilip-1 as a peripheral early stage AD biomarker. Findings in cerebrospinal fluid (CSF) and blood plasma showed Vilip-1 levels were elevated in individuals with AD compared to cognitively normal control subjects (Tarawneh et al., 2011). Additionally, CSF levels of Vilip-1 were predictive of the progression of cognitive decline, with higher concentrations at time of collection indicating a more rapid loss in mental faculties over the duration of the illness (Tarawneh et al., 2012). Some studies suggest that the CSF elevation of Vilip-1 is specific to AD, as CSF collected from other neurodegenerative disorders, like Lewy Body dementia, show no change compared to cognitively normal controls (Tarawneh et al., 2011, Luo et al., 2013).

To date, there is limited information about the status of Vilip-1 in human AD brain tissue. Data from mRNA and protein studies suggests that Vilp-1 expression is decreased in the temporal cortex, parts of the limbic system, and the entorhinal cortex (Loring et al., 2001, Schnurra et al., 2001). In a whole-genome expression profiling study investigating the frontal cortex of AD subjects with varying degrees of disease severity, expression of Vilip-1 mRNA was shown to correlate with NFT burden and MMSE scores (Wilmot et al., 2008). In addition to the frontal cortex data, downregulation of Vilip-1 mRNA in the hippocampus has also been observed (Miller et al., 2008, Gomez Ravetti et al., 2010). Furthermore, qualitative immunohistochemistry data has suggested an association of Vilip-1 with neuritic plaques and neurofibrillary tangles in the neocortex of AD subjects (Schnurra et al., 2001).

Recently, in a microarray study investigating VSNL1 expression in 209 cognitively normal subjects spanning the adult age range we found that VSNL1 is present and unaffected across the adult lifespan. In addition, VSNL is significantly coexpressed with genes related to AD pathways, including APP (***Appendix B***).

Finally, genetics studies evaluating putative psychosis risk genes in AD with psychosis (AD+P), a phenotype of AD characterized by a more severe trajectory of cognitive deterioration than seen in AD subjects without psychosis (Murray et al., 2014b), have identified an association of VSNL1, the gene that encodes the protein Vilip-1 (Hollingworth et al., 2012). This data coincides with findings of reduced expression of VSNL1 mRNA and protein in the brain tissue of schizophrenia subjects (Martins-de-Souza et al., 2009, Braunewell et al., 2011).

Collectively these findings suggest a role for Vilip-1 in the AD pathogenesis, but it is unknown to what extent it participates, particularly in regards to Aβ-mediated pathways.

1.3 GOALS AND RELEVANCE OF THIS DISSERTATION

AD is a devastating neurodegenerative disease that is a top leading cause of death in the United States. Here in the General Introduction (***Chapter 1.0***), I have presented evidence that increased synaptic pathology and neuronal loss underlie cognitive decline in AD. Further, while the specific mechanisms underlying neuronal loss in AD are not fully understood, a growing pool of evidence implicates soluble amyloid-β (Aβ) oligomers as a primary neurotoxic agent. Previous work has demonstrated that Aβ disrupts neuronal Ca^{2+} homeostasis, initiating a cascade of pathological events that ultimately culminate in widespread neuronal death. Recent human data has shown an association of neuronal calcium sensing protein Vilip-1 and AD. CSF and plasma Vilip-1 concentrations are elevated in AD subjects compared to cognitively normal control subjects. This CSF phenomenon appears to be AD-specific, as other neurodegenerative disorders, like FTLD, do not exhibit a change. In addition, Vilip-1 mRNA is significantly coexpressed with genes related to AD across normal aging, notably APP, which is cleaved in the pathogenesis of AD to form Aβ. Vilip-1 immunoreactivity also associates with neuritic plaques in the neocortex of the human AD brain. Finally, overexpression of Vilip-1 in PC12 cells increased death rates following a Ca^{2+} challenge suggesting Vilip-1 may play a functional role in neuronal loss.

Based on this evidence, we proposed a model (Figure 1.1) where Vilip-1 protein expression is altered in response to Aβ, increasing vulnerability to Aβ-induced neuronal death in AD. Understanding the distinct causal neurobiological factors, like the role of Vilip-1 in AD, will lead to improved therapeutic strategies and profoundly impact patients, caregivers, and society as a whole.

The purpose of this dissertation is to determine how Vilip-1 is altered in the AD brain and whether it is actively participating in the process of Aβ-initiated neuronal loss. This dissertation aims to address this purpose by answering the following questions: 1) Are Vilip-1 levels altered in the brain tissue of individuals with Alzheimer disease? (***Chapter 2.0***); 2) Does Aβ cause increased Vilip-1 expression in model systems? (***Chapter 3.0***); 3) Are rates of Aβ-induced neuronal death influenced by neuronal Vilip-1 expression level? (***Chapter 4.0***).

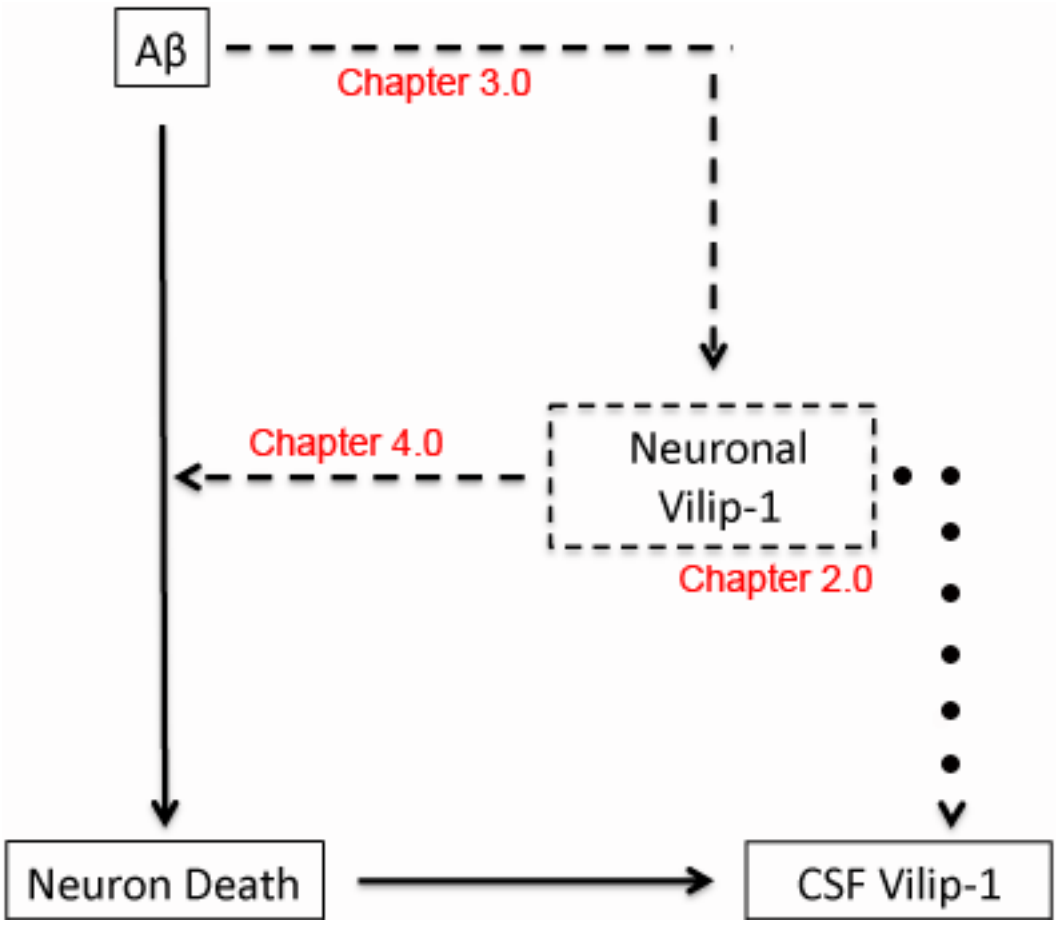

Figure 1.1 Proposed model of Vilip-1 interactions in AD. Vilip-1 protein expression is altered in response to Aβ, increasing vulnerability to Aβ-induced neuronal death in AD and resulting in Vilip-1 release into the CSF. Solid lines are established in the literature and dashed lines are hypothesized based on supportive preliminary data.

2.0 VILIP-1 LEVELS ARE ALTERED IN THE BRAIN TISSUE OF INDIVIDUALS WITH ALZHEIMER DISEASE

2.1 ABSTRACT

Recent studies have implicated the neuronal calcium-sensing protein visinin-like 1 protein (Vilip-1) as a peripheral biomarker in Alzheimer disease (AD), however little is known about expression of Vilip-1 in the AD brain. We used targeted and quantitative mass spectrometry to measure Vilip-1 peptide levels in early to moderate stage AD within two brain regions of varying neuronal loss: the entorhinal cortex (ERC) and the superior frontal gyrus (SF). In an initial cohort of 12 AD subjects and 12 normal controls, we found Vilip-1 levels were significantly lower in the ERC, a region with prominent neuronal death even at early stages of the disease. However, in the SF, a region with lower levels of neuronal loss, Vilip-1 levels did not differ from normal control subjects. Additionally, in a group of frontotemporal lobar degeneration (FTLD) subjects (n = 10), Vilip-1 levels in the SF were significantly lower compared to normal controls, suggesting a potential role for Vilip-1 as a neuronal integrity biomarker, at least within ERC.

2.2 INTRODUCTION

Alzheimer disease (AD) is the leading cause of dementia in the United States affecting more than 5 million people. Clinically, this progressive neurodegenerative disease is characterized by loss of memory, decline in cognitive abilities, and behavioral changes that worsen over time. Neuropathologically, AD is classified by two major hallmarks: extracellular amyloid plaques comprised of the amyloid-β (Aβ) peptide and intracellular neurofibrillary tangles composed of hyperphosphorylated tau protein (Selkoe, 2004, Ballatore et al., 2007). In addition to accumulating protein aggregates, AD also exhibits gross anatomical changes, such as dramatic shrinkage of the brain tissue that results from prominent neuronal death, synapse loss, and gliosis (Gomez-Isla et al., 1996, Ingelsson et al., 2004).

Several studies have identified the primarily brain-expressed neuronal calcium sensing protein, visinin-like protein 1 (Vilip-1), as a peripheral early stage AD biomarker. Findings in cerebrospinal fluid (CSF) and plasma showed Vilip-1 levels were elevated in individuals with AD compared to cognitively normal control subjects (Tarawneh et al., 2011). Additionally, CSF levels of Vilip-1 were predictive of the progression of cognitive decline, with higher concentrations at time of collection indicating a more rapid loss in mental faculties over the duration of the illness. Some studies suggest that Vilip-1 CSF elevation phenomenon is specific to AD, as CSF collected from other neurodegenerative disorders, like Lewy Body dementia, show no change compared to cognitively normal controls (Tarawneh et al., 2011, Luo et al., 2013).

Recently we have shown mRNA evidence for VSNL1, the gene that encodes the Vilip-1 protein, is significantly coexpressed with genes related to AD pathways, such as amyloid precursor protein (APP), throughout normal aging (***Appendix B***) (Lin et al., 2015). Furthermore,

qualitative immunohistochemistry data has suggested an association of Vilip-1 with neuritic plaques and neurofibrillary tangles in the neocortex of AD subjects (Schnurra et al., 2001). However, to date, relatively little is known about the levels of Vilip-1 in AD brain tissue.

Additionally there is limited data indicating a potential a role for Vilip-1 in cell death. One previous study found that overexpression of Vilip-1 in PC12 cells increased cell death in response to a calcium challenge (Schnurra et al., 2001).

Based on these studies, we hypothesized that Vilip-1 would be altered in the brain tissue of AD and associated with neuronal loss. To test this hypothesis we examined two different brain regions (ERC and SF) of early to moderate stage AD subjects. We found that Vilip-1 levels were decreased in the entorhinal cortex (ERC) of AD subjects and unchanged in the superior frontal gyrus (SF) compared to normal controls. In the SF, the primarily affected area in another neurodegenerative disease, frontotemporal lobar degeneration (FTLD), subjects had significantly lower levels of Vilip-1 compared to normal controls, suggesting that decreased Vilip-1 levels may reflect neuronal loss.

2.3 METHODS

2.3.1 Subjects

2.3.1.1 AD subjects & FTLD subjects. Fifty-eight AD subjects and 10 FTLD subjects (Table 2) were identified through the brain bank of the Alzheimer Disease Research Center (ADRC) at the University of Pittsburgh, using protocols approved by the University of Pittsburgh Institutional Review Board and Committee for Oversight of Research Involving the Dead. Individuals

underwent neurologic, neuropsychological, and psychiatric diagnostic evaluations at successive time points as part of the participation in the Clinical Core of the ADRC as previously described (Sweet et al., 2000, Lopez et al., 2013).

Postmortem interval (PMI) was recorded at the time of brain removal. At autopsy, the brain was removed intact, examined grossly, and divided in the midsagittal plane. Gray matter samples from the right entorhinal cortex (ERC) and superior frontal gyrus (SF) were dissected and frozen at −80°C. The left hemibrain was immersion fixed in 10% buffered formalin for at least one week, sectioned into 1.0 cm coronal slabs, and sampled according to CERAD protocol for neuropathological diagnosis of AD. AD pathology was evaluated using modified Bielschowsky silver stain and immunohistochemical staining for tau and beta-amyloid (4G8. Neuritic plaque density was assessed according to CERAD criteria (Mirra et al., 1991); distribution of tau pathology was classified according to Braak stages (Braak et al., 2006). Lewy body pathology was assessed by alpha-synuclein immunohistochemistry and classified into brainstem-predominant, limbic and neocortical types following consensus criteria (McKeith et al., 2005). Immunohistochemical staining for TDP-43 was performed on sections of middle frontal gyrus and mesial temporal lobe as previously described (Vatsavayi et al., 2014). Sections were evaluated for the absence or presence of TDP-43 positive neuronal cytoplasmic inclusions, neuronal intranuclear inclusions and dystrophic neurites.

Neuropathologic diagnoses of Alzheimer disease were made according to CERAD criteria (Mirra et al., 1991), although all AD subjects also met NIA-Reagan criteria (Hyman and Trojanowski, 1997) for intermediate to high probability that their dementia was due to AD lesions. Neuropathologic diagnosis of FTLD-TDP, FTLD-FUS or FTLD-tau was determined following consensus criteria (Cairns et al., 2007, Mackenzie et al., 2010, Mackenzie et al., 2011).

When TDP pathology was present in cases that fulfilled diagnostic criteria for another neurodegenerative disease, no distinct diagnosis of FTLD-TDP was rendered following consensus recommendations (Mackenzie et al., 2009).

2.3.1.2 Normal control subjects. Two normal control subject brain specimens were obtained through the ADRC as described above. The remaining 10 normal control subject brain specimens were obtained through the Allegheny County Medical Examiner's Office, with consent obtained from the subjects' next-of-kin. The protocol used to obtain consent was approved by the University of Pittsburgh Institutional Review Board and Committee for Oversight of Research Involving the Dead. An independent committee of experienced clinicians made consensus DSM-IV diagnoses for each subject, using information obtained from clinical records and structured interviews with surviving relatives. Samples from subjects without any DSM-IV diagnosis (i.e. including no diagnosis of a cognitive disorder) were used in this study.

The right hemisphere was blocked coronally at 1-2 cm intervals and the resultant slabs snap frozen in 2-methyl butane on dry ice, and stored at -80°C. Samples from the frontal pole, hippocampus, ERC, and cerebellum were collected and an experienced neuropathologist reviewed sections stained using hematoxylin and eosin, Bielschowsky silver stain, amyloid β immunohistochemistry, and alpha-synuclein immunohistochemistry were determined to be without evidence of any neurodegenerative disease. Tissue slabs containing either the SF immediately caudal to the genu of the corpus collosum or the ERC were indentified. From these slabs, SF and ERC were removed as single blocks. Gray matter was collected by cutting 40 μM sections and frozen at −80°C.

Table 2.1 Descriptive information of subjects in Cohort 1. Mean values ± SD or number of subjects with percentage of group in parentheses. Groups not sharing superscript letters differ significantly on these variables.

Variable	AD N = 12	Control N = 12	FTLD N = 10
Age (years)	84.5 ± 8.9[a]	70.7 ± 9.4[b]	74.7 ± 10.4[b]
Range	71 - 101	62 - 90	56 - 89
Sex			
Male	5 (42)[a]	8 (67)[a]	4 (40)[a]
Female	7 (58)	4 (33)	6 (60)
Post mortem interval (hours)	5.1 ± 2.9[a]	12.2 ± 5.9[b]	6.2 ± 2.3[a]
Range	2 - 10	4 - 20	2 - 9
Age of onset (years)	76.0 ± 9.0		
Range	63 - 90		
Duration of Illness (years)	7.9 ± 3.0		
Range	4 - 13		
Lewy Body Stage			
Negative	12 (100)		
Brainstem/Transitional	0 (0)		
Neocortical	0 (0)		
Braak Stage			
4	3 (25)		
5	9 (75)		

Table 2.2 Descriptive information of subjects in Cohort 2. This expanded cohort contains all subjects from Cohort 1 with an additional 46 AD subjects.

Variable	AD N = 58
Age (years)	84.2 ± 7.0
Range	68 - 101
Sex	
Male	29 (50)
Female	29 (50)
Post mortem interval (hours)	6.1 ± 3.4
Range	2 - 17
Age of onset (years)	75.9 ± 7.0
Range	57 - 90
Duration of Illness (years)	8.2 ± 3.3
Range	2 - 18
Lewy Body Stage	
Negative	30 (52)
Brainstem/Transitional	15 (26)
Neocortical	13 (22)
Braak Stage	
3	6 (10)
4	20 (35)
5	32 (55)

It is of note that AD and FTLD subjects had significantly lower postmortem intervals (PMIs) than normal controls. However, using quantitative Western blot, we have previously established the stability of Vilip-1 protein across a 48-hour PMI in a mouse model (Figure 2.1), and therefore did not match subjects groups on PMI.

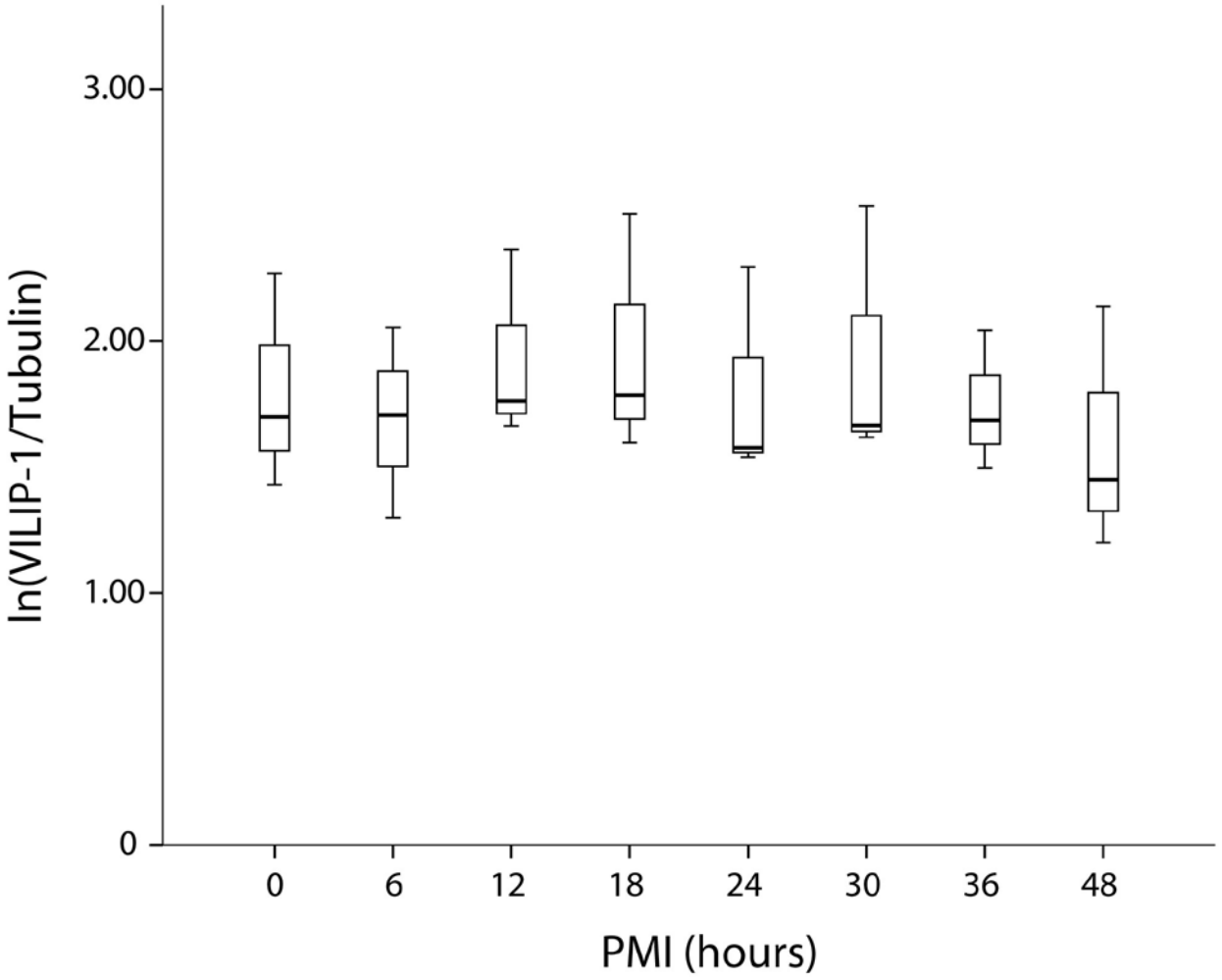

Figure 2.1 Postmortem interval (PMI) of Vilip-1 expression from mouse whole brain homogenate. ANOVA analysis of Vilip-1 protein levels normalized to tubulin showed no significant change over 48 hours ($p = 0.952$).

2.3.2 Sample Preparation

Tissue homogenates were prepared from fresh frozen human SF and ERC gray matter. Total protein was extracted using SDS extraction buffer (0.125 M Tris – HCl (pH 7), 2% SDS, and 10% glycerol) at 70°C. Using bicinchoninic acid assay (Micro BCATM Protein Assay, Pierce) protein concentration was measured. A pooled technical replicate sample composed of homogenate aliquots from all subjects was also prepared for each experiment (SF and ERC). 20

ug of total protein from the gray matter homogenate or pooled sample was mixed with Lysine 13C6 Stable Isotope Labeled Neuronal Proteome Standard (13C6 STD; 20 ug) for on gel trypsin digestion. To evenly distribute AD, FTLD, and normal control subjects throughout preparation, on-gel digestion, and analysis, samples were organized in a block distribution. For the SF experiment, each block was composed of 7 subjects and one pooled technical replicate, for a total of 12 blocks. For the ERC experiment each block was also composed of 7 subjects and one pooled technical replicate, for a total of 4 blocks. Each block was run on a single 10 well 4-12% BisTris gel with two SeeBlue® Plus2 Pre-stained Protein Standards. On-gel trypsin digestion was performed as previously described (MacDonald et al., 2012) with samples being run 4 cm into the gel and divided into two fractions (above and below 65kd).

2.3.3 LC-SRM/MS

Vilip-1 and MAP2 peptides were selected for analysis based on the presence of a lysine, the amino acid labeled in the 13C6STD, and 100% homology across mouse and human sequences (determined by Uniprot BLAST search). Five peptide sequences were identified from the Vilip-1 protein for quantification as indicated as underlined text in the following Vilip-1 amino acid sequence:

MGKQNSKLAPEVMEDLVKSTEFNEHELKQWYKGFLKDCPSGRLNLEEFQ
QLYVKFFPYGDASKFAQHAFRTFDKNGDGTIDFREFICALSITSRGSFEQK
LNWAFNMYDLDGDGKITRVEMLEIIEAIYKMVGTVIMMKMNEDGLTPEQ
RVDKIFSKMDKNKDDQITLDEFKEAAKSDPSIVLLLQCDIQK

Additionally, four peptide sequences were identified from the microtubule-associated protein 2 (MAP2) protein for quantification (Figure 2.2) to assess neuronal loss.

LC-SRM/MS analyses were conducted as previously described. (MacDonald et al., 2012) In brief, peptide peaks were detected using a TSQ Quantiva triple stage quadrupole mass spectrometer (Thermo Scientific) with an UltiMate 3000 Nano LC Systems (Thermo scientific). 2 µl (~1 µg protein) of sample was loaded/desalted on a PepMap100 Nano-Trap column (Thermo scientific) at 8 µl/min for 2 min and separated on a Reprosil-pur 3 µm PicoChip column (New Objective) at 400 nl/min over a 20 min gradient from 2-35% mobile phase B (Acetonitrile containing 0.1% formic acid). SRM transitions were timed using 1.5 min retention windows. Transitions were monitored, allowing for a cycle time of 1 sec, resulting in a dynamic dwell time, never falling below 2 msec. The MS instrument parameters were as follows: capillary temperature 275 °C, spray voltage 1100 V, and a collision gas of 1.4 mTorr (argon). The resolving power of the instrument was set to 0.7 Da (Full Width Half Maximum) for the first and third quadrupole. All samples were analyzed in triplicate. Using Skyline, integrated peak areas for both "light" human peptides and the "heavy" 13C6STD peptides were calculated for each of the peptide sequences. The light:heavy integrated area ratio was calculated to obtain peptide measures using multiple transitions per peptide.

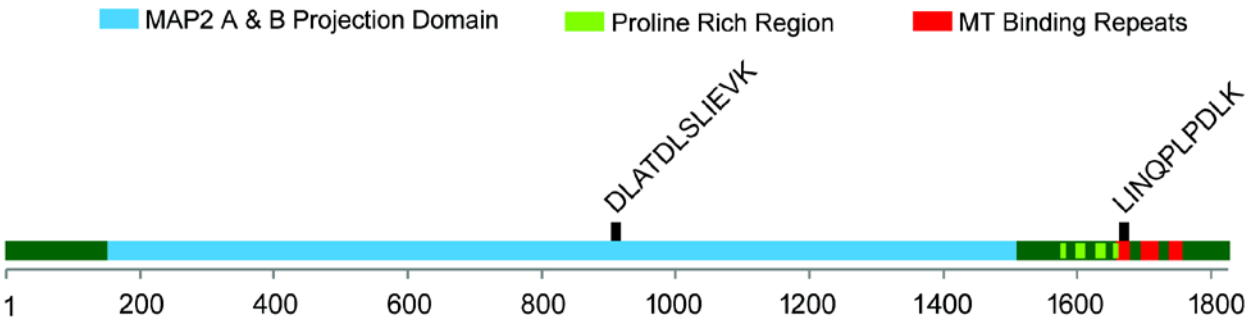

Figure 2.2 Two peptide sequences were identified for LC-SRM/MS quantification as shown in their respective locations within the MAP2 protein. (Modified from (Shelton et al., 2015))

2.3.4 Measurement of soluble Aβ and phospho-tau by sandwich enzyme-linked immunosorbent assay

Levels of soluble $A\beta_{1-40}$ and $A\beta_{1-42}$ and of tau protein had been previously performed in a subset of study subjects. (Murray et al., 2012, Koppel et al., 2014) Briefly, $A\beta_{1-40}$ and $A\beta_{1-42}$ levels were quantified from SF gray matter brain tissue samples that were homogenized on ice in phosphate-buffered saline (PBS; 150 mg/mL). Samples were then rehomogenized in tissue homogenization buffer (250 mM sucrose, 20 mM Tris base, and 10 μL Sigma P8340 protease inhibitor cocktail [Sigma-Aldrich, St. Louis, Missouri, USA]) and prepared in diethylamine (DEA)-soluble fractions for $A\beta_{1-40}$ and $A\beta_{1-42}$ peptide concentration quantification as described previously (Ikonomovic et al., 2008). The DEA-soluble fraction was prepared by centrifuging the homogenate aliquot at 135,000 x g at 4 °C for 1 hour followed by neutralizing the supernatant with 0.5 M Tris-Cl. Colorimetric 3,3′,5,5′-tetramethylbenzidine (TMB)-based ELISA (Invitrogen, Carlsbad, California) was used to measure Aβ concentrations. Capture antibodies specific for the NH2 terminus of human Aβ (amino acids 1-16) and neoepitopes at either the 40- or the 42-amino acid COOH-terminus of Aβ were used to detect peptide levels and measurements were read at 450 nm. Peptide concentration values were extrapolated using standard curves generated by synthetic Aβ peptide (Invitrogen, Carlsbad, California) and expressed as picomoles per gram wet brain tissue.

Levels of tau were quantified as previously described.(Acker et al., 2013) Briefly, SF gray matter brain tissue samples were homogenized in a Tris-buffer saline solution (pH 7.4) containing 10 mM NaF, 1 mM NaVO3 and 2 mM EGTA with a complete Mini protease inhibitor (Roche). Prior to use, samples were stored at – 80 °C. For analysis, thawed homogenates, spun at 14,000 g for 10 minutes at 4 °C, were diluted in 20% superblock in 1 x

Tris-buffered saline (TheroScientific). Sandwich enzyme linked immunosorbent assay (ELISA) measurements using monoclonal antibodies targeted against different forms of tau and phospho-tau were performed for quantification of tau peptide concentrations. Capture antibodies DA31 (amino acids 150-190), PHF1 (pSer396/404), CP13 (pSer202), and RZ3 (pThr231) were used at a concentration of 6 μg/mL in 4 separate ELISA measurements. DA31 was used to measure peptide concentrations of total tau. PHF-1 is used to quantify Ser396/404 phospho-tau (pSer396/404), a form of phosphorylated tau that is present in early and late Braak stages and is observed in a range of early to mature tau aggregates (Mondragon-Rodriguez et al., 2014). CP13 was used to quantify Ser202 phospho-tau that is detected in early neuritic pathology (Janocko et al., 2012). RZ3 was used to quantify Thr231 phospho-tau, a conformational epitope often phosphorylated even in pretangles (Augustinack et al., 2002). Detection antibody DA9-HRP (amino acids 102-140) was used at a concentration of 0.3 μg/mL for all assays.

ELISAs were performed in 96-well plates coated with capture antibodies at a concentration of 6 mg/mL in coating buffer for at least 48 hours at 4 ℃. To avoid non-specific binding, plates were washed 3 x in wash buffer and blocked for 1 hour at room temperature using StartingBlock (Thermoscientific). 50 μL of SF brain tissue sample was combined with 50 μL of DA9-HRP detection antibody and added to the appropriate well. Plates were incubated overnight shaking at 4 °C. The following day wells were washed 9 x in wash buffer and 1-Step ULTRA TMB-ELISA (Thermoscientific) was added for 30 minutes at room temperature before stopping the reaction with 2 M H2SO4. Plates were read with an Infinite m200 plate reader (Tecan) at 450 nm.

2.3.5 Statistical Analysis

All light:heavy ratios were log2 transformed for statistical analysis. Replicate peptide values were averaged prior to analysis. Assessment of demographic, clinical, and pathological differences between groups was performed using analysis of variance (ANOVA), t-tests, and $\chi 2$ tests. Initial comparison of Vilip-1 and MAP2 peptide levels between AD subjects and normal control subjects used independent samples T-tests for both the ERC and SF regions. A repeated measure ANOVA was employed to evaluate the brain region by diagnosis interaction. In the SF region, ANCOVA was used to assess whether demographic, clinical, and pathological subgroups affected individual Vilip-1 and MAP2 peptide levels.

2.4 RESULTS

2.4.1 Alterations in VILIP-1 levels in brain regions with and without prominent cell death

In an initial comparison of 12 AD subjects and 12 cognitively normal control subjects (Table 2.1), Vilip-1 levels were assessed in two brain regions: ERC and SF. The ERC is a brain region with prominent cell death in AD, including in earlier disease stages, whereas the SF has comparatively little neuronal loss in AD. Vilip-1 peptide levels in the ERC were significantly decreased in AD subjects compared to cognitively normal controls (Figure 2.3; Table 2.3). However, in the SF, Vilip-1 levels were not significantly different from cognitively normal controls. Additionally, for three of the five Vilip-1 peptides (STE, LNL, and LNW), there was a significant region by diagnosis interaction (Figure 2.3; Table 2.3).

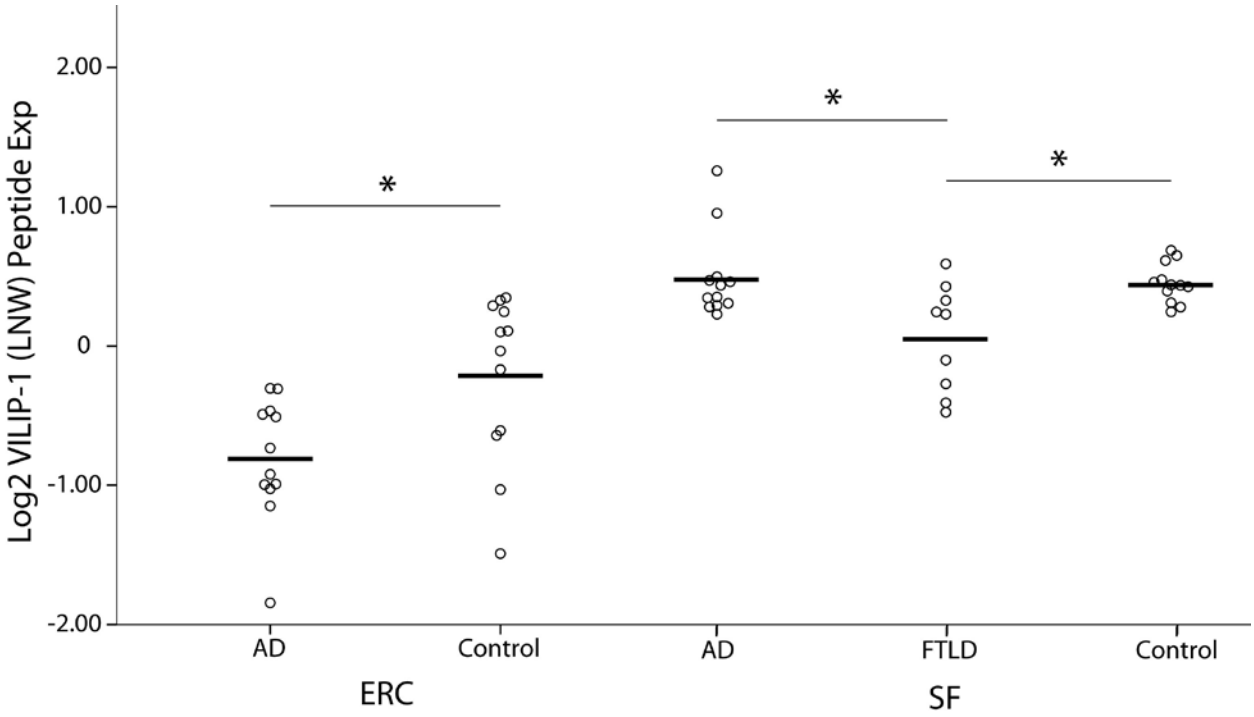

Figure 2.3 Log2-transformed expression ratios of a representative peptide, Vilip-1 (LNW), in the entorhinal cortex (ERC) and the superior frontal gyrus (SF) comparing AD subjects (n =12) and cognitively normal control subjects (n=12). * indicates $p < 0.05$.

Table 2.3 Summary of Vilip-1 peptide expression in ERC and SF brain regions and the effect of region by diagnosis from 34-subject Cohort 1 (AD: n = 12; cognitively normal control: n = 12; FTLD: n = 10)

	ERC			SF			Region by Diagnosis	
Peptide	**AD:Control**	**t, df**	**p**	**AD:Control**	**t, df**	**p**	**F, df**	**p**
STE	0.650	2.618, 22	*0.016*	1.117	-0.858, 22	0.400	6.406, 22	*0.019*
LNL	0.666	2.322, 22	*0.030*	1.112	-0.944, 22	0.355	5.560, 22	*0.028*
LNW	0.641	2.788, 22	*0.011*	1.047	-0.399, 22	0.694	6.540, 22	*0.018*
VEM	0.619	2.621, 22	*0.016*	1.042	0.387, 22	0.702	2.326, 22	0.141
SDP	0.667	2.48, 22	*0.021*	1.003	0.366, 22	0.718	4.060, 22	0.056

Because the restriction of the observed decrease in Vilip-1 levels to the ERC suggested it resulted from neurodegeneration rather than a specific AD-related pathology, we analyzed Vilip-1 peptide levels from FTLD subjects (Table 2.1) in the SF, a brain region that in FTLD is primarily affected by widespread neuronal loss, and found that SF Vilip-1 levels in FTLD were significantly lower than in cognitively normal controls (Figure 2.3; Table 2.4).

Table 2.4 Summary Vilip-1 peptide expression diagnosis differences from expanded AD subject group (n = 58) in comparison to FTLD (n = 10) and cognitively normal controls (n = 12).

	AD vs Control		AD vs FTLD		FTLD vs Control	
Peptide	**AD:Control**	**p**	**AD:FTLD**	**p**	**FTLD:Control**	**p**
STE	1.024	0.161	1.335	*0.002*	0.767	*< 0.001*
LNL	0.746	0.478	1.300	*< 0.001*	0.773	*< 0.001*
LNW	0.984	0.592	1.254	*0.002*	0.784	*0.003*
VEM	0.996	0.245	1.376	*0.017*	0.724	*0.003*
SDP	0.934	0.618	1.600	*0.002*	0.5837	*0.004*

To confirm this interpretation, we assessed levels of MAP2, a marker that is reduced by neuron loss (Huh et al., 2003) in the ERC and SF of all subjects. MAP2 levels were significantly decreased in ERC of AD subjects compared to normal controls (all $p < 0.001$; Table 2.5), and decreases in the ERC exceeded those in the SF of these subjects. In the SF of the expanded cohort of subjects, the magnitude of reduction in MAP2 levels was greater in FTLD subjects than in AD (Table 2.6).

Table 2.5 Summary of MAP2 peptide expression in ERC and SF brain regions and the effect of region by diagnosis from 34-subject Cohort 1 (AD: n = 12; cognitively normal control: n = 12; FTLD: n = 10)

	ERC			SF			Region by Diagnosis	
Peptide	AD:Control	t, df	p	AD:Control	t, df	p	F, df	P
LIN	0.242	4.638, 21	*< 0.001*	0.63	2.106, 22	*0.047*	7.792, 22	*0.011*
DLA	0.299	5.119, 21	*< 0.001*	0.805	1.375, 22	0.183	19.993, 22	*< 0.001*

Table 2.6 Summary MAP2 peptide expression diagnosis differences from expanded AD subject group (n = 58) in comparison to FTLD (n = 10) and cognitively normal controls (n = 12)

	AD vs Control		FTLD vs Control		AD vs FTLD	
Peptide	AD:Control	p	FTLD:Control	p	AD:FTLD	p
LIN	0.554	*0.010*	0.358	*< 0.001*	1.439	0.054
DLA	0.729	0.065	0.507	*< 0.001*	1.549	*0.013*

2.4.2 VILIP-1 levels in SF of AD subjects and indicators of disease severity

We examined SF Vilip-1 levels in an expanded group of AD subjects (Table 2.2) to assess whether indicators of greater disease severity would be associated with reduced SF Vilip-1 in AD. In this expanded group the comparison of Vilip-1 peptide levels to controls remained non-significant (all $p > 0.1$). No association was observed between increasing Braak stage and Vilip-1

levels in the SF of AD (Figure 2.4). Nor were Vilip-1 levels in the SF correlated with levels of soluble $A\beta_{1-42}$, $A\beta_{1-40}$, total tau or phosphorylated tau (Figure 2.5). Additionally, history of psychosis, Lewy body stage, Mini–Mental State Examination (MMSE) score at death, age at death, age of disease onset, and duration of illness were not significantly associated with SF Vilip-1 levels (Figure 2.4).

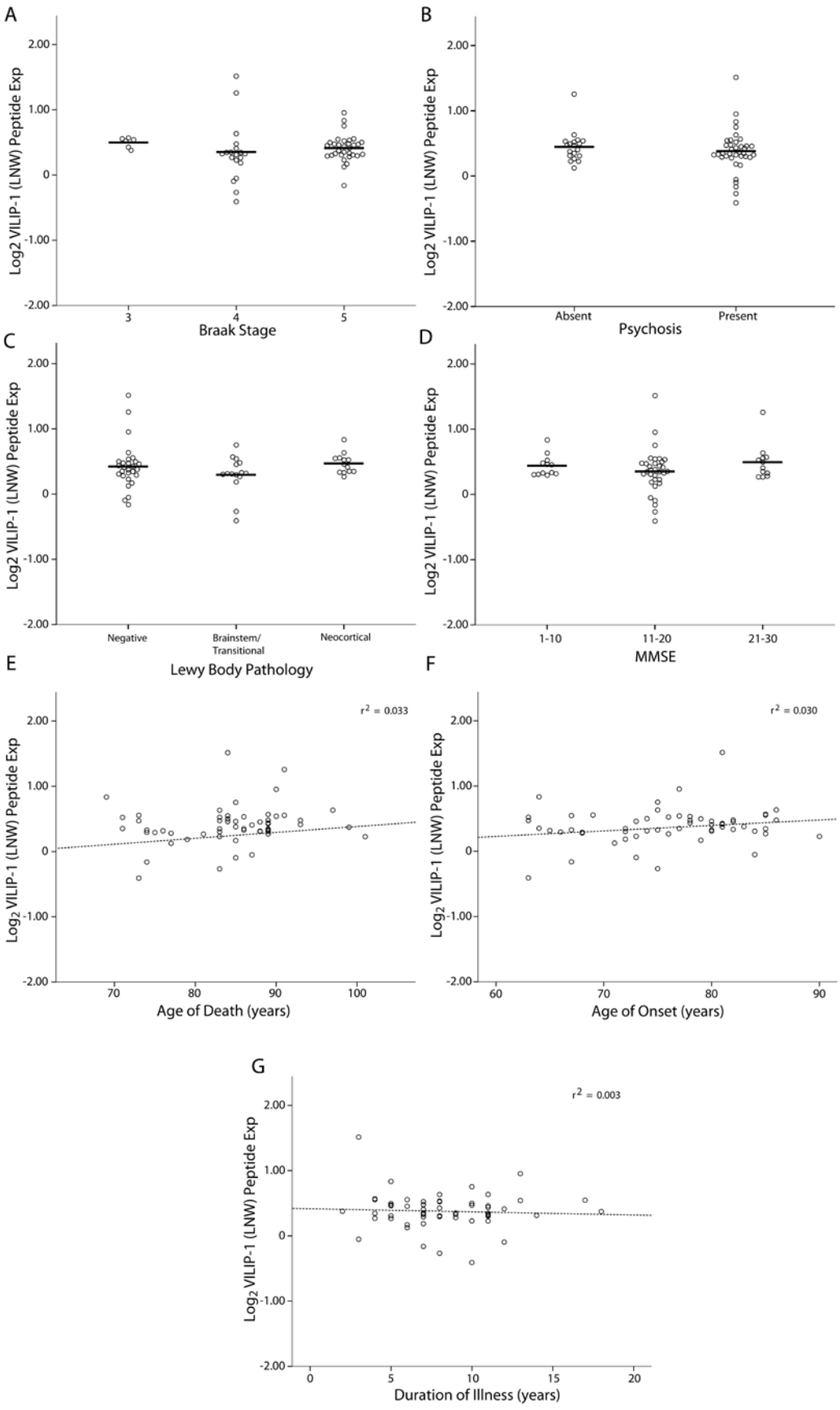
A
Log2 VILIP-1 (LNW) Peptide Exp
2.00
1.00
0
-1.00
-2.00
3
4
5
Braak Stage
B
Log2 VILIP-1 (LNW) Peptide Exp
Absent
Present
Psychosis
C
Log2 VILIP-1 (LNW) Peptide Exp
Negative
Brainstem/ Transitional
Neocortical
Lewy Body Pathology
D
Log2 VILIP-1 (LNW) Peptide Exp
1-10
11-20
21-30
MMSE
E
Log2 VILIP-1 (LNW) Peptide Exp
r2 = 0.033
70
80
90
100
Age of Death (years)
F
Log2 VILIP-1 (LNW) Peptide Exp
r2 = 0.030
60
70
80
90
Age of Onset (years)
G
Log2 VILIP-1 (LNW) Peptide Exp
r2 = 0.003
0
5
10
15
20
Duration of Illness (years)

Figure 2.4 Log2-transformed expression ratios of a representative peptide, Vilip-1 (LNW), in the superior frontal gyrus (SF) of AD subjects (n=58,Table 2) looking at (A) Braak stage, (B) Psychosis status in Alzheimer disease, (C) Lewy body pathologic stage, (D) Mini-Mental State Examination, (E) Age at death, (F) Age of disease Onset, and (G) Disease duration.

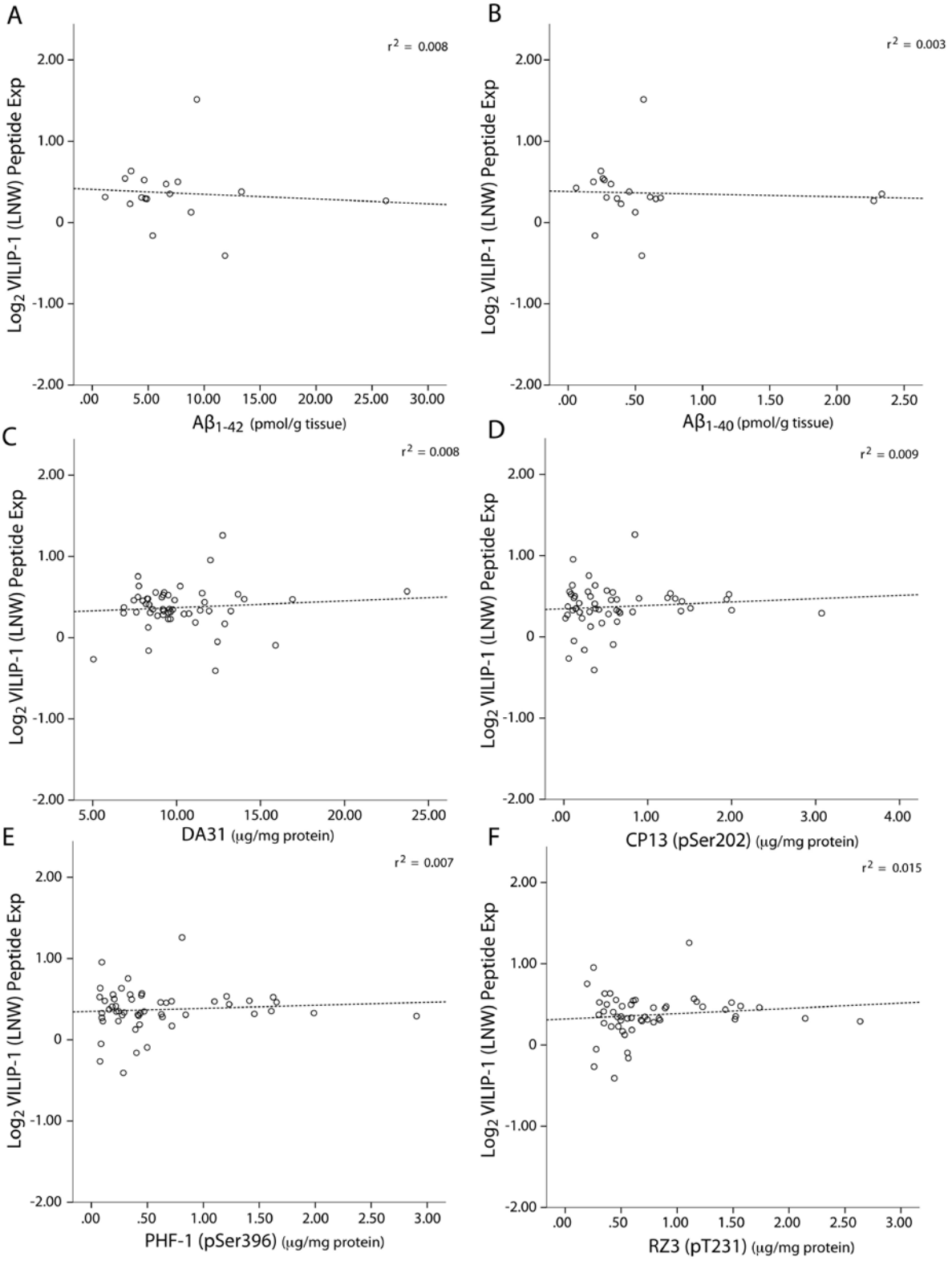

Figure 2.5 Correlation of $\log_2$-transformed expression ratios of a representative peptide, Vilip-1 (LNW), in the superior frontal gyrus (SF) of AD subjects with (A) $A\beta_{1\text{-}42}$, (B) $A\beta_{1\text{-}40}$, (C) DA31, (D) CP13, (E) PHF-1, and (F)

RZ3. For soluble $A\beta_{1-42}$ and $A\beta_{1-40}$ data was available for 23 AD subjects. For total and phosphotau measures, data was available for 53 AD subjects.

2.5 DISCUSSION

We evaluated the hypothesis that Vilip-1 is altered in AD and associated with neurodegeneration by assessing Vilip-1 brain protein levels in two different regions with varying degrees of neuronal loss. We found Vilip-1 levels were decreased in the ERC of AD subjects, an area of prominent neuronal loss even at early stages of the disease. However, in the SF, an area with comparatively less neuronal loss in early to moderate disease stages, Vilip-1 levels did not differ from normal control subjects. In contrast, FTLD is characterized by profound neuronal loss in the frontal and temporal lobes of the brain. Vilip-1 levels in the SF were decreased in these subjects. Additionally, in an expanded group of AD subjects, Vilip-1 levels in the SF did not associate with other indicators of disease severity including Braak stage, soluble $A\beta_{1-42}$, $A\beta_{1-40}$, total and phosphorylated tau levels. These findings provide evidence that Vilip-1 is altered in AD and may be more closely associated with neuronal loss than with upstream pathologies such as Aβ and phosphorylated tau accumulation or synaptic pathology.

Recent studies have identified a potential role for Vilip-1 as a biomarker in AD. CSF and plasma Vilip-1 levels have been shown to be elevated in mild cognitive impairment and AD compared to normal control subjects (Lee et al., 2008, Tarawneh et al., 2011, Mroczko et al., 2015). Additionally, Vilip-1 CSF levels were predictive of progressive cognitive decline, as higher Vilip-1 levels indicate a more rapid deterioration in cognitive performance (Tarawneh et al., 2012, Fagan et al., 2014, Mroczko et al., 2015). While CSF Vilip-1 levels are elevated in AD,

our findings, which are the first reported quantitative levels of Vilip-1 in human brain tissue, indicate decreased levels of Vilip-1 in the ERC of AD subjects. Many different scenarios may explain this disparity between elevated CSF and decreased brain levels. The most parsimonious explanation is that as ERC neurons die, intraneuronal Vilip-1 is released into the interstitium and reaches the CSF. For example, Vilip-1 has also been shown to be elevated in the CSF of a rat model of stroke and within the plasma of patients after stroke (Laterza et al., 2006, Stejskal et al., 2011).

Further CSF findings have suggested a disease-specific association of Vilip-1 by showing increased Vilip-1 levels in AD compared to other non-AD dementia subjects, including individuals with FTLD, progressive supranuclear palsy, and Lewy body dementia (Tarawneh et al., 2011). In contrast to CSF, we have shown that in SF brain tissue, Vilip-1 levels were unaffected in AD and significantly decreased in FTLD subjects compared to normal control subjects. Without having measurements from a neuropathologically verified population of FTLD subjects it is difficult to know for certain whether CSF Vilip-1 levels are unchanged in this neurodegenerative disorder. Future CSF studies involving larger numbers of FTLD subjects will be necessary to definitively determine that CSF Vilip-1 is not increased in FTLD. Confirming this discrepancy between CSF and brain findings in AD and FTLD would support further evaluation of additional mechanisms including: active secretion of Vilip-1 into the CSF from the ERC in AD; poor clearance of Vilip-1 from the CSF in AD, or; Vilip-1 released from ERC neurons has more direct influence on the CSF compartment sampled by lumbar puncture than when released from SF neurons.

Previous reports have qualitatively described Vilip-1 associating with other AD pathologies, like neuritic plaques and neurofibrillary tangles in the neocortex (Braunewell et al.,

2001a) and shown correlations with CSF levels of tau and phosphorylated tau (Tarawneh et al., 2011). Others have indicated that Vilip-1 may play an active role in tau phosphorylation (Schnurra et al., 2001). However, we found that Vilip-1 levels in the SF did not correlate with any indicators of disease severity including Braak stage, soluble $A\beta_{1-42}$, $A\beta_{1-40}$, total or phosphorylated tau levels. The discrepancy between findings may be in part due to the approach used. We used quantitative LC-SRM/MS of gray matter brain homogenate to measure total levels of Vilip-1 peptide in brain tissue, an approach that allowed for simultaneous measurement and quantification of five Vilip-1 peptides with high precision and reproducibility. Peptide detection was linear and over repeated runs we observed low variability in peptide measures. Similarly, we used a highly specific ELISA assay to measure total and phosphorylated tau with multiple antibodies. In contrast, the prior finding indicating an association of Vilip-1 with tau pathology used qualitative immunohistochemistry (IHC) (Braunewell et al., 2001a), and thus could not speak to the amount of Vilip-1 present. Additionally, albeit only an indirect indicator of increased tau pathology, psychosis status in AD was not associated with altered Vilip-1 levels in our cohort (Murray et al., 2014b).

One potential limitation of this study was the significantly younger normal control group. We opted to utilize a neuropathologically normal control group, as previous Western blot data from our laboratory (not shown) has suggested decreased levels of Vilip-1 in controls with some level of neuropathology, such as mesial temporal sclerosis and cerebrovascular disease, despite no clinical diagnosis of a cognitive disorder. Additionally, selection of age-matched control subjects is complicated as many biomarker and neuroimaging studies have demonstrated that the AD disease process can begin decades prior to the emergence of cognitive symptoms (Resnick et al., 2010, Tosun et al., 2013). Thus to obtain neuropathologically normal subjects, many subjects

of advanced ages similar to the AD group did not meet this criteria. Despite these obstacles in selecting a proper control group, several observations make it unlikely that age is associated with the alterations we observed in Vilip-1. First, it would be difficult to explain an age effect that led to differential expression of Vilip-1 only in the ERC, but not SF, of the same subjects. Second, we have shown using mRNA microarray analysis of cognitively normal adults that VSNL1 is unaffected by age across the adult lifespan (***Appendix B***) (Lin et al., 2015). Finally, our FTLD subjects were substantially younger than our AD cohort, yet still had significantly different Vilip-1 protein levels compared to controls. Another potential confound in human tissue studies is matching normal control subjects as closely as possible on PMI. Our study included AD with significantly lower PMIs than normal controls, however we previously established the stability of Vilip-1 protein across a 48-hour PMI in a mouse model (Figure 2.1), a much greater range than in the current study. Moreover, as for age difference, it would be difficult to reconcile a PMI effect with differential expression of Vilip-1 only in the ERC, but not SF, of the same subject pairs.

Neuronal loss occurs prominently in the ERC of AD subjects and the SF of FTLD subjects (Gomez-Isla et al., 1996, Cairns et al., 2003). Conversely, despite reductions in cortical volume, stereological studies have found no global change in neuron number within the neocortex of females with severe AD (Regeur et al., 1994). As a confirmatory measure to assess neuronal loss with the ERC and SF brain regions in our study, we measured MAP2 peptide levels. MAP2 is a neuron-specific protein that interacts with microtubules and the cell cytoskeleton (Dehmelt and Halpain, 2005). Being among the most vulnerable cytoskeletal proteins, MAP2 immunoreactivity is lost in neuronal death (Huh et al., 2003). We found that MAP2 levels were significantly decreased in the ERC of AD subjects compared to normal

controls. MAP2 levels were also down in the SF of AD subjects compared to normal controls, however, in FTLD subjects the magnitude of reduction was greater, suggesting a larger amount of neuronal loss in FTLD compared to AD. In addition, our lab has previously reported that MAP2 peptide levels are unchanged in schizophrenia subjects, a disease without neuronal loss (Shelton et al., 2015).

Our findings of decreased Vilip-1 expression levels in brain regions with prominent cell death in both AD and FTLD, but not in the SF of AD where cell death is more limited suggest that Vilip-1 may serve as a neuronal integrity biomarker, at least within ERC. The role of Vilip-1 in cell death, whether it is an active participant in the process or an innocent bystander, requires further investigation. For example, prior reports have shown that expression of Vilip-1 in PC12 cells reduced cell survival rate compared to untransfected cells. When transfected cells were exposed to ionomycin, a known neurotoxic reagent that increases intracellular calcium concentration, an even higher cell death rate was observed, indicating a role for Vilip-1 in Ca^{2+}-mediated cell death (Schnurra et al., 2001). Future studies using in vitro techniques and animal models of Aβ overproduction will help clarify the role of Vilip-1 in AD-related neuronal death.

3.0 THE IMPACT OF AB ON VILIP-1 EXPRESSION

3.1 ABSTRACT

Soluble Aβ oligomers are widely considered to have a central etiological role in Alzheimer disease, binding synapses and initiating a cascade of neurotoxic events in the cells that culminate in neuron death. Recently, we have shown that mRNA for VSNL1, the gene that encodes the protein Vilip-1, a peripheral early stage biomarker for Alzheimer disease (AD), is coexpressed with genes associated with AD throughout normal aging. Notably, the gene that encodes the amyloid precursor protein, which is cleaved to form Aβ peptide, is correlated with the Vilip-1 mRNA expression. Additionally, Vilip-1 has been shown to associate with neuritic plaques in AD brain tissue. However, whether Aβ impacts Vilip-1 expression is unknown. To assess the effect of Aβ on Vilip-1 expression we used two model systems: a transgenic mouse model of Aβ-overexpression and exogenous Aβ exposure in primary cortical neuronal cultures. We found that Vilip-1 expression was unchanged in both systems by the presence of Aβ peptide.

3.2 INTRODUCTION

The amyloid-β (Aβ) peptide chiefly comprises extracellular amyloid plaques, one of the major neuropathological hallmarks in Alzheimer disease (AD). Soluble Aβ oligomers have been

strongly implicated in the pathogenesis of AD and are posited to initiate a cascade of pathological events that involve neuronal Ca^{2+} dysregulation, synaptic impairment and dysfunction, loss of dendritic spines, tau phosphorylation and aggregation, and ultimately neuronal death.

Visinin-like protein 1 (VILIP-1) is a primarily brain-expressed neuronal calcium-sensing protein that has recently been identified by a number of studies as a peripheral early stage biomarker in AD. Individuals with AD have elevated levels of Vilip-1 in their cerebrospinal fluid (CSF) that correlate with measures of amyloid load in the brain (Tarawneh et al., 2011). Recently, in an mRNA microarray study examining expression of VSNL1, the gene that encodes for the Vilip-1 protein, we showed that VSNL1 is coexpresses with genes associated with AD across normal aging (***Appendix B***) (Lin et al., 2015). This included a high degree of correlation of VSNL1 expression with that of amyloid precursor protein (APP) (***Appendix B***) (Lin et al., 2015). Additionally, qualitative immunohistochemistry data from AD subjects has suggested an association between Vilip-1 and neuritic plaques in several neocortical brain regions (Braunewell et al., 2001a). However, whether amyloid overexpression and exposure to soluble Aβ can induce elevations in Vilip-1 is not known.

In the present study, we hypothesized that Vilip-1 expression would be increased in the presence of Aβ peptides. Using two model systems to evaluate this relationship, a mouse model of Aβ-overexpression and primary cortical neuronal cultures treated with Aβ peptide, we found that Vilip-1 expression is unchanged by the presence of Aβ peptide.

3.3 METHODS

3.3.1 Experimental Animals

3.3.1.1 B6.Cg-Tg(APPswe,PSEN1dE9)85Dbo/Mmjax mouse model. Six-month-old double transgenic B6.Cg-Tg(APPswe,PSEN1dE9)85Dbo/Mmjax (PSAPP; n = 5) and wild-type (n = 5) male mice were studied. Double transgenic PSAPP (The Jackson Laboratory, Bar Harbor, Maine; Catalog #: 005864) and wild-type mice for study were generated by mating male PSAPP mice with female kalirin heterozygous mice that were generated as previously described by inserting the neomycin resistance cassette in place of exons 27-28 (Cahill et al., 2009) and subsequently maintained on a C57BL/6NJ background. PSAPP mice express chimeric mouse/human amyloid precursor protein carrying a mutation linked to familial AD (Mo/HuAPP695swe) and a mutant human presenilin 1 (PSEN1dE9), which is also linked to familial AD (Hardy, 1997). The double transgenic increases the ratio of $A\beta_{1-42}$:$A\beta_{1-40}$ as compared to mice carrying the APPswe mutation alone (Jankowsky et al., 2004). Both mutations are under the control of the mouse prion protein promoter, which directs transgene expression largely to central nervous system neurons. PSAPP mice show detectable Aβ deposits by 4 months of age and an overall increase in levels of soluble and insoluble levels of two Aβ isoforms ($A\beta_{1-40}$ and $A\beta_{1-42}$) by twelve months of age, with $A\beta_{1-42}$ being the predominantly expressed Aβ species (Garcia-Alloza et al., 2006). In Figure 3.1, we demonstrate an increase in 6E10 antibody immunoreactivity (directed against the N-terminus of human Aβ peptide; biotinylated, SIG-39340; Covance, Emeryville, CA) in the PSAPP genotype in comparison to wild type. Behaviorally, by 6 months mutant mice have learning and memory deficits compared

to wild-type littermates (Gimbel et al., 2010, Phillips et al., 2011). All studies were approved by the University of Pittsburgh Institutional Animal Care and Use Committee.

3.3.1.2 C57BL/6NJ. Primary neuronal culture experiments were performed on newborn (P0) C57BL/6NJ mice (The Jackson Laboratory, Bar Harbor, Maine).

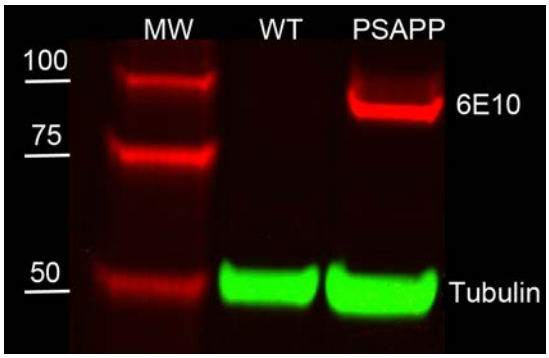

Figure 3.1 Representative 6E10 Western blot of 6-month-old wild type brain tissue versus PSAPP. A marked increase in APP expression is observed within the PSAPP animals.

3.3.2 LC-SRM/MS

3.3.2.1 Sample preparation. Tissue homogenates were prepared from fresh frozen PSAPP and wild-type mouse cortex. Total protein was extracted using SDS extraction buffer (0.125 M Tris – HCl (pH 7), 2% SDS, and 10% glycerol) at 70°C. Using bicinchoninic acid assay (Micro BCATM Protein Assay, Pierce) protein concentration was measured. 20 ug of total protein from the whole brain homogenate was mixed with Lysine 13C6 Stable Isotope Labeled Neuronal Proteome Standard (13C6 STD; 20 ug) for on gel trypsin digestion. Samples were run on a single 10 well 4-12% BisTris gel with two SeeBlue® Plus2 Pre-stained Protein Standards. On-gel trypsin digestion was performed as previously described (MacDonald et al., 2012) with samples

being run 4 cm into the gel and divided into two fractions (above and below 65kd). The samples were randomly distributed in a block design across three 10-well gels with each gel containing seven samples, one pooled internal control, and two lane markers.

3.3.2.2 LC-SRM/MS. VILIP-1 peptides were selected for analysis based on the presence of a lysine, the amino acid labeled in the 13C6STD. Five peptide sequences were identified from the VILIP-1 protein for quantification as indicated as underlined text in the following VILIP-1 amino acid sequence:

MGKQNSKLAPEVMEDLVKSTEFNEHELKQWYKGFLKDCPSGRLN
LEEFQQLYVKFFPYGDASKFAQHAFRTFDKNGDGTIDFREFICALSITSRG
SFEQKLNWAFNMYDLDGDGKITRVEMLEIIEAIYKMVGTVIMMKMNEDG
LTPEQRVDKIFSKMDKNKDDQITLDEFKEAAKSDPSIVLLLQCDIQK

LC-SRM/MS analyses were conducted as previously described. (MacDonald et al., 2012) In brief, SRMs were monitored using a TSQ Quantiva triple stage quadrupole mass spectrometer (Thermo Scientific) with an UltiMate 3000 Nano LC Systems (Thermo scientific). 2 µl (~1 µg protein) of sample was loaded/desalted on a PepMap100 Nano-Trap column (Thermo scientific) at 8 µl/min for 2 min and separated on a Reprosil-pur 3 µm PicoChip column (New Objective) at 400 nl/min over a 20 min gradient from 2-35% mobile phase B (Acetonitrile containing 0.1% formic acid). SRM transitions were timed using 1.5 min retention windows. Transitions were monitored, allowing for a cycle time of 1 sec, resulting in a dynamic dwell time, never falling below 2 msec. The MS instrument parameters were as follows: capillary temperature 275 °C, spray voltage 1100 V, and a collision gas of 1.4 mTorr (argon). The resolving power of the

instrument was set to 0.7 Da (Full Width Half Maximum) for the first and third quadrupole. Using Skyline, integrated peak areas for both “light” PSAPP peptides and the “heavy” 13C6STD peptides were calculated for each of the five VILIP-1 peptide sequences. The light:heavy integrated area ratio was calculated to obtain peptide measures using multiple transitions per peptide. A sample chromatogram is shown in Figure 3.2.

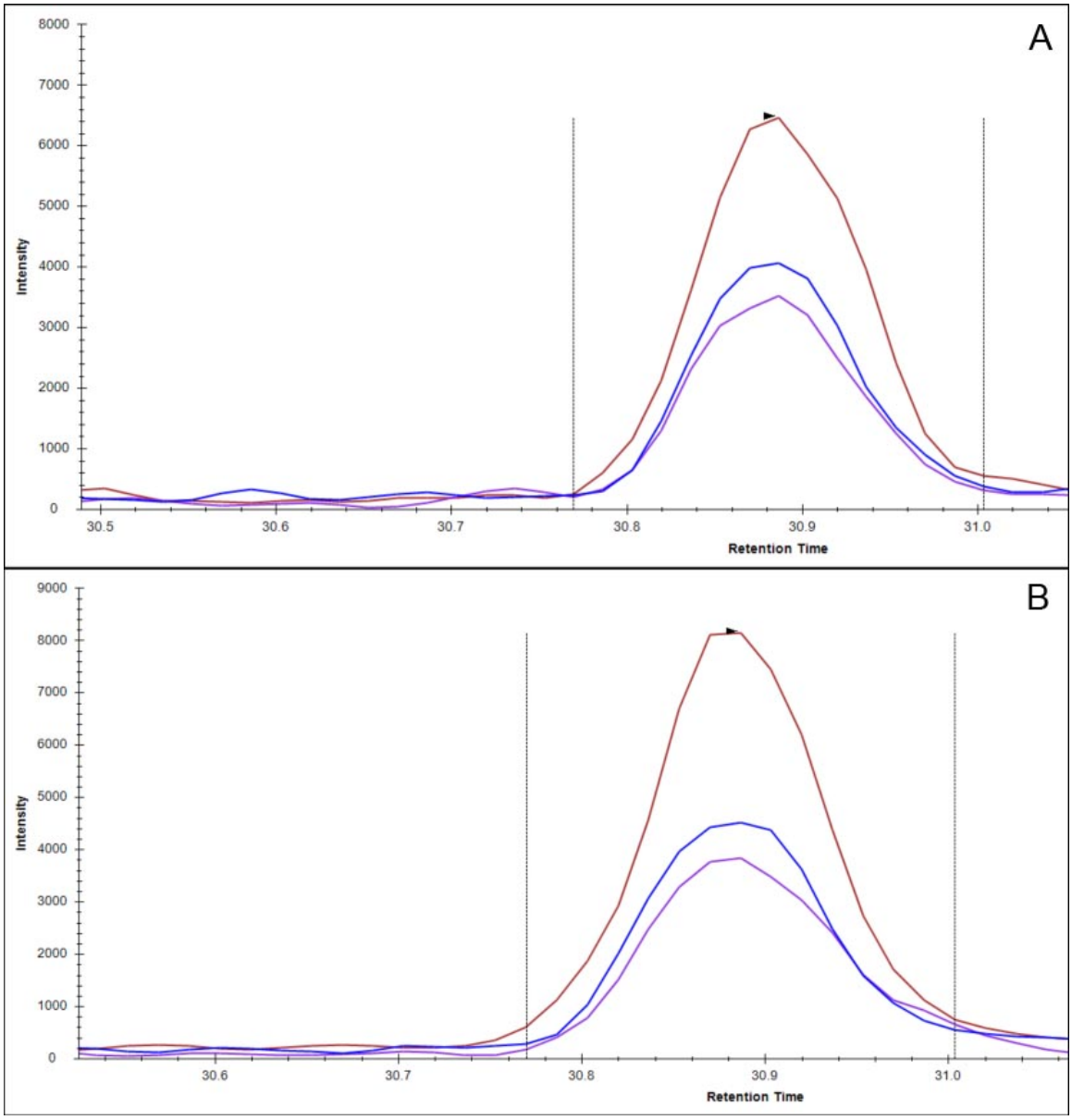

Figure 3.2 Representative mass chromatogram of Vilip-1 LNLEEFQQLYVK product ions for the light (A) and heavy (B) peptide SRM measures.

3.3.3 Cell Culture

3.3.3.1 Primary neuronal culture generation. Primary neuronal cultures were generated as previously described (Beaudoin et al., 2012) with modifications. Mouse cortical neurons were

prepared from newborn (P0) mice. Pups were euthanized by decapitation and heads were placed in dissection medium (1X Hank's Balanced Salt Solution (Ca^{2+} and Mg^{2+} free; Gibco; Catalog #: 14185), 100X sodium pyruvate (Sigma-Aldrich; Catalog #: P-2256), 20% glucose (Sigma-Aldrich; Catalog #: G-6152), 1 M HEPES (Sigma-Aldrich; Catalog #: H0887)). Skin on top of the head was gently dissected to expose the skull and using fine scissors, the skull was opened by making an incision at the base of the brain. The two halves of the skull were separated and removed exposing the brain. The brain was pinched off from the base in a scooping motion and transferred to a fresh dish of dissection media kept on ice. Under the dissecting scope, a sagittal cut was made down the midline of the brain, separating the two halves. The midbrain and thalamic tissues were then removed leaving the intact hemisphere containing the cortex and the hippocampus. Meninges were removed from each hemisphere by gently peeling them off. Forceps were then used to dissect out the hippocampus from the neighboring cortical tissue. Using a pipette, cortical tissue was collected and placed in an Eppendorf tube with 500 µL of dissection media. Following the competition of dissection of all brains, the tissue was resuspended in 500 µL of fresh dissection media and 50 µL of 2.5% trypsin solution (Gibco; Catalog #: 15090046) and incubated at 37°C in a water bath for 20 minutes. After 20 minutes, 20 µL of DNase (Thermo Scientific; Catalog #: EN0525) was added and tissue was incubated at room temperature for 5 minutes. Following incubation, the media was aspirated and washed twice with 1 mL of dissection medium followed by two washes with temperature-equilibrated (37°C) plating medium (Minimum Essential Medium with Earle's salts, Gibco, Catalog #: 41090-036), 100 mM pyruvic acid (Sigma-Aldrich; Catalog #: P-2256), 20% glucose, 10% Horse serum (Gibco; Catalog #: 26050-070)). Tissue was then carefully triturated between ten to fifteen times to dissociate cells. Cell numbers were estimated using exclusion of trypan blue

(Sigma-Aldrich; Catalog #: T8154) staining and a hemocytometer. In 60 mm dishes with five poly-d-lysine (PDL) coated glass coverslips (neuVitro; Catalog #: GG-18-pdl), neurons were plated at 100,000 cells/dish. Cortical neurons were maintained in Neurobasal Medium (Gibco; Catalog #: 21103-049), supplemented with 2% B27 Supplement (Gibco; Catalog #: 17504-44), penicillin/streptomycin (100 U/mL and 100 mg/mL, respectively; Gibco; Catalog #: 15145-014), and 2 mM glutamine (Sigma-Aldrich; Catalog #: G3126) with replacement of one half of the media in each well every 3 days. Neurons were incubated at 37 °C, with 5% CO2.

3.3.3.2 Aβ Exposure. Human amyloid β-peptide (1-42) (Tocris, Bristol, UK; Catalog #: 1428) is considered to be the predominant and most toxic Aβ-peptide species in Alzheimer disease patients. The $A\beta_{1-42}$ amino acid sequence is: DAEFRHDSGYEVHHQKLVFFAEDVGSNKGAIIGLMVGGVVIA. 100 μg of $A\beta_{1-42}$ was solubilized at 1 mg/mL in 50 mM Tris buffer (PH 7.0) creating a 221.5 μM $A\beta_{1-42}$ stock solution and vortexed vigorously for 1 minute. Next, 225.7 μL of solublized stock $A\beta_{1-42}$ was added to 1 mL of B27 maintenance media and vortexed again for 1 minute before adding the solution to the 4 mL of conditioned media present in the dish with the coverslips, bringing the final concentration to10 μM $A\beta_{1-42}$. Our $A\beta_{1-42}$ stock solution preparation was determined to be largely dimeric with some higher molecular weight oligomeric species (Figure 3.3). Primary mouse cortical cultures (DIV 8 or 10) were incubated in $A\beta_{1-42}$ or media only for 24 hours. Directly following $A\beta_{1-42}$ exposure, primary cortical neurons were immersion-fixed in cold 4% paraformaldehyde for 20 minutes, and stored in HBSS at 4°C until immunohistochemistry.

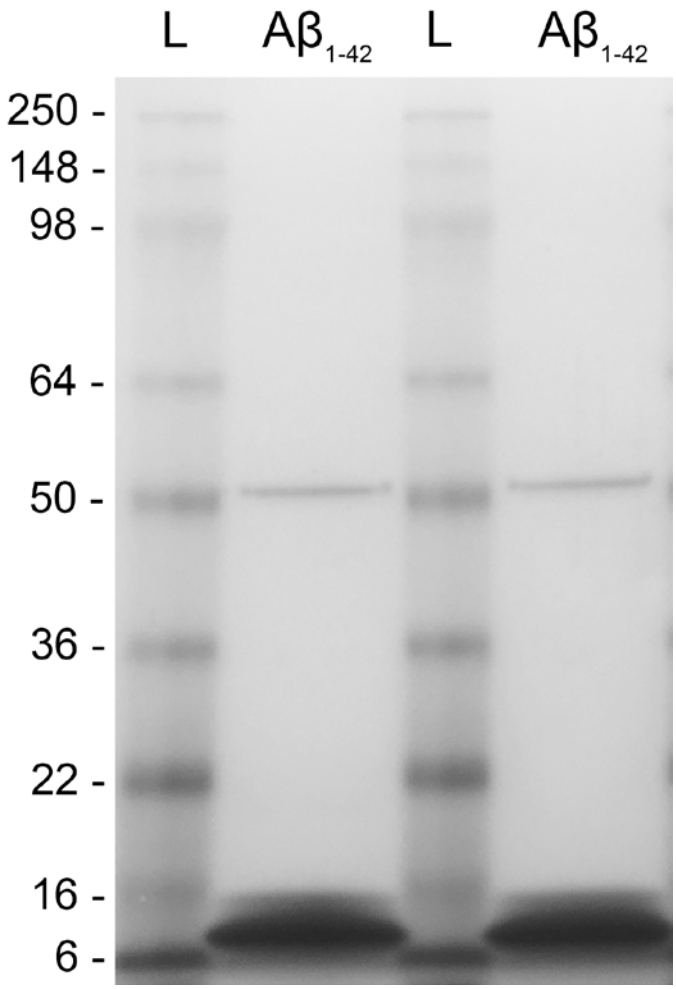

Figure 3.3 $A\beta_{1-42}$ preparation was largely dimeric with some higher molecular weight oligomeric species.

3.3.3.3 Immunohistochemistry. Monoclonal Vilip-1 antibody, 3A8.1 (kind gift of Jack Ladenson, Washington University, St. Louis, MO), was raised against Vilip-1 protein with a combination of DNA and protein injections (Laterza et al., 2006). Polyclonal rabbit anti-MAP2 (antiserum 266 raised against MAP2; kind gift of Shelley Halpain, UCSD, San Diego, CA) primarily recognizes the high molecular weight MAP2 doublet (MAP2a and MAP2b) and is unaffected by phosphorylation state of the protein (Halpain and Greengard, 1990). Fixed cells were permeabilized with 0.2% Triton for 10 minutes and rinsed three times for 3 minutes each in Hank's Balanced Salt Solution (HBSS). Cells were then incubated for 20 minutes in HBSS

containing 2% normal goat serum, followed by a 45 minute incubation at room temperature in HBSS containing 1% normal goat serum, a 1:500 dilution of Vilip-1 antibody, and a 1:500 dilution of 266 antibody. Next cells were incubated for 45 minutes at room temperature in the dark in HBSS containing 1% normal goat serum, 1:500 dilution of goat anti-rabbit secondary antibody conjugated to Alexa Fluor 405 (Invitrogen), and a 1:500 dilution of goat anti-mouse secondary antibody conjugated to Alexa Fluor 568 (Invitrogen). Coverslips were mounted onto glass slides with Vectashield hardset (Vector Laboratories, Burlingame, CA).

3.3.3.4 Microscopy. Data acquisition was performed on an Olympus (Center Valley, PA) BX51 WI upright microscope equipped with an Olympus spinning disk confocal (SDCM) using an Olympus PlanAPO N 60X 1.40 NA super corrected oil immersion objective. The SDCM was equipped with an ORCA-R2 camera (Hamamatsu, Bridgewater, NJ), MBF CX9000 front-mounted digital camera (MicroBrightField, Inc., Natick, MA), BioPrecision2 XYZ motorized stage with linear XYZ encoders (Ludl Electronic Products Ltd., Hawthorne, NY), excitation and emission filterwheels (Ludl Electronic Products Ltd.), and equipped with a Sedat Quad 89000 filter set (Chroma Technology Corp., Bellows Falls, VT). The microscope was controlled by Stereo Investigator (MicroBrightField, Inc.) and SlideBook (Intelligent Imaging Innovations) software and samples were illuminated using a Lumen 220 metal halide lamp (Prior Scientific, Rockland, MA).

Using Stereo Investigator software, the glass coverslip was first outlined and a systematic random sampling grid was then randomly rotated and applied. 3-dimensional image stacks, consisting of image planes of 512 X 512 pixels (~3,058 μm2) that were separated by 0.1 μm, were acquired throughout the thickness of the cell starting at the slide. At each plane, data were collected using the following filters: 488 nm channel- excitation 490 ± 10 nm/emission 528 ±19

nm, and 568 nm channel-excitation 555 ± 14 nm/emission 617 nm ± 37 nm. Exposure times were set at 1,000 milliseconds for Vilip-1 (568 nm channel) for all sites and optimized at each site for the MAP2 (488 nm channel) for both experiments. Vilip-1 exposure times were standardized in order to compare intensity values across image stacks, whereas MAP2 intensity was optimized to ensure best visualization of the cell for the masking procedure described below. There were no instances of pixel saturation in any stack. In two independent experiments, between ten and twelve sites were imaged per coverslip (2 coverslips per condition: Aβ and media).

3.3.3.5 Image processing. In SlideBook, two-dimensional sum-projection images were made of each three-dimensional image stack. Next, a binary mask of the MAP2 channel was created by manual threshold segmentation and used to assess Vilip-1 fluorescence intensity values (Figure 3.4).

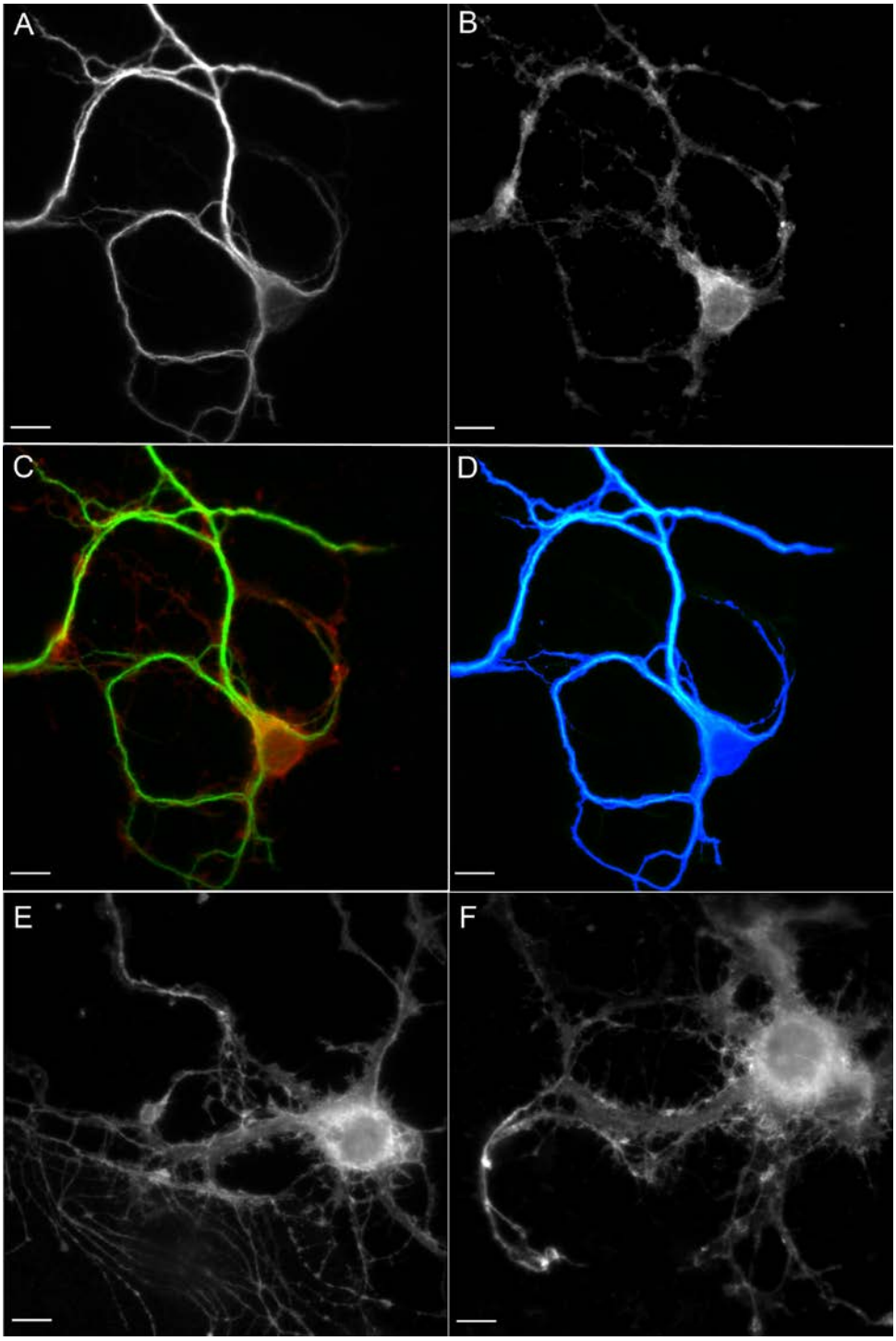

Figure 3.4 Multichannel view of neuron labeled with MAP2 (A), Vilip-1 (B), the merged image (C), and the MAP2 threshold mask (D). Representative Vilip-1 immunofluorescence in an Aβ treated cell (E) versus a control media only cell (F). Scale bars represent 10 μm.

3.3.4 Statistical analysis

All light:heavy ratios were log2 transformed for statistical analysis. Comparison of Vilip-1 peptide levels between Vilip-1 heterozygous animals and wild-type animals used independent samples T-tests.

Comparison of sum VILIP-1 fluorescence intensity levels between 10 μM $A\beta_{1-42}$ and media conditions for two independent culture experiments used independent samples T-tests. All Vilip-1 intensity measurements used in the analyses were normalized to the mean sum Vilip-1 intensity control condition (media only) within an experiment to account for assay variability.

3.4 RESULTS

3.4.1 VILIP-1 levels in a mouse model of Aβ overexpression

In a comparison of 5 PSAPP and 5 wild-type 6 month old mice, Vilip-1 levels were not significantly different between groups for any of the peptides (Figure 3.5; Table 3.1).

Table 3.1 Summary of Vilip-1 peptide expression in PSAPP and WT cortical brain tissue (PSAPP: n = 5; WT n = 5)

Peptide	PSAPP:WT	t, df	p
LAP	0.973	0.183, 8	0.859
STE	1.079	-0.456, 8	0.660
LNL	1.066	-0.328, 8	0.751
VEM	0.756	1.522, 8	0.167
SDP	1.019	-0.107, 8	0.918

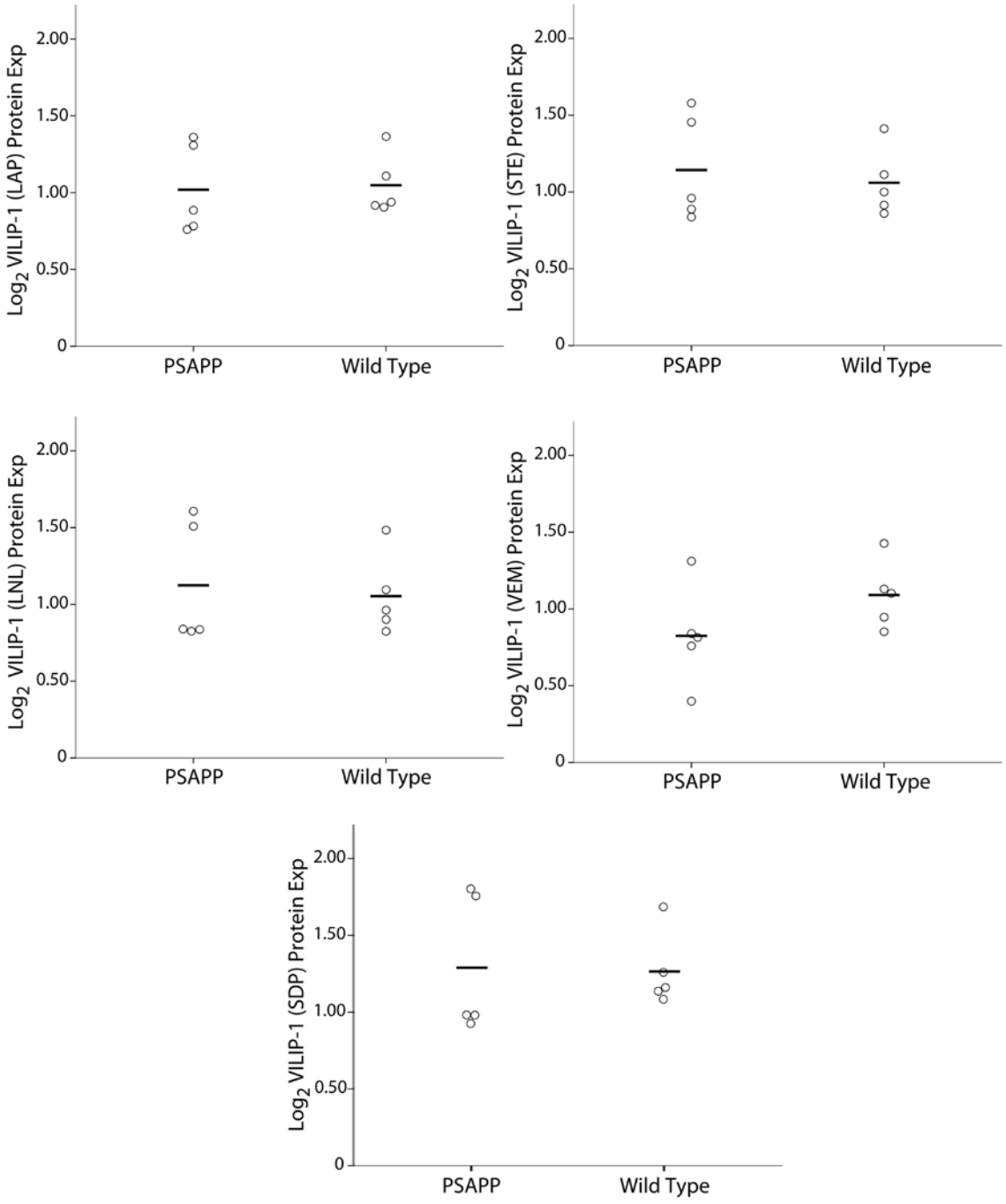

Figure 3.5 Log2-transformed expression ratios of VILIP-1 peptides in whole brain homogenate comparing PSAPP (n = 5) and wild-type (n=5) mice. No peptide levels differed significantly between groups.

3.4.2 VILIP-1 levels following Aβ exposure in culture

We examined Vilip-1 levels in neurons in following a 24 hour 10 μM $A\beta_{1-42}$ exposure. Vilip-1 levels in the $A\beta_{1-42}$ exposed group (n = 40) did not differ significantly from the control neurons in media only (n = 42) (Figure 3.6).

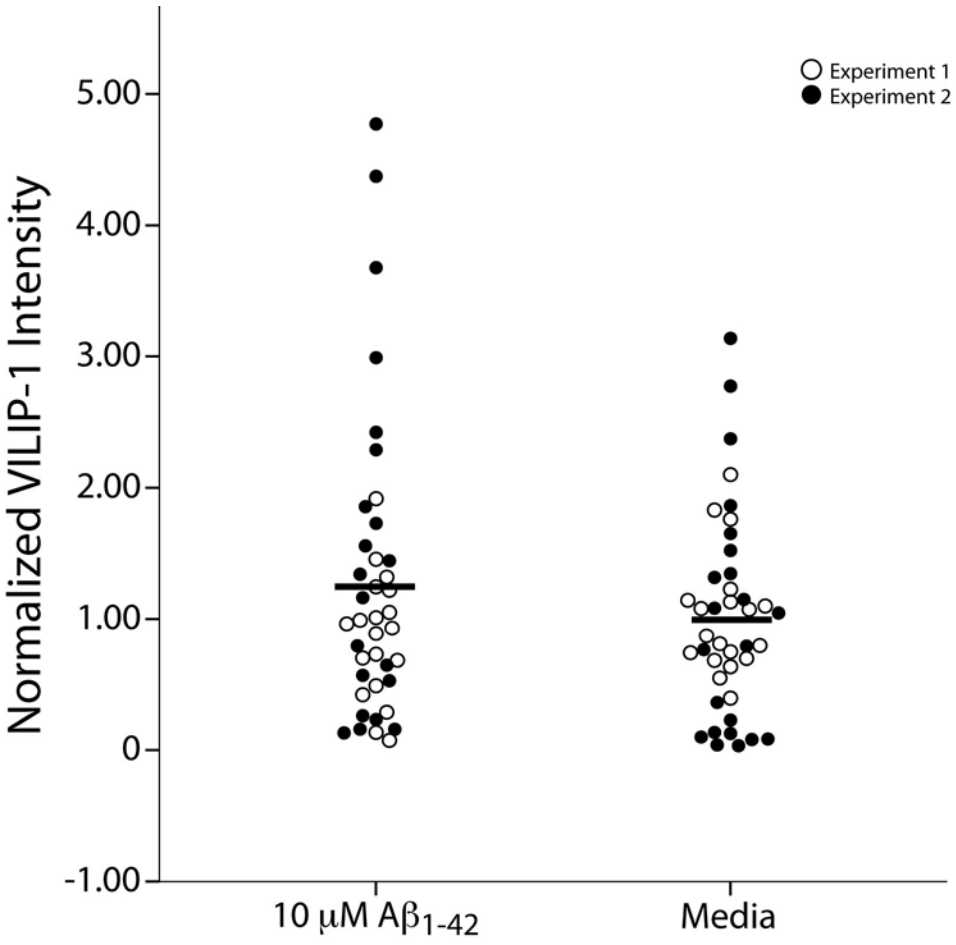

Figure 3.6 Vilip-1 immunoreactivity (sum Vilip-1 fluorescence intensity) in C57BL/6NJ primary cortical neuronal cultures normalized to the average control Vilip-1 sum fluorescence intensity in each experiment. Aβ and media conditions are not significantly different (p = 0.219). Two independent experiments are represented.

3.5 DISCUSSION

Here we provide evidence that Vilip-1 expression is unaltered in the presence of Aβ in two model systems: an animal model of Aβ overexpression and primary cortical neuronal cultures treated with Aβ peptide. These congruent findings from different experimental modalities suggest that Aβ is unlikely to lead to elevated neuronal Vilip-1 in AD.

Several lines of evidence have suggested an association between Vilip-1 and Aβ in the pathogenesis of AD. First, studies looking at cerebrospinal fluid (CSF) Vilip-1 levels and amyloid load using positron emission tomography imaging with Pittsburgh Compound-B, an histological dye that easily crosses the blood-brain barrier and binds amyloid, have demonstrated a positive correlation between these markers in preclinical AD (Tarawneh et al., 2012). Additionally, combining CSF Vilip-1 levels with CSF $A\beta_{1\text{-}42}$ (Vilip-1/$A\beta_{1\text{-}42}$) levels has also been shown to predict the rate of cognitive decline in AD (Tarawneh et al., 2012). Second, an immunohistochemistry study looking at Vilip-1 in AD brain tissue also found a qualitative association of Vilip-1 with neuritic plaques in the neocortex (Braunewell et al., 2001a). Third, we have shown using mRNA microarray analysis that VSNL1, the gene that encodes Vilip-1 protein, is co-expressed with amyloid precursor protein (APP) throughout normal aging (***Appendix B***) (Lin et al., 2015).

While collectively the above data is suggestive of a link between Aβ and Vilip-1, in this study we provide the first functional evaluation of this relationship, finding that Aβ does not drive Vilip-1 expression using two model systems. Our findings are consistent with our observation in ***Chapter 1.0*** that VILIP-1 levels did not correlate with soluble $A\beta_{1\text{-}42}$ or $A\beta_{1\text{-}40}$ levels within human brain tissue in the superior frontal gyrus. Unlike studies using human subjects, the current use of both in vivo and in vitro models has the advantage of focusing on the

impact of Aβ in isolation. For example, neither model is characterized by the other predominant AD neuropathology, neurofibrillary tangles (Kurt et al., 2003). Nor is the PSAPP mouse model characterized by prominent neuronal loss (Irizarry et al., 1997, Takeuchi et al., 2000). Finally neither model has been associated with any of the other frequent comorbid neuropathologies found in AD subjects, such as vascular lesions, Lewy bodies, and TAR DNA-binding protein 43 (TDP-43) aggregates.

One limitation of this study is that primary cortical cultures were only exposed to one 10 μM concentration of $A\beta_{1-42}$. We used this relatively high concentration of peptide to ensure that we would have robust biological effects (as confirmed in our evaluation of neuronal death, see ***Chapter 3.0***). While the $A\beta_{1-42}$ isoform is widely considered the most toxic Aβ species (Klein et al., 1999, Sanchez et al., 2011, Pauwels et al., 2012) and we used a primarily dimeric preparation with some higher molecular weight species that are known to induce pathological changes in culture (Shankar et al., 2008, O'Nuallain et al., 2010), it is unknown whether lower concentrations of $A\beta_{1-42}$ would elicit a different response in Vilip-1 expression.

Another potential study limitation is the age at which PSAPP and wild-type mice were examined using LC-SRM/MS. While we have demonstrated that these animals have a clear elevation in APP expression at 6 months (Figure 3.1), it is possible that Vilip-1 levels could be altered at a later time point (e.g. 12 months) due to greater amyloid load. However, this seems an unlikely scenario given that neuronal cultures exposed to high levels of Aβ did not differ significantly from untreated neurons.

While Aβ does not appear to drive increased Vilip-1 expression, this does not exclude Vilip-1 from being engaged by Aβ-induced molecular alterations that ultimately result in neuronal death. As shown in ***Chapter 1.0*** in human brain tissue, decreases in Vilip-1 are present

in regions with prominent neuronal loss. Further investigation into whether Vilip-1 actively participates in the process of Aβ-induced neuronal death will be addressed in ***Chapter 3.0***.

4.0 THE EFFECT OF VILIP-1 EXPRESSION ON AB-INDUCED NEURONAL DEATH

4.1 ABSTRACT

Through mechanisms that are not yet entirely clear, Aβ oligomers perturb neuronal Ca^{2+} homeostasis and initiate a cascade of pathological events in the cell that ultimately results in neuronal death. In ***Chapter 1.0***, we observed significantly reduced Vilip-1 levels in brain regions associated with significant neuronal loss. In this study, we investigated the effect of manipulating Vilip-1 levels on Aβ-induced neuronal death in primary cortical neuronal cultures using fluorescence microscopy. We found that the extent of Vilip-1 expression did not influence neuronal death, indicating that Vilip-1 unlikely mediates Aβ-induced neuronal loss.

4.2 INTRODUCTION

A substantial body of evidence exists supporting the theory that Aβ oligomers disrupt neuronal Ca^{2+} homeostasis. Several studies have demonstrated that exogenous exposure of cultured neurons to synthetic Aβ oligomers results in a sustained elevation in intracellular Ca^{2+} levels (Mattson et al., 1992, Guo et al., 1999, Demuro et al., 2005). Similarly, multiphoton imaging in

mouse models of Aβ overexpression has shown Ca^{2+} overload in neurites and dendritic spines as a function of amyloid plaque proximity (Kuchibhotla et al., 2008).

Importantly, dendritic spine loss, neuron death, and subsequent cognitive impairments in AD may arise from pathologic disruption of Ca^{2+} homeostasis by soluble Aβ. Previous in vivo and in vitro work has shown that Aβ-induced activation of Ca^{2+}-dependent phosphatase calcineurin is sufficient to induce dendritic spine loss and neurite dystrophy (Kuchibhotla et al., 2008, Wu et al., 2010). Additionally, application of exogenous Aβ to primary neuronal cultures has been shown to trigger Ca^{2+}-influx-induced apoptosis through generation of reactive oxygen species (Ekinci et al., 2000).

Neuronal Ca^{2+}-sensing (NCS) protein, visinin like protein 1 (Vilip-1) has previously been implicated as a potential mediator in neuronal death. As described in ***Chapter 1.0***, in AD, we observed significantly diminished levels of the protein within the entorhinal cortex, a brain region characterized by prominent neuronal loss. However, in a brain region with comparatively little neuronal loss, the superior frontal gyrus (SF), Vilip-1 levels were unaltered in the same subjects. Further evidence supporting an association of Vilip-1 and neuronal loss is that we saw similar reductions as observed in the ERC of AD subjects within the SF of frontotemporal lobar degeneration (FTLD) individuals, which is a region primarily effected by widespread neuronal loss.

In vitro studies have also provided evidence for a role of Vilip-1 in neuronal death. One previous report found that Vilip-1 overexpression in pheochromocytoma cells (PC12) lead to increased Ca^{2+}-mediated cell death (Schnurra et al., 2001). Additionally, overexpression of the highly homologous NCS family member hippocalcin has been shown to facilitate cell survival in

the face of a Ca^{2+} challenge, suggesting this family of NCS proteins could hold different functional roles in modulating cell death (Mercer et al., 2000).

In this study we used fluorescence microscopy to evaluate Aβ-induced neuronal death in primary cortical neuronal cultures that differ by extent of Vilip-1 expression. We found that Vilip-1 levels did not impact neuronal death, indicating that Vilip-1 is unlikely to play a role in Aβ-mediated neuronal death.

4.3 METHODS

4.3.1 VSNL1$^{tm1(KOMP)Vlcg}$ mouse model

Primary cortical culture experiments were carried out using heterozygous and wild-type newborn (P0) mice. Transgenic VSNL1tm1(KOMP)Vlcg were generated by the Knockout Mouse Program (KOMP) using embryonic stem cells provided by the International Knockout Mouse Consortium by inserting the ZEN-UB1 Velocigene cassette (beta-galactosidase coding sequence from E. coli LacZ gene) into the VSNL1 gene, deleting exon 2 spanning Chromosome 12:11,393,779-11,393,606. The construct was introduced into C57BL/6N-derived VGB6 embryonic stem cells and correctly targeted embryonic stem cells were injected into B6(Cg)-TyrC-2J/J blastocysts. The resulting chimeric males were bred to C57Bl/6NJ females. Homozygous knockout of the VSNL1 gene is embryonic lethal. Vilip-1 is expressed in the neocortex, among other brain regions, at postnatal day zero (http://www.informatics.jax.org). Heterozygous VSNL1tm1(KOMP)Vlcg are viable and fertile, demonstrating approximately

50% reduction in Vilip-1 protein levels (Figure 4.1). Heterozygous and wildtype P0 mice were generated by crossing heterozygous VSNL1tm1(KOMP)Vlcg male mice with C57BL/6NJ females. All studies were approved by the University of Pittsburgh Institutional Animal Care and Use Committee.

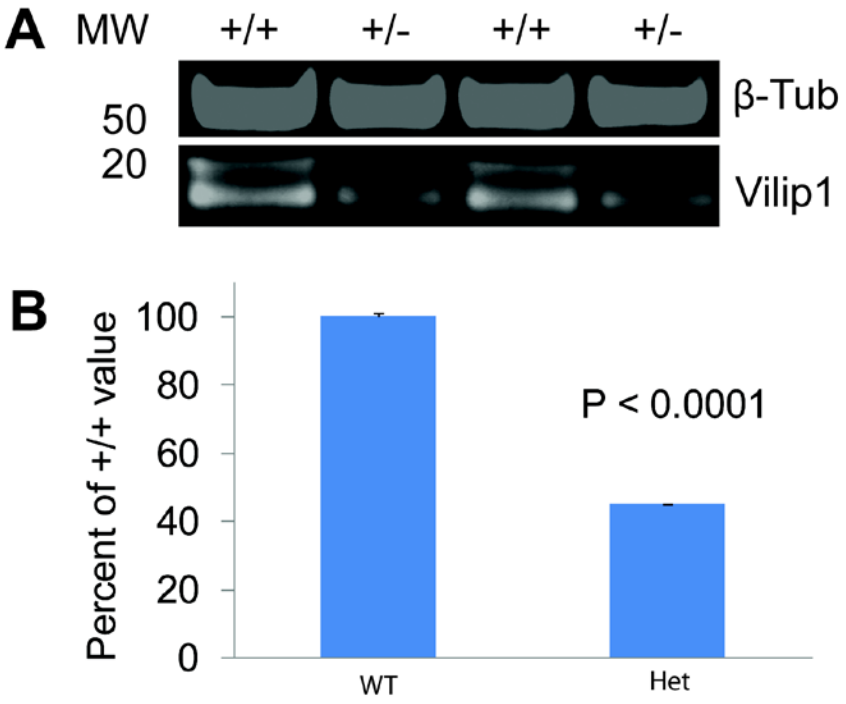

Figure 4.1 Vilip-1 levels in heterozygous and wild-type mice. (A). An example blot from the comparison of subjects with wild-type (+/+) and Vilip-1 heterozygous (+/-) mice (B) Quantification of wild-type (WT) and heterozygous (Het) Vilip-1 levels.

4.3.2 Cell culture

Primary neuronal cultures were generated as previously described (Beaudoin et al., 2012) with modifications. Mouse cortical neurons were prepared from newborn (P0) mice. Importantly, throughout the entire preparation, individual mouse brains were kept, processed, and plated separately to ensure that genotypes were not mixed. Tail samples for genotyping were collected

at the time of decapitation. Pups were euthanized by decapitation and heads were placed in dissection medium (1X Hank's Balanced Salt Solution (Ca^{2+} and Mg^{2+} free; Gibco; Catalog #: 14185), 100X sodium pyruvate (Sigma-Aldrich; Catalog #: P-2256), 20% glucose (Sigma-Aldrich; Catalog #: G-6152), 1 M HEPES (Sigma-Aldrich; Catalog #: H0887)). Skin on top of the head was gently dissected to expose the skull and using fine scissors, the skull was opened by making at incision at the base of the brain. The two halves of the skull were separated and removed exposing the brain. The brain was pinched off from the base in a scooping motion and transferred to a fresh dish of dissection media kept on ice. Under the dissecting scope, a sagittal cut was made down the midline of the brain, separating the two halves. The midbrain and thalamic tissues were then removed leaving the intact hemisphere containing the cortex and the hippocampus. Meninges were removed from each hemisphere by gently peeling them off and the hippocampus was dissected out from the neighboring cortical tissue with forceps. Using a pipette, cortical tissue was collected and placed in an Eppendorf tube with 500 µL of dissection media on ice. Following the competition of dissection of all brains, the tissue was resuspended in 500 µL of fresh dissection media and 50 µL of 2.5% trypsin solution (Gibco; Catalog #: 15090046) and incubated at 37°C in a water bath for 20 minutes. After 20 minutes, 20 µL of DNase was added and tissue was incubated at room temperature for 5 minutes. Following incubation, the media was aspirated and washed twice with 1 mL of dissection medium followed by two washes with temperature-equilibrated (37°C) plating medium (Minimum Essential Medium with Earle's salts (Gibco, Catalog #: 41090-036), 100 mM pyruvic acid (Sigma-Aldrich; Catalog #: P-2256), 20% glucose, 10% horse serum (Gibco; Catalog #: 26050-070)). Tissue was then carefully triturated between ten to fifteen times to dissociate cells. Cell numbers were estimated using exclusion of trypan blue (Sigma-Aldrich; Catalog #: T8154) staining and a

hemocytometer. In 60 mm dishes with five poly-d-lysine (PDL) coated glass coverslips (neuVitro; Catalog #: GG-18-pdl), neurons were plated at 100,000 cells/dish. Cortical neurons were maintained in Neurobasal Medium (Gibco; Catalog #: 21103-049), supplemented with 2% B27 Supplement (Gibco; Catalog #: 17504-44), penicillin/streptomycin (100 U/mL and 100 mg/mL, respectively; Gibco; Catalog #: 15145-014), and 2 mM glutamine (Sigma-Aldrich; Catalog #: G3126) with replacement of one half of the media in each dish every 3 days. Neurons were incubated at 37 °C, with 5% CO2.

4.3.3 Aβ Exposure

Human amyloid β-peptide (1-42) (1428; Tocris, Bristol, UK) is considered to be the predominant and most toxic Aβ-peptide species in Alzheimer disease patients. The $A\beta_{1-42}$ amino acid sequence is: DAEFRHDSGYEVHHQKLVFFAEDVGSNKGAIIGLMVGGVVIA. 100 μg of $A\beta_{1-42}$ was solubilized at 1 mg/mL in 50 mM Tris buffer (PH 7.0) creating a 221.5 μM $A\beta_{1-42}$ stock solution and vortexed vigorously for 1 minute. Next, 225.7 μL of solublized stock $A\beta_{1-42}$ was added to 1 mL of B27 maintenance media and vortexed again for 1 minute before adding the solution to the 4 mL of conditioned media present in the dish with the coverslips, bringing the final concentration to10 μM $A\beta_{1-42}$. Our $A\beta_{1-42}$ stock solution preparation was determined to be largely dimeric with some higher molecular weight oligomeric species (***Chapter 3.0***, Figure 3.3). Primary mouse cortical cultures (DIV 8 or 10) were incubated in $A\beta_{1-42}$ or media only for 24 hours. Directly following $A\beta_{1-42}$ exposure, primary cortical neurons were immersion-fixed in cold 4% paraformaldehyde for 20 minutes, and stored in HBSS at 4°C until immunohistochemistry.

4.3.4 Immunohistochemistry

Histochemical detection of apoptotic cell death in primary cortical neurons was accomplished with the In Situ Cell Death Detection Kit, Fluorescein (11684795910; Roche, Indianapolis, IN). This kit features the TUNEL reaction, which predominantly labels apoptotic-generated DNA strand breakage through the use of terminal deoxynucleotidyl transferase (TdT) that catalyzes the polymerization of labeled modified nucleotides to free DNA 3'-OH termini in a template-independent fashion. Cortical neurons were labeled with Guinea pig polyclonal anti-NeuN antibody (ABN90; Millipore, Temecula, CA), which recognizes the N-terminus of the DNA-binding, neuron-specific nuclear protein (NeuN).

Fixed cells were incubated in the In Situ Cell Death Detection Kit TUNEL reaction mixture for 60 minutes at 37 °C in the dark. Next cells were rinsed in Hank's Balanced Salt Solution (HBSS) and permeabilized with 0.2% Triton for 10 minutes. Cells were then incubated for 20 minutes in HBSS containing 2% normal goat serum, followed by a 45-minute incubation at room temperature in the dark in HBSS containing 1% normal goat serum and a 1:500 dilution of NeuN antibody. Cells were then incubated for 45 minutes at room temperature in the dark in HBSS containing 1% normal goat serum and a 1:500 dilution of goat anti-guinea pig secondary antibody conjugated to Alexa Fluor 568 (Invitrogen). Coverslips were mounted onto glass slides with Vectashield hardset (Vector Laboratories, Burlingame, CA).

4.3.5 Microscopy

Data acquisition was performed on an Olympus (Center Valley, PA) BX51 WI upright microscope equipped with an Olympus spinning disk confocal (SDCM) using an Olympus

PlanAPO N 10X 0.40 NA air objective. The SDCM was equipped with an ORCA-R2 camera (Hamamatsu, Bridgewater, NJ), MBF CX9000 front-mounted digital camera (MicroBrightField, Inc., Natick, MA), BioPrecision2 XYZ motorized stage with linear XYZ encoders (Ludl Electronic Products Ltd., Hawthorne, NY), excitation and emission filterwheels (Ludl Electronic Products Ltd.), and equipped with a Sedat Quad 89000 filter set (Chroma Technology Corp., Bellows Falls, VT). The microscope was controlled by Stereo Investigator (MicroBrightField, Inc) and SlideBook (Intelligent Imaging Innovations) software (MicroBrightField, Inc.) and samples were illuminated using a Lumen 220 metal halide lamp (Prior Scientific, Rockland, MA).

Using Stereo Investigator software, the glass coverslip was first outlined and a systematic random sampling grid was then randomly rotated and applied. Each two-dimensional image consisted of an image plane that was 512 X 512 pixels (~3,058 μm2). At each plane, data were collected using the following filters: excitation 490 ± 10 nm/emission 528 ±19 nm and excitation 555 ± 14 nm/emission 617 nm ± 37 nm. Exposure times were set at 1,000 milliseconds for both the TUNEL (488 nm), and NeuN (568 nm) channels.

4.3.6 Image processing

Intensity histograms for each channel were manually adjusted to the mode of the histogram for the low setting and a standard value for the high setting for each channel that was optimized for visualization. TUNEL-positive, NeuN-positive and objects positive for both TUNEL and NeuN (Tunel-NeuN-positive) were manually counted at each site (Figure 4.2).

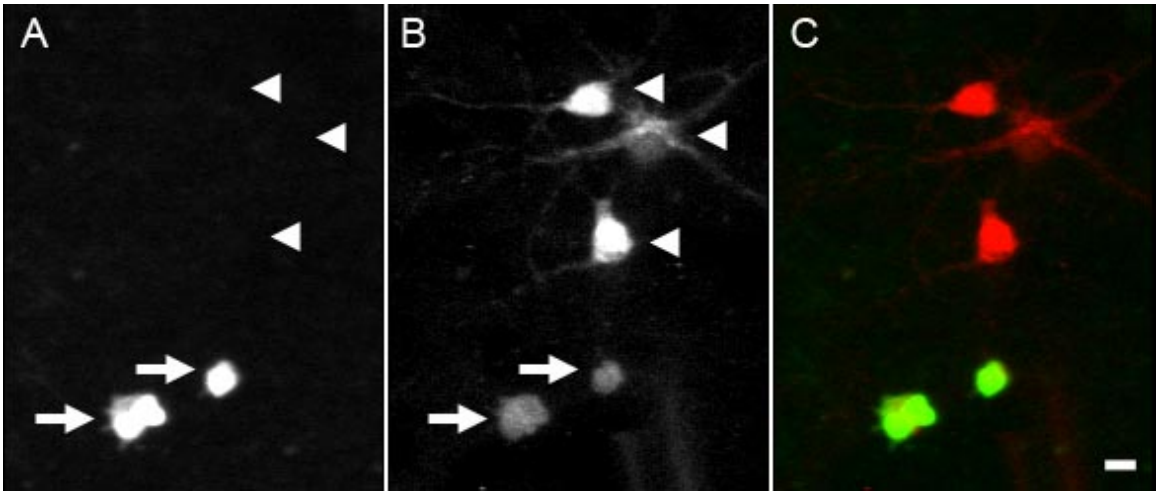

Figure 4.2 Primary cortical cultures labeled for TUNEL (A) and NeuN (B). Channels are merged in Panel C. Arrows represent TUNEL-NeuN-positive objects. Arrowheads represent NeuN cells that are TUNEL-negative. Scale bars represent 10 μm.

4.3.7 Statistical analysis

Apoptotic neuronal counts were normalized by taking the number of Tunel-NeuN-positive objects per site and dividing by the average number of NeuN objects per site within condition and experiment. Normalization helped account for varying total cell numbers across coverslips. Comparisons of normalized cell death counts between experimental conditions, genotypes, and the interaction between genotype and condition were made using two-way ANOVA.

4.4 RESULTS

4.4.1 Alterations in Vilip-1 heterozygous neuron death following Aβ exposure

In a comparison of Vilip-1 heterozygous neurons to wild-type neurons following $A\beta_{1-42}$ exposure, genotype did not significantly affect neuronal death ($p = 0.977$). $A\beta_{1-42}$ exposure in the wild-type group resulted in a 48% increase in cell death over the media control condition ($p = 0.005$). Heterozygous cells had a 60% increase in cell death after $A\beta_{1-42}$ exposure ($p = 0.001$) (Figure 2). There was no significant interaction of genotype x condition ($p = 0.700$).

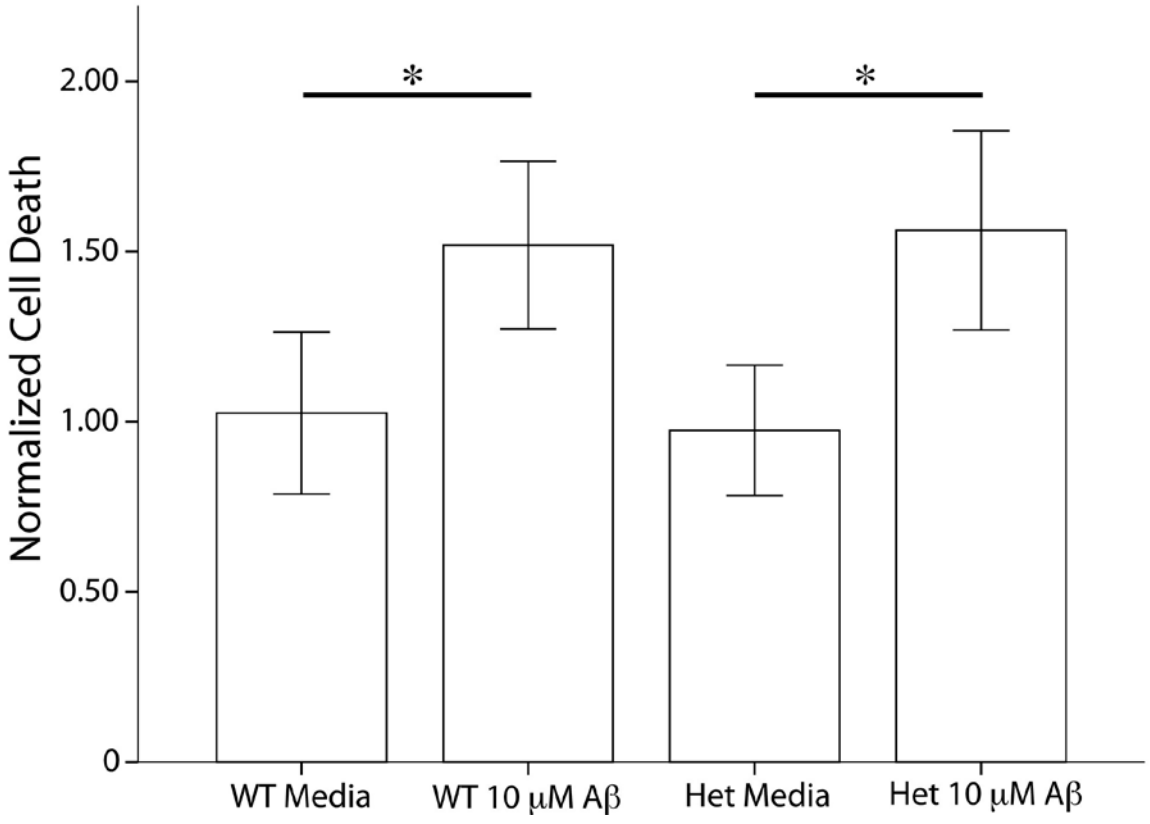

Figure 4.3 Normalized cell death counts across two independent experiments ([# of TUNEL-NeuN + objects per site/average # NeuN objects per site within condition and experiment]/average # of NeuN objects in the WT media

condition). WT Aβ and Vilip-1 Het Aβ conditions were not significantly different ($p = 0.819$). * $p < 0.05$. Bars indicate SEM.

4.5 DISCUSSION

In primary cortical cultures of Vilip-1 heterozygous and wild type mice, we found that reductions in Vilip-1 did not alter the amount of Aβ-induced neuronal death. This finding provides evidence that Vilip-1 is unlikely a mediator of Aβ-induced neuronal loss. Additionally, it suggests that lower levels of Vilip-1 may not be neuroprotective.

Previous work has revealed a potential role for Vilip-1 in cell death. As described in ***Chapter 1.0***, we observed reductions in Vilip-1 protein levels in disease within brains regions characterized by prominent neuronal loss: the entorhinal cortex (ERC) of AD subjects and in the superior frontal gyrus (SF) of frontotemporal lobar degeneration (FTLD). However, in a region with comparatively less neuronal death – the SF of AD subjects – Vilip-1 expression was unaltered, suggesting a potential link between the NCS protein and neuronal loss. In addition, a previous study has further suggested a more functional role for Vilip-1 in cell death showing that expression of Vilip-1 in PC12 increased sensitivity to Ca^{2+}-mediated cell death (Schnurra et al., 2001). Despite these potential connections to neuronal loss, our findings in primary cortical neuronal cultures that differ by extent of Vilip-1 expression show unaltered neuronal death levels, indicating that Vilip-1 unlikely plays a role in Aβ-mediated neuronal death.

A major factor contributing to discrepancy between our finding and the previous study is the use of different cell types. We used primary cortical neurons that naturally express Vilip-1 (Figure 4.1), whereas PC12 cells (a cell line derived from the rat adrenal gland) do not express

Vilip-1 and were transfected for analysis (Braunewell et al., 2001b). Thus, in our study we compared naturally occurring Vilip-1 levels to a reduction in heterozygous animals and the previous report by Schnurra and colleagues assessed overexpression of the protein in PC12 cells.

Additionally, in our study we directly tested Aβ-induced neuronal death and the prior PC12 cell report investigated cell death following Ca^{2+} challenge via the Ca^{2+} ionophore ionomycin. The extent of mechanistic overlap between these two cytotoxic challenges is currently unclear. While the particular manner by which Aβ oligomers perturb neuronal Ca^{2+} homeostasis and increase neurotoxicity is complex and still a matter of debate, there are a number of theories. Aβ oligomers have been shown to fuse with lipid bilayers creating annular structures that function as artificial pores or channels in the membrane, allowing for increased cation flux into the cell (Arispe et al., 1993). They also have been shown to induce membrane-associated oxidative stress leading to Ca^{2+} influx (Butterfield, 2002). Others have postulated that Aβ can stimulate the release of Ca^{2+} from internal stores through altering the sensitivity of inositol triphosphate receptor (IP3R) and ryanodine receptor (RyR) channels in the endoplasmic reticulum (Stutzmann et al., 2004, Bezprozvanny and Mattson, 2008). As for ionomycin, it is thought to act primarily through the release from internal calcium stores (Himmel et al., 1990, Morgan and Jacob, 1994). While it is widely accepted that Aβ does perturb Ca^{2+} homeostasis in neurons, a potential caveat is that we did not measure changes in Ca^{2+} following Aβ exposure. Different amounts of calcium may have impacted the apoptotic-pathway in the condition of reduced Vilip-1 levels.

As previously described in ***Chapter 2.0***, a limitation of this study is the single 10 μM concentration exposure of neurons to $A\beta_{1-42}$. At lower concentrations of Aβ, neuronal death levels in the heterozygous cultures may be altered due to reduced Vilip-1 and therefore we may

not be seeing an effect due to the high levels of toxicity in the cultures. In addition to Aβ concentration, the Aβ exposure time length could impact the neuronal death response. We selected a 24-hour Aβ exposure to ensure that we observed neuronal death but shorter or longer time frames may also impact the apoptotic process in the presence of reduced levels of Vilip-1.

Another possible caveat is the stage of neuronal death that we assessed. In this study we used the Terminal deoxynucleotidyl transferase dUTP nick end labeling (TUNEL) reaction that detects DNA fragmentation by labeling free DNA 3'-OH termini of nucleic acids to assess apoptosis. This assay measures late stages of apoptosis after extensive DNA degradation has occurred to the cell. However, use of an earlier apoptotic marker, such as caspase-3 would have provided more information about cells at risk for progression to apoptotic cell death. Previous work in culture has demonstrated that the caspase-3 apoptotic-pathway is activated by Aβ (Takuma et al., 2004). We attempted to label neurons with caspase-3, however the antibody failed to label cells even at high concentrations. Future work could focus on a different early apoptotic marker, such as YO-PRO-1 Iodide, a DNA marker for cells with a compromised plasma membrane.

A technical factor to keep in consideration is that our methodology of exogenously exposing rodent neuronal cultures to Aβ does not recapitulate all of the pathological aspects of AD. Mouse models of Aβ overexpression have demonstrated hyperphosphorylation of mouse tau but not aggregation into neurofibrillary tangles as human tau does in disease. Additionally, these mice do not exhibit neuronal loss (Games et al., 1995, Stancu et al., 2014). Also, other pathologies in addition to tau aggregation, such as Lewy bodies, are not present in these Aβ models. Thus, it is possible that Aβ-induced neuronal death in human brain engages additional pathways not assessed in this mouse neuronal culture system.

Accepting the caveats associated with the $A\beta_{1-42}$ exposure parameters and cell culture model discussed above, our findings suggest, in combination with evidence presented in ***Chapters 1.0*** and ***2.0***, that Vilip-1 is not an active participant in AD-related cell death, but rather a passive bystander that decreases in the brain as a consequence of neuronal loss. Furthermore, when considering the findings of increased CSF Vilip-1 in AD patients, that Vilip-1 is likely released upon neuronal death, accumulating in the CSF.

5.0 GENERAL DISCUSSION

5.1 5.1 SUMMARY OF FINDINGS

Alzheimer disease (AD) is a prevalent, progressive neurodegenerative disorder that is characterized clinically by declining memory, progressive loss of cognitive ability, and behavioral impairments that result from pathogenic protein accumulation, synapse impairment, and widespread neuronal loss that culminates in end-organ (brain) failure. The fundamental neurobiological mechanisms underlying neuron death in AD are not yet fully understood, however amassing evidence implicates soluble Aβ oligomers as a primary neurotoxic agent in AD. Aβ oligomers are thought to exact their detrimental effects on the brain by initiating a cascade of neurotoxic events involving neuronal Ca^{2+} dysregulation, synaptic impairment and dysfunction, loss of dendritic spines, tau phosphorylation and aggregation, and ultimately neuronal death. In addition to understanding the neurobiology behind AD, a research priority has been working on identifying AD biomarkers in order to accurately detect early pathologic processes in hopes of early intervention. Recently, Vilip-1 protein has been identified as a peripheral biomarker of AD and is predictive of the rate of cognitive decline. It is unknown to what extent Vilip-1 contributes to AD pathogenesis, particularly through Aβ-mediated pathways. The goal of this dissertation was to determine how Vilip-1 is altered in the AD brain and using *in vivo* and *in vitro* model systems, determine whether it is an active participant in Aβ-mediated

neuronal death or merely an innocent bystander in the process that ends up being discarded into the CSF. We demonstrated that Vilip-1 is reduced within brain regions characterized by prominent neuronal loss in both AD and frontotemporal lobar degeneration (FTLD) (***Chapter 2.0***). We reported that Vilip-1 expression is not driven by Aβ (***Chapter 3.0***). Finally, we examined Aβ-initiated neuron death in neurons with differing levels of Vilip-1 protein and found that neuron death was unaffected by the extent of Vilip-1 expression (***Chapter 4.0***). In the following sections, we will review the findings of the experimental chapters and discuss the broader implications for these Vilip-1 findings in AD. We will also address the caveats associated with model systems of AD and the experimental challenges associated with neuronal culture systems.

5.2 UTILITY OF VILIP-1 AS A PERIPHERAL AD BIOMARKER: DIFFERENTIAL ACCESS FOR MEDIAL TEMPORAL LOBE STRUCTURES

5.2.1 CSF regional proximity

As discussed in the General Introduction (***Chapter 1.0***), Vilip-1 has recently been identified as an AD-specific, prognostic, peripheral biomarker of cognitive decline and disease severity. CSF and plasma Vilip-1 levels are elevated in mild cognitive impairment and AD compared to normal control subjects (Lee et al., 2008, Tarawneh et al., 2011, Mroczko et al., 2015). In addition, higher CSF Vilip-1 concentrations correlate with reduced Mini Mental State Examination (MMSE) scores and are predictive of a more rapid deterioration in cognitive performance (Tarawneh et al., 2012, Fagan et al., 2014, Mroczko et al., 2015). Notably, a number of studies

indicates that Vilip-1 CSF concentrations are elevated as part of an AD-specific phenomenon, as other non-AD neurodegenerative disorders like Lewy Body dementia, progressive supranuclear palsy, and FTLD do not exhibit changes in CSF Vilip-1 compared to normal controls (Tarawneh et al., 2011, Luo et al., 2013). While AD demonstrates elevated CSF Vilip-1 concentrations, our findings indicate that Vilip-1 levels are reduced only in brain regions associated with prominent neuronal loss: the entorhinal cortex (ERC), but not the superior frontal gyrus (SF), in AD and the SF in FTLD. The disparity between CSF and postmortem brain tissue findings suggest that Vilip-1 released from ERC neurons upon neuronal death may have a more direct influence on the CSF compartment sampled by lumbar puncture compared to SF neurons.

While alterations in CSF fluid dynamics in AD are not fully understood, there are likely a number of contributing factors. First, proximity of the affected brain region to the ventricular system could impact protein diffusion and penetration into the CSF. In a dual neuroimaging-CSF study investigating how brain Aβ deposition is reflected in the CSF, researchers correlated tracer carbon-11-labeled Pittsburgh Compound B (PiB), which binds cerebral plaque and non-plaque amyloid deposits in the brain, with CSF $A\beta_{1\text{-}42}$ concentrations in 30 patients with probable AD. Grimmer and colleagues found that the relationship between CSF Aβ concentrations and amyloid load in the brain were strongest within brain regions surrounding the ventricles, suggesting that CSF protein levels may chiefly reflect pathology localized to brain regions in the vicinity of the ventricular system (Grimmer et al., 2009). Additional support of this idea comes from a study investigating region-specific uptake of CSF-administered radiocarbon labeled glutamate (^{14}C-glutamate) in rats. Results showed that the cerebral cortex had the lowest uptake of ^{14}C-glutamate as it is farthest from the CSF ventricular system (Al-Sarraf and Philip, 2003). Notably, this idea of access via proximity of the affected brain region to the ventricle is

consistent with the anatomy of our observed Vilip-1 reductions in brain regions with significant neuronal loss. The hippocampus, which is anatomically juxtaposed to the ERC, is located in the temporal cortex, medial to the inferior horn of the lateral ventricle. The hippocampal-CSF interface runs the entire length of lateral ventricle in each hemisphere of the brain, while the frontal cortex is located relatively far from the ventricular system (Johanson et al., 2005). In addition to proximity, MRI studies have demonstrated the breakdown of the ventricular lining in AD, rendering it more accessible to proteins in the local interstitium (Scheltens et al., 1995), which could include Vilip-1 released upon neuronal death in the ERC. The possibility of additional AD-specific mechanisms for ERC Vilip-1 penetration exists, however, based on the currently available data, both proximity and thinning of the ventricular lining provide the most parsimonious explanations for this phenomenon. Altogether, these data suggest that Vilip-1 may be a good marker of neuronal integrity for neurodegeneration in affected brain regions within close proximity to the ventricles, like the ERC in AD but not the SF in FTLD.

5.2.2 Plasma and blood brain barrier permeability

Vilip-1 levels are also increased in the plasma of AD patients compared to normal control subjects, which could be impacted by regional blood-brain barrier (BBB) vulnerability (Tarawneh et al., 2011). A number of factors have the ability to influence BBB integrity including aging and early stages of neurodegenerative disease. A recent MRI study looking at regional BBB breakdown during normal aging and mild cognitive impairment (MCI) found that BBB deterioration begins with the hippocampus in normal aging and worsens with MCI (Montagne et al., 2015). Additionally, integrity in cortical regions remains intact throughout both normal aging and MCI aging, demonstrating a regional disparity that is exacerbated with

cognitive decline (Montagne et al., 2015). This regional pattern for BBB integrity is consistent with the observed regional discrepancies between reduced Vilip-1 levels in regions associated with prominent neuronal loss (ERC in AD; SF in FTLD), but not other cortical regions in AD (SF), and AD Vilip-1 biomarker positivity in plasma. While the specific mechanisms underlying BBB vulnerability in AD are not fully understood, these studies demonstrate that regional differences exist within the capacity of the tissue to mediate BBB permeability changes, and present a possible mechanism for Vilip-1 plasma elevations observed in AD patients.

5.3 VILIP-1: POTENTIAL AS A NOVEL BIOLOGICAL INDICATOR OF NEURONAL INTEGRITY AND LOSS IN BRAIN TISSUE

At autopsy, AD patients show gross cortical atrophy, predominantly affecting the medial temporal lobes, while the primary motor, sensory, and visual cortices are left relatively intact (Serrano-Pozo et al., 2011). However, stereological studies have demonstrated that while there is significant neuronal loss at early to moderate stages of disease in medial temporal structures, like the hippocampus and entorhinal cortex, the extent of neuron loss in the neocortex is comparatively less robust (Regeur et al., 1994, Gomez-Isla et al., 1996).

In the ERC, we observed decreased levels of Vilip-1 in AD subjects compared to normal controls (***Chapter 2.0***). Consistent with this observation, microtubule-associated protein 2 (MAP2) levels were severely decreased in AD subjects compared to normal controls in this region. In the brain, MAP2 is a neuron-specific protein like Vilip-1 (Bernstein et al., 1999). MAP2 functions in microtubule stability and plasticity and is vulnerable to cytotoxic insults on the cell. Loss of MAP2 immunoreacitvity is considered an early indicator of neuronal damage

and has been shown to occur following neuronal insults such as ischemia, brain injury, and notably, Aβ exposure (Fifre et al., 2006). In the SF of AD subjects, Vilip-1 levels were unchanged compared to normal controls. MAP2 levels in the SF were decreased compared to normal controls, however the magnitude of reduction was considerably less than the measured loss in the ERC, consistent with stereological reports of limited neuron loss in the SF even at moderate stages of disease (Regeur et al., 1994).

Interestingly, Vilip-1 levels in FTLD subjects were significantly decreased compared to both AD and normal control subjects in the SF. In contrast to AD, FTLD is characterized by severe cerebral atrophy that is relatively selective for the frontal and anterior temporal lobes and that is accompanied by neuronal loss in these regions (Mackenzie et al., 2009, Rabinovici and Miller, 2010). In our study, FTLD subjects also showed substantially decreased MAP2 levels in the SF compared to normal controls. The magnitude of the reduction was similar to the level of reduction observed in the ERC of AD subjects and consistent with extensive neuronal loss in the SF in FTLD. Importantly, in the SF, FTLD subjects had significantly decreased Vilip-1 levels compared to AD subjects. Taken together, our data suggest that Vilip-1 levels coincide well with established patterns of neuronal loss in both AD and FTLD cases, making its potential as a biologic indicator of neuronal loss promising.

In addition to observed Vilip-1 elevation in the CSF of AD, Vilip-1 has also been shown to be elevated in the CSF of a rat model of stroke (Laterza et al., 2006, Stejskal et al., 2011). The rat model of stroke involves occluding the middle cerebral artery either temporarily or permanently, which results in massive neuronal injury (Longa et al., 1989). While CSF alterations in stroke patients have yet to be demonstrated, if ischemic damage is widespread enough, including areas located within the medial temporal lobe, it is unsurprising that Vilip-1

concentrations would increase in the CSF as observed in the rat model. Stroke findings further indicate a role for Vilip-1 in determining degree of neuronal integrity, both in CSF and brain tissue.

While the current gold standard for determination of unbiased estimates of neuron counts is design-based stereology, use of Vilip-1 as a biological indicator of neuronal integrity and loss in brain tissue may prove beneficial for several reasons. Stereology employs mathematical principles and systematic random sampling to provide estimates of the number of objects within a three-dimensional region of interest from two-dimensional information (Geuna and Herrera-Rincon, 2015). While the stereological approach provides highly accurate cell counts, there are limitations to this technique. Chiefly, the process of counting cells in human tissue sections is highly time consuming. Often immunohistochemical stains must be performed prior to the study to identify characteristic chemical profiles or cytoarchitectural features of the region of interest. In addition, if multiple brain regions are being considered, independent counting procedures must be performed for each individual region (Geuna and Herrera-Rincon, 2015, Herculano-Houzel et al., 2015). Other challenges such as tissue shrinkage, distinguishing between neurons and glia, appropriate sample size to ensure representative counts, and human error also factor into this technique. Identifying a novel, less labor-intensive marker, like Vilip-1 or perhaps an approach incorporating Vilip-1 and MAP2, for accurately measuring neuronal integrity and determining relative amounts of neuronal loss in brain tissue would be beneficial in human brain tissue studies, particularly in scenarios where constraints on tissue availability and equipment exist.

5.4 IMPLICATIONS FOR THE RELATIONSHIP OF VILIP-1 WITH AD PATHOLOGY AND PSYCHOSIS PHENOTYPE

In AD, soluble Aβ oligomers play a central etiological role in the pathogenesis of the disease. Widely considered the most toxic form of Aβ, soluble oligomers are hypothesized to initiate a pathological cascade of neurotoxic events involving Ca^{2+} dysregulation, synaptic disruption, and tau hyperphosphorylation and aggregation that culminate in neuron death. As described in ***Appendix B***, VSNL1 coexpresses with genes associated with AD throughout normal aging, in particular the amyloid APP gene, which encodes the transmembrane protein that is cleaved to form Aβ peptide (Lin et al., 2015). In addition to the association with APP, Vilip-1 has been shown to abnormally localize with neuritic plaques in AD brain tissue (Braunewell et al., 2001a). Given these associations, we hypothesized that Aβ-induced pathology drives Vilip-1 expression. In ***Chapter 2.0*** we investigated this hypothesis in two model systems: a transgenic mouse model of Aβ-overexpression and exogenous Aβ exposure in primary cortical neuronal cultures. Vilip-1 expression levels were unaltered in both systems by the presence of Aβ peptide. While these results suggest that Vilip-1 expression is not driven by Aβ, it does not exclude Vilip-1 from potentially having a role in other major AD pathophysiological processes, such as tau hyperphosphorylation and aggregation in a manner that could contribute in various ways to disease phenotype.

Notably, increased hyperphosphorylation of tau is a characteristic of a prevalent, heritable, and more severely progressive phenotype of AD, AD with psychosis (AD+P). Distinguished by the presence of hallucinations and delusions, AD+P occurs frequently, in upwards of 40% of AD cases. Familial aggregation is observed in AD+P with an estimated heritability of any occurrence of psychotic symptoms in AD of 30%, which increases to 61% for

multiple/recurrent symptoms (Bacanu et al., 2005). A substantial body of evidence indicates that the presence of psychotic symptoms in AD is linked to both greater cognitive impairment and more rapid cognitive decline (Ropacki and Jeste, 2005).

Although data on the link between Aβ pathology burden and AD+P are conflicting, studies have indicated a consistent connection between psychosis and increased indices of tau pathology in the neocortex (Murray et al., 2014b). For example, we recently reported on phosphorylated tau in the prefrontal cortex of 45 AD cases with and without psychosis using immunohistochemistry. Intraneuronal tau concentration was higher in AD+P subjects, while the extent of phosphorylated tau spread throughout the DLPFC was unchanged. In addition, phosphorylated tau concentrations correlated inversely with scores on the MMSE and the Digit Span Backwards test that evaluates executive function and depends in part on the DLPFC (Murray et al., 2014a). These findings suggest that tau phosphorylation may be accelerated in AD+P.

In conjunction with increased levels of hyperphosphorylated tau and decreased neuronal integrity attributed to AD+P, genetic studies evaluating putative psychosis risk genes in AD have identified an association of VILIP-1 with AD+P (Hollingworth et al., 2012). Qualitative immunohistochemistry data from human AD brain has also shown Vilip-1 immunoreactivity associates with extracellular tangles in the cortex (Braunewell et al., 2001a). Finally, Vilip-1-transfected PC12 cells exposed to an ionomycin Ca^{2+} challenge demonstrated an increase in tau phosphorylation, suggesting that Vilip-1 may enhance this process (Schnurra et al., 2001). As described in ***Chapter 2.0***, our data indicates that neither total tau levels nor phosphorylated tau levels were correlated with Vilip-1 in the SF of AD subjects. Additionally, history of psychosis was not significantly associated with SF Vilip-1 levels.

While our data suggest that it is unlikely that Vilip-1 is a critical component in further propagating disease related processes in either AD with or without psychosis, the possibility of an interaction between Vilip-1 and tau pathology needs to be further evaluated in alternative model systems. Neither the *in vitro* or B6.Cg-Tg(APPswe,PSEN1dE9)85Dbo/Mmjax (PSAPP) *in vivo* models used in this dissertation are ideal for the evaluation of tau pathology as they do not recapitulate all of the neurofibrillary tangle pathology observed in AD (detailed in ***Chapter 5.6 Methodological Considerations***). Thus examining a model with more complete tau pathology and manipulating Vilip-1 levels in an Aβ environment would provide additional insight into a potential role for Vilip-1 in the pathogenesis of AD. One example might involve knocking down Vilip-1 expression in neurons from transgenic mutant tau mice and exposing the cultures to soluble Aβ to determine if reducing the protein expression is protective against neuron death in a model involving both major neuropathological components associated with AD.

5.5 A ROLE FOR VILIP-1 IN AB-MEDIATED DISEASE PATHOLOGY?

5.5.1 Neuron death

Several lines of evidence support the amyloid cascade hypothesis in which Aβ oligomers initiate a set of events that perturb neuronal Ca^{2+} homeostasis and ultimately kill neurons. However, the full extent of neuropathological mechanisms engaged in the Aβ-mediated apoptotic process are not yet fully understood and remain a matter of investigation. Vilip-1, a neuronal calcium sensing protein, has previously been implicated as a potential mediator in neuronal death. Vilip-1

overexpression in PC12 cells has been shown to increase cell vulnerability to Ca^{2+}-mediated cell death (Schnurra et al., 2001). In contrast, another NCS family member, hippocalcin, which is highly homologous to Vilip-1, is neuroprotective against Ca^{2+}-mediated death in neural cell lines (Mercer et al., 2000). Together these data suggest that Vilip-1 may play a functional role in mediating Aβ-initiated neuronal death, specifically we hypothesized that downregulation of Vilip-1 expression would be neuroprotective against Aβ-mediated neuron death. Using primary cortical cultures of Vilip-1 heterozygous and wild type mice, we found that the extent of Vilip-1 expression did not influence neuronal death, indicating that Vilip-1 unlikely mediates Aβ-induced neuronal loss.

Further clarification of the complex cascade of events involving Aβ-induced apoptosis will provide additional insight into whether differential pathways of activation exist and if Vilip-1 potentially participates in a disease mechanism our experiment did not fully recapitulate. Currently, Aβ induction of apoptosis can occur through a number of hypothesized calcium dyshomeostasis mechanisms including artificial membrane pore formation (Arispe et al., 1993), oxidative stress buildup at the cell membrane (Butterfield, 2002), and altering internal calcium stores through endoplasmic reticulum channels (Stutzmann et al., 2004, Bezprozvanny and Mattson, 2008). This Ca^{2+} dysregulation is thought to lead to caspase activation, which can initiate an apoptosis cascade (Sharma and Rohrer, 2004, Tantral et al., 2004). However, the extent to which Aβ-induced caspase activation definitely leads to neuronal death, as opposed to primarily remodeling dendrites and spines, is currently debated (Hyman, 2011). While we were unsuccessful in our attempt to measure caspase-3 expression following Aβ treatment as described in ***Chapter 4.0***, understanding the response of more specific aspects involved in this

complex cascade of apoptotic events would identify additional pathways affected by altering Vilip-1 levels, albeit to an extent that does not result in a change in neuron death.

5.5.2 Synaptic Plasticity

While our current data suggest that Vilip-1 does not participate in the Aβ-mediated neuronal death cascade, this NCS protein may have a role in Aβ-synaptic plasticity changes. Vilip-1, like other NCS subfamily members, seems to be involved in modifying receptor recycling (Braunewell and Klein-Szanto, 2009). With a higher affinity for Ca^{2+} than calmodulin, Vilip-1 binds Ca^{2+} inducing a conformational change that exposes a hydrophobic myristoyl group allowing Vilip-1 to translocate and interact with cellular membranes and target proteins (Burgoyne and Weiss, 2001, Spilker and Braunewell, 2003). Specifically, Vilip-1 has been shown to interact with $\alpha_4\beta_2$ nicotinic acetylcholine receptors and several types of receptors involved in cyclic guanosine monophosphate (cGMP) signaling, modulating surface expression and function (Braunewell et al., 2001b, Lin et al., 2002, Braunewell and Klein-Szanto, 2009). Another NCS protein family member, hippocalcin, appears to modify receptor trafficking via GluR endocytosis and promote NMDAR-dependent LTD (LTD_{NMDAR}). Expression of a dominant negative hippocalcin that cannot detect Ca^{2+} occludes LTD (Palmer et al., 2005). Although the effects of VILIP-1 on GluR, NMDAR, and LTP/LTD are largely unknown, Vilip-1's highly homologous structure to hippocalcin suggests a role in a similar LTD_{NMDAR} mechanism. LTD mechanisms (in conjunction with LTP) are widely thought to mediate dendritic spine size and stability (Yang et al., 2008), and thus cognitive function (Kasai et al., 2010). However, quantitative Western blot data from our lab suggests that Vilip-1 may not play a prominent role in LTD_{NMDAR} mechanisms as reducing expression levels does not change

expression of key synaptic proteins. In particular, no significant alteration in the expression of synaptophysin, spinophilin, postsynaptic density protein 95(PSD-95), glutamate receptor 1 and 2 (GluR1, GluR2), N-methyl D-aspartate receptor subtypes 1 and 2B (NR1, NR2b), or glutamate decarboxylase 65 (GAD65) was observed between Vilip-1 heterozygous and wild-type mice (data not shown). Future studies examining spine loss in Vilip-1 heterozygous/PSAPP mice, or in primary neuronal culture derived from Vilip-1 heterozygous and wild type mice exposed to Aβ, would provide further insight into a potential role for Vilip-1 in pathologic synapse alterations.

5.6 METHODOLOGICAL CONSIDERATIONS

5.6.1 Mouse models of Aβ deposition

Many transgenic mouse lines model aspects of AD, but as with other complex psychiatric diseases, there is no one model that accurately recapitulates the neuropathology of the human disease in its entirety (Chin, 2011). However, the most widely used genetically engineered mouse models generate major neuropathological hallmarks of AD, like amyloid plaques and neurofibrillary tangles, and provide insight into mechanisms underlying the disease.

As described in ***Chapter 3.0***, we selected the PSAPP mouse model for our study investigating whether Aβ drives Vilip-1 expression. This double transgenic model expresses chimeric mouse/human amyloid precursor protein carrying two mutations linked to familial AD: the Swedish mutation (Mo/HuAPP695swe) and mutant human presenilin 1 (PSEN1dE9) (Hardy, 1997). The double transgenic increases the ratio of $A\beta_{1-42}$:$A\beta_{1-40}$ as compared to mice carrying

the APPswe mutation alone (Jankowsky et al., 2004). Both mutations are under the control of the mouse prion protein promoter, which results in primarily central nervous system transgene expression. At 4 months of age, the PSAPP mouse model presents with detectable Aβ deposits. By 12 months of age there is a global increase in levels of soluble and insoluble levels of two Aβ isoforms ($A\beta_{1-40}$ and $A\beta_{1-42}$), with $A\beta_{1-42}$ being the predominantly expressed Aβ species (Garcia-Alloza et al., 2006).

Aβ-based mouse models, like PSAPP, recapitulate many of the key features of AD including production of neurotoxic Aβ species and subsequent amyloid plaque deposition, synapse loss, tau phosphorylation, dystrophic neurites, reactive gliosis, and cognitive deficits. However, neurofibrillary tangles and neuron loss are notably absent (Kurt et al., 2003, Chin, 2011). While familial AD mutations involving APP and/or presenilin always develop into typical AD with amyloid plaques and neurofibrillary tangles, it is unknown why these same mutations expressed within mouse models fail to display a more complete set of neuropathological disease attributes, such as the presentation of detectable tangles.

Tau appears to be a critical component of the Aβ-initiated neurodegeneration cascade, as demonstrated by knockout studies. Complete removal of tau in neuronal cultures exposed to exogenous Aβ prevented characteristic neurite degeneration (Rapoport et al., 2002) and Aβ-induced impairment of long-term potentiation (LTP) (Shipton et al., 2011). In addition, reducing endogenous levels of tau in APP overexpressing transgenic mice prevented cognitive deficits (Roberson et al., 2007). However the extents to which neurofibrillary tangles and subsequent neuron loss play a role are not fully realized in models in which only mutant APP and/or presenilin are overexpressed. A few mouse models contain both amyloid and tau-related mutations, which can be useful for investigating the interaction between Aβ and tau. However,

since there are no known AD-specific tau mutations, these mice express familial tau mutations associated with FTLD (Gotz et al., 2007). Understanding the underlying mechanisms between Aβ-cascade initiation and tau aggregation through other model systems, like primary neuronal culture from transgenic mutant tau mice exposed to Aβ, may lead to new insights into how transgenic mouse models can more completely recapitulate the more complex nuances of AD neuropathology.

5.2.1 Challenges and strategies for neuronal culture and Aβ treatment

Over the past century, neuronal culture has advanced our fundamental understanding of nervous system function. Evolving from the hanging drop culture technique, which first demonstrated that cells could be maintained outside of the body, to better mimicking the brain and gaining precise spatiotemporal fluidic control by pioneering neuron growth in three-dimensional microenvironments, *in vitro* studies are pushing boundaries and providing new insight across all fields in neuroscience (Millet and Gillette, 2012). A variety of neuronal culture techniques are in use today, each with their own benefits and challenges. Disparities observed between different approaches can present certain challenges in reproducing results and reviewing data across laboratories and experiments. This section will discuss some of the strengths and limitations associated with the primary cortical neuronal culture methodology employed in this dissertation and the strategies used to overcome encountered challenges.

5.6.1.1 Variability associated with primary cortical neuronal cultures. The first major consideration in culture system selection is the type of cells being cultured. A number of options exist including neuronal cell line models, primary hippocampal and cortical neuronal cultures,

and hippocampal organotypic slice cultures, among others. We selected primary cortical cultures, a well-established system for investigating Aβ-induced neuronal toxicity. In addition, in AD with psychosis neuroimaging and postmortem studies have shown impairments associated with psychotic symptoms in neocortical regions (particularly in DLPFC), but not in hippocampus. Primary cortical cultures have several advantages over available immortalized neuronal cell lines. These include the natural production of Vilip-1, our protein of interest, and that they are not tumor derived, more accurately recapitulating *in vivo* neuronal properties. Additionally, they more accurately recapitulate the *in vivo* environment of the brain by providing a population of neurons that extend axons and dendrites, and create functional synapses between the cells. However, the lack of immortality limits the number of neurons obtained from each animal cortex.

Initially we employed the use of a bilaminar co-culture system consisting of primary cortical neurons and glia. This approach involves late embryonic stage neurons being plated on a glass coverslip, which are then inverted over a glial feeder cell layer (Shimizu et al., 2011). While this technique is ideal for examining cell morphology as it can sustain extremely low-density cultures, it is technically challenging. Individual paraffin feet must be crafted onto the coverslip and be of equal size to ensure even diffusion of glial survival factors across all cells on the coverslip and prevent coverslips from sliding on top of each other. Additionally, an issue arose with glial adherence to the tissue culture dish following inversion of neuronal coverslips, which was caused by switching the cells from glial maintenance media to neuronal media. Ultimately, we switched our approach to a more widely employed technique yielding more consistent results, that of primary cortical culture supplementation with B27 reagent.

B27 is a serum-free supplement that is designed to promote the growth and maintenance of low or high density mixed cortical neuronal cultures. While sufficient for the originally intended purpose of maintaining neurons, its proprietary formulation later presented unforeseen problems in attempts to measure protein release into the media. B27 inhibited the lactate dehydrogenase (LDH) cell death reaction that is used to measure the cytosolic enzyme upon release into the medium following cell membrane breakdown following apoptosis. LDH levels would have served as another neuronal integrity measure in conjunction with our neuron-specific nuclear protein (NeuN)/TUNEL cell counts. Additionally, future work investigating Vilip-1 protein release upon neuronal death via western blot or LC-SRM/MS is complicated as an unknown component of the B27 supplement reacts with the bicinchoninic acid assay used to measure protein concentration in a sample. To further pursue these avenues, new serum-free media supplements may need to be investigated.

While neuron-glia interactions in the central nervous system are important for normal function, presence of both cell-types in mixed cortical cultures presents some additional limitations in terms of cell discrimination. To circumvent this issue and ensure our neuronal death counts did not include glia, we developed an assay using NeuN antibody paired with TUNEL staining. NeuN has been vetted as a neuron-specific nuclear protein in vertebrates and is widely expressed across neuronal types with a few exceptions including cerebellar Purkinje cells, olfactory bulb mitral cells, and retinal photoreceptor cells (Mullen et al., 1992). However, these exceptions did not present an issue with the use of primary cortical cultures in our experiments.

Other methodological modifications we made to limit assay variability and improve neuronal survival included plating higher neuron densities, switching the cell attachment and adhesion substrate from poly-L-lysine, which can be digested by cells, to coverslips coated with

poly-D-lysine, and replacing L-glutamine with GlutaMAX, a reagent that is a stabilized form of L-glutamine that better withstands degradation and better supports the energy demands of cells.

5.6.1.2 Aβ. In addition to the variability associated with culture systems, a number of factors influence the design of an Aβ-treatment experiment. First, amyloid peptide application can either be exogenously applied or endogenously produced from overexpression of mutant APP. For exogenous application, synthetic Aβ forms are most commonly utilized, however naturally secreted peptides from human AD brains can be extracted. Aβ peptides exist in a number of conformations that produce varying levels of toxicity including: monomers, dimers, oligomers, or fibrils. Additionally Aβ exists in variety of lengths, with Aβ1-40, 1-42, 1-43, and 25-35 being the most commonly studied. Finally, Aβ fibrils may aggregate into plaques. *In vivo*, plaques may actually serve as reservoirs for Aβ oligomers in which there is a constant interconversion between nonfibrillar and fibrillar forms of Aβ in the plaque surround (Koffie et al., 2009, Kirkwood et al., 2013). The kinetics and structure of Aβ in culture can be difficult to discern, particularly after the peptide preparation goes into culture as these self-aggregating peptides are influenced by factors such as pH and temperature (Valerio et al., 2008, Zhang et al., 2013). Aβ concentration and exposure time length also factor into study design because exposing neurons to lower concentrations and/or shorter exposure times can exact more subtle effects on dendritic spines than higher concentrations and/or longer exposure times, which can result in neuron death.

We used a commercially available synthetic form of human $A\beta_{1\text{-}42}$, which is the predominant form of the peptide found in the human AD brain (Mann et al., 1996). As described in ***Chapter 3.0***, we demonstrated that we applied primarily dimeric and some higher molecular weight Aβ species to our culture system, which have shown to have significant toxic effects on

cells (Ono et al., 2009). Cultures were exposed for 24 hours to ensure induction of neuronal death.

Many factors impact the design of an Aβ-exposure culture experiment with the list including but not limited to: cell type, cell density, culture supplementation, Aβ type, Aβ concentration, and Aβ exposure duration. However despite the number of factors that can impact an experiment, as research continues to uncover more about how Aβ induces toxicity in AD, these variables can be honed into a more precise model.

5.7 CONCLUSIONS AND FUTURE DIRECTIONS

In summary, this dissertation begins to address the critical gap in knowledge associated with the role of Vilip-1 in AD. Identified as an AD-specific peripheral biomarker and further implicated in the disease process by genetic and immunohistochemical studies, to date evidence for a functional role of Vilip-1 in the pathogenesis of AD is limited. Studies conducted in this dissertation highlight two important points about the potential utility of Vilip-1 protein as a marker of neuronal integrity. First, Vilip-1 appears to be a general marker for neuronal loss in brain tissue instead of part of an AD-specific pathological process, however due to differential access to the CSF and plasma for structures in the medial temporal lobe, which are particularly affected in AD, it is a reliable biomarker for the disease in comparison to other neurodegenerative disorders that impact different brain regions. Second, Vilip-1 may have value as a marker for relative amounts of neuronal loss in human brain tissue, which would save resources and time in studies that require a general evaluation of the measure.

Future mechanistic *in vivo* and *in vitro* studies investigating the potential roles of Vilip-1 in other AD-associated neuropathologies such as tau hyperphosphorylation or its impact on other aspects of neurodegeneration, like synaptic plasticity and spine loss, will aid in the development of a more comprehensive picture of whether Vilip-1 plays a functional role in AD. Based on the findings in this dissertation Vilip-1 does not present as a promising therapeutic target for intervening in Aβ-mediated neuronal loss, however, it cannot be fully ruled out in the neuropathogenesis of AD until more extensive work evaluating multiple aspects of the disease is completed.

APPENDIX A

TITLE DENDRITIC SPINE DENSITY, MORPHOLOGY, AND FIBRILLAR ACTIN CONTENT SURROUNDING AMYLOID-B PLAQUES IN A MOUSE MODEL OF AMYLOID-B DEPOSITION

Caitlin M. Kirkwood, BSE,[1] Jennifer Ciuchta, BS,[1] Milos D. Ikonomovic, MD,[1,2,3] Kenneth N. Fish, PhD,[1] Eric E. Abrahamson, PhD,[2] Patrick S. Murray, PhD,[1,4] William E. Klunk, MD, PhD,[1,2] and Robert A. Sweet, MD[1,2,4]

[1] Translational Neuroscience Program, Department of Psychiatry, University of Pittsburgh School of Medicine, Pittsburgh, Pennsylvania [2] Department of Neurology, University of Pittsburgh School of Medicine, Pittsburgh, Pennsylvania [3] Geriatric Research, Education and Clinical Center, VA Pittsburgh Healthcare System, Pittsburgh, Pennsylvania [4] VISN 4 Mental Illness Research, Education and Clinical Center, VA Pittsburgh Healthcare System, Pittsburgh, Pennsylvania.

Send correspondence and reprint requests to: Robert A. Sweet, 3811 O'Hara Street, BST W1645, Pittsburgh, PA 15213. Phone: (412)383-8548; Fax: (412) 624-9910; Email: sweetra@upmc.edu

Note on my contributions to this paper: *I contributed to the study design, data collection, analysis, interpretation and writing of this manuscript.*

A.1 ABSTRACT

Dendritic spines are the site of the majority of excitatory synapses, the loss of which correlates with cognitive impairment in patients with Alzheimer disease. Substantial evidence indicates that amyloid-β (Aβ) peptide, either insoluble fibrillar Aβ deposited into plaques or soluble non-fibrillar Aβ species, can cause spine loss but the concurrent contributions of fibrillar Aβ and non-fibrillar Aβ to spine loss has not been previously assessed. We used multiple-label immunohistochemistry to measure spine density, size, and f-actin content surrounding plaques in the cerebral cortex in the PSAPP mouse model of Aβ deposition. Our approach allowed us to measure fibrillar Aβ plaque content and an index of non-fibrillar Aβ species concurrently. We found that spine density was reduced within 6 μm of the plaque perimeter, remaining spines were more compact, and f-actin content per spine was increased. Measures of fibrillar Aβ plaque content were associated with reduced spine density near plaques, whereas measures of non-fibrillar Aβ species were associated with reduced spine density and size, but not altered f-actin content. These findings suggest that strategies to preserve dendritic spines in AD patients may need to address both non-fibrillar and fibrillar forms of Aβ and that non-fibrillar Aβ may exert spine toxicity through pathways not mediated by depolymerization of f-actin.

A.2 INTRODUCTION

Alzheimer disease (AD) is the most common form of dementia and is characterized clinically by progressive loss of memory and cognitive function and progressive impairments in behavior. A number of neurodegenerative changes underlie these clinical manifestations. Two neuropathologic hallmarks of AD are extracellular amyloid plaques composed of amyloid-β (Aβ) peptide and intracellular neurofibrillary tangles, consisting of hyperphosphorylated microtubule-associated protein tau (Selkoe, 2004, Ballatore et al., 2007). Other pathologic changes include widespread cortical synapse loss, neuronal loss, and reactive gliosis (Ingelsson et al., 2004). Of these pathologic alterations, loss of synapses is the best structural correlate of cognitive impairments in AD (DeKosky and Scheff, 1990, Scheff et al., 2007). Genetic, in vitro, and in vivo studies have implicated soluble Aβ as a primary cause of the synapse loss in AD (Walsh and Selkoe, 2007).

In cerebral cortex, dendritic spines are the site of the majority of excitatory synapses. Substantial evidence indicates that progressive loss of dendritic spines in AD is due to effects of Aβ, either insoluble fibrillar Aβ deposited into amyloid plaques, or non-fibrillar Aβ species lacking amyloid structure, the latter including soluble oligomers and protofibrils (Walsh et al., 2005). In organotypic slice culture, both exogenous exposure to soluble Aβ and overexpression of endogenous Aβ by neurons dramatically reduce dendritic spine density (Hsieh et al., 2006, Shankar et al., 2007). Transcranial multiphoton imaging studies in transgenic mouse models of AD have shown that dendrites passing through or near fibrillar Aβ plaques undergo spine loss (Tsai et al., 2004, Spires et al., 2005). Transgenic mouse model studies have also revealed that fibrillar Aβ plaques are surrounded by a halo of oligomeric Aβ and have reported a loss of excitatory synapses within this halo region (Koffie et al., 2009). Confocal microscopy in the

PSAPP mouse model and in AD autopsy brain tissue has confirmed reduced densities of dendritic spines in proximity to fibrillar Aβ plaques (Grutzendler et al., 2007). While informative, these studies did not address the relative contributions to dendritic spine loss of fibrillar Aβ in plaques and concurrently measured non-fibrillar (soluble) Aβ species.

Current understanding of dendritic spine maintenance and elimination has focused mainly on the regulation of the spine f-actin network. Long-term potentiation (LTP) is a form of activity-dependent synaptic plasticity that is widely believed to be the cellular basis for learning and memory. Enlargement of single spines has been shown to be associated with LTP (Matsuzaki et al., 2004), and requires polymerization of g-actin into f-actin (Okamoto et al., 2004). Conversely, long-term depression (LTD), another form of activity-dependent plasticity, has been shown to induce dendritic spine shrinkage and elimination via f-actin depolymerization (Nagerl et al., 2004, Okamoto et al., 2004, Zhou et al., 2004). Studies conducted in rodent hippocampus have demonstrated that soluble Aβ oligomers can enhance LTD and inhibit LTP, suggesting that Aβ-induced spine loss engages mechanisms that reduce f-actin content in spines. (Wang et al., 2002, Shankar et al., 2008).

In the present study, we used a novel multiple-label immunohistochemical approach in the PSAPP transgenic mouse model of Aβ deposition to measure spine density, size, and f-actin content surrounding plaques in the cerebral cortex. In addition, our approach allowed us to concurrently measure fibrillar Aβ plaque content and an index of non-fibrillar Aβ species, examining their relationship to spine parameters. We found that dendritic spine density was reduced and remaining spines were more compact within 6 μm of the plaque perimeter, with a concomitant increase in f-actin content per spine. Measures of fibrillar Aβ plaque content were associated with reduced spine density near plaques, while measures of non-fibrillar Aβ species

were associated with reduced spine density, size, and shape complexity, but not with altered f-actin content.

A.3 MATERIALS AND METHODS

A.3.1 Transgenic Animals

Double transgenic PSAPP mice were generated by mating male APP Tg2576 (K670N/M671L) mice (Hsiao et al., 1996) (Taconic Farms, Germantown, NY) with female M146L PS1 mice (mutant PS1, line 6.2, University of South Florida) (Duff et al., 1996). The Tg 2576 mice were derived from a C57B6/SJL × C57B6 background; the M146L PS1 animals were derived from a Swiss-Webster/B6D2F1 × B6D2F1 background (Holcomb et al., 1998). Food and water were available ad libitum and a 12/12-hour light/dark cycle was maintained. All studies were approved by the University of Pittsburgh Institutional Animal Care and Use Committee. All mice were male to circumvent concerns about estrous cycling.

A.3.2 Tissue Preparation and Immunohistochemistry

PSAPP mice were anesthetized with isoflurane and perfused transcardially with phosphate buffer followed by cold 4% paraformaldehyde. Brains were removed, immersion-fixed in cold 4% paraformaldehyde for 24 hours and cryoprotected in a series of 15% and 30% sucrose solutions. Sections were cut coronally at 40 μm on a freezing sledge microtome and stored at −20°C in cryoprotectant solution (Watson et al., 1986). A single section was selected for analysis from

each of 4 12-week-old, 3 15-week-old, and 4 18-week-old mice, matched for rostral-caudal level using cytoarchitectonic features (~bregma −2.30 mm [(Paxinos G, 2004)]).

Histochemical staining of fibrillar Aβ plaques was performed using X-34, a highly fluorescent Congo red derivative, which binds peptides and proteins in fibrillar β-pleated sheet conformations ("amyloid") with a high affinity (Ikonomovic et al., 2006). Because immunoreactivity of fibrillar Aβ plaques to anti-Aβ antibodies is weak unless a formic acid pre-treatment is used to break up the fibrillar β-pleated sheet structure (Ikonomovic et al., 2006), we used 3 different antibodies, each in the absence of formic acid pre-treatment, to visualize non-fibrillar Aβ. The 6E10 antibody (biotinylated, SIG-39340; Covance, Emeryville, CA) is directed against the N-terminus of human Aβ peptide. The 4G8 antibody (biotinylated, SIG-39240, Covance) is directed against Aβ amino acids 17–24. Western blot analyses provide clear evidence that 6E10 and 4G8 are reactive with soluble monomeric and oligomeric species of Aβ (Kayed et al., 2010, Zempel et al., 2010). Because both of these antibodies may cross-react with the Aβ precursor protein (APP), we also used the anti-$A\beta_{x-40}$ antibody (AB5074P; Millipore, Temecula, CA), which is directed against the neo-epitope at amino acid 40 of the Aβ peptide and has human and mouse species reactivity. This antibody predominantly labels Aβ 1-40, and does not label longer Aβ forms (e.g. 1-42) or full-length APP (Kamal et al., 2001). Histochemical staining of dendritic spines was accomplished with the f-actin binding mushroom toxin phalloidin, conjugated to Alexa Fluor 568 (A12380; Invitrogen, Eugene, OR) (Capani et al., 2001). Although a direct, linear relationship specifically between phalloidin fluorescence intensity and f-actin concentration has not been firmly established, we have previously shown that detected fluorescence intensity is directly related to the intensity of fluorescent microspheres

embedded in thick sections, and can be used to measure protein concentration accurately (Sugiyama et al., 2005, Fish et al., 2008).

Free-floating tissue sections were incubated in 1% NaBH4 for 30 minutes followed by a 3-hour incubation at room temperature in phosphate buffered saline (PBS) containing 5% normal human serum, 5% goat serum, and 0.3% Triton X-100, and then incubated with PBS containing 5% normal human serum, 5% goat serum, and a 1:1000-dilution of biotinylated 6E10 antibody, a 1:1000 dilution of biotinylated 4G8 antibody, or a 1:100 dilution of anti-$A\beta_{x-40}$ antibody for 24 hours at 4°C. Next tissue sections were incubated for 24 hours at 4°C in PBS containing 5% normal human serum, 5% goat serum, phalloidin conjugated to Alexa Fluor 568 at a concentration of 1.5 μL/mL and either a 1:500 dilution of streptavidin conjugated to Alexa Fluor 488 (Invitrogen) or 1:500 goat anti-rabbit secondary antibody conjugated to Alexa Fluor 488 (Invitrogen). All tissue sections were then mounted on slides and after drying for 1 hour the sections were rehydrated for 5 minutes in PBS. Sections were incubated for 10 minutes in 100 μM stock solution of X-34, and then dipped in distilled water and incubated in 0.2% sodium hydroxide made in 80% unbuffered ethanol for 2 minutes; they were then soaked in distilled water for 10 minutes. Sections were coverslipped with Vectashield hard set (Vector Laboratories, Burlingame, CA). Final mean section thickness was 10.45 ± 4.409 μm (SD). Sections were processed and analyzed in 2 separate immunohistochemistry runs.

A.3.3 Microscopy

Data acquisition was performed on an Olympus (Center Valley, PA) BX51 WI upright microscope equipped with an Olympus spinning disk confocal (SDCM) using an Olympus

PlanAPO N 60X 1.42 N.A. oil immersion objective. The SDCM was equipped with an ORCA-R2 camera (Hamamatsu, Bridgewater, NJ), MBF CX9000 front mounted digital camera (MicroBrightField, Inc., Natick, MA), BioPrecision2 XYZ motorized stage with linear XYZ encoders (Ludl Electronic Products Ltd., Hawthorne, NY), excitation and emission filter wheels (Ludl Electronic Products Ltd), and equipped with a Sedat Quad 89000 filter set (Chroma Technology Corp., Bellows Falls, VT). The microscope was controlled by Stereo Investigator software (MicroBrightField, Inc.) and illuminated using a Lumen 220 metal halide lamp (Prior Scientific, Rockland, MA).

Using Stereo Investigator software, the cerebral cortex of each tissue section was first outlined and a systematic random sampling grid was then randomly rotated and applied to each tissue section (Figure, Supplemental Digital Content 1, http://links.lww.com/NEN/A474). At each site, defined by the intersection of the grid with the cortical gray matter, the investigator determined if a visible single plaque (defined by the presence of X-34-positive staining) was present within the 512 × 512 field of view at high power. When a single plaque was present it was then recentered in the field of view and, if it fit within the 512 × 512 pixels window of uniform fluorescence illumination, it was used for quantification, that is, an image stack was collected.

Each 3-dimensional image stack consisted of image planes of 512 × 512 pixels (~ 3058 μm^2) that were separated by 0.25 μm and acquired throughout the tissue section starting at the slide. At each plane, data were collected using the following filters: excitation 403 ± 6 nm/emission 457 ± 25 nm, excitation 490 ± 10) nm/emission 528 ± 19 nm, and excitation 555 ± 14 nm/emission 617 nm ± 37 nm. Exposure times (150 seconds, 1000 seconds, and 1100

seconds, respectively) were maintained for all experiments and there were no instances of pixel saturation in any stack.

A.3.4 Image Processing

To control for differences in background fluorescence intensity across animals, sections, and image stacks, the mode of the histogram was identified and subtracted. The choice of this approach reflected several considerations. First, because labeled objects of interest (i.e. dendritic spines) represent a minority of the voxels, the modal value is reflective of the background. Second, this approach is without the potential for operator bias. Third, non-specific background fluorescence is variable between sites and across samples (Luther et al., 2004), particularly in tissue sections.

Following background subtraction, the phalloidin channel was transformed to enhance automated detection of dendritic spines. Specifically, the final output was a subtraction of Gaussian filter channels of 2 different standard deviations of the Gaussian distribution s(σ) ([σ = 0.7] − [σ = 2.0]). Figure Supplemental Digital Content 2, http://links.lww.com/NEN/A475, demonstrates this concept with a 500-nm fluorescent bead. Data segmentation of the Gaussian filter transformation of the phalloidin channel to create binary mask objects was performed as previously described (Fish et al., 2008) except that threshold settings were evenly spaced (50 grey levels; Figure A.1.A). This approach provides for quantification of large numbers of phalloidin-labeled objects, with little contribution of non-specific fluorescent signal (Figure, Supplemental Digital Content 3, http://links.lww.com/NEN/A476). Image channels for non-fibrillar Aβ, fibrillar Aβ plaques and phalloidin, but not the Gaussian filter transformation channel, were deconvolved using the constrained iterative algorithm included in SlideBook 5.13.

After deconvolution, a region of interest containing the entire fibrillar Aβ plaque was manually defined and a threshold segmentation set at 50 grayscale units above background was applied to the X-34 channel intensity to generate a binary mask object of the plaque. Twelve contiguous 3-dimensional concentric shells were constructed around the outer edge of the fibrillar Aβ plaque (Figure A.1.B). Each shell was created using the mask dilation command in SlideBook, which allowed each shell mask, starting with the mask of the plaque, to be increased in radial size by exactly 2 μm from the prior mask. The prior mask was then subtracted from this larger mask to create each shell. The coordinates of the centroid for each phalloidin channel mask object were used to assign each mask object to a single shell, allowing for the analysis of dendritic spine density, morphology, and relative fluorescence intensity at known distances from the fibrillar Aβ plaque.

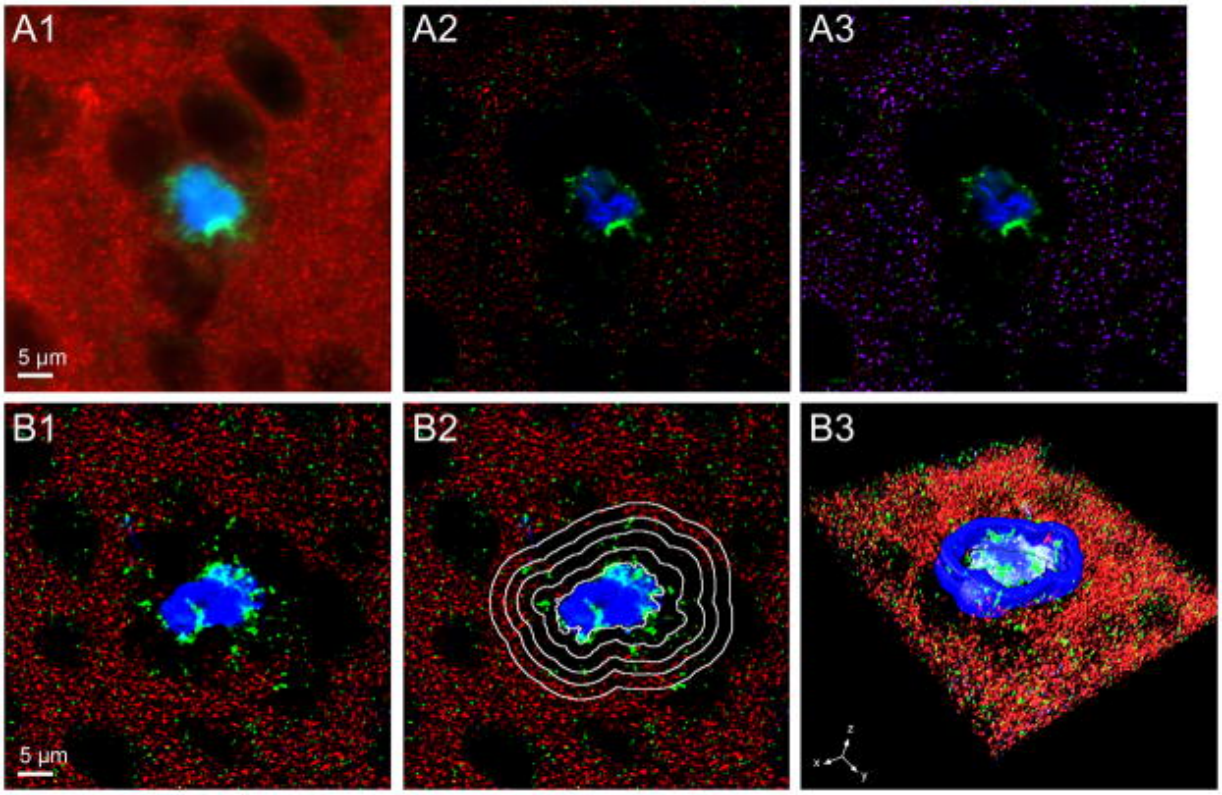

Figure A.1 Approach to image processing. (**A.1–A.3**) Image processing. Raw single plane image of dendritic spines labeled with phalloidin (red), amyloid-β (Aβ)-Immunoreactivity (green), and fibrillar Aβ plaque (blue) (**A.1**). The raw image was processed using the constrained iterative (CI) algorithm deconvolution for the Aβ-Immunoreactivity (green) and fibrillar Aβ plaque (blue) and the Gaussian filter transformation for dendritic spines (red). Dendritic spines are now clearly defined punctate structures and the amyloid and Aβ-Immunoreactive structures are refined (**A.2**). Generation of a binary mask (blue) using Iterative threshold segmentation of the Gaussian filter transformation (red) from the image seen in (**A.2**) shows the precision of dendritic spine coverage achieved using this processing technique. For extraction of relative fluorescence intensity within spines, the mask shown is overlayed on the CI deconvolved phalloidin channel (**A.3**). (**B.1–B.3**) Three-dimensional shells surrounding a plaque. A single plane from a CI deconvolved image with dendritic spines (red), Aβ-Immunoreactivity (green), and fibrillar Aβ plaque (blue) (**B.1**). Outline of the first 4 (of 12) shells used in the analysis; each is expanded by 2 µm from the edge of the fibrillar Aβ plaque overlayed on (A) (**B.2**). Three-dimensional surface rendering of lower half of the same image stack with a representative shell shown in dark blue (**B.3**).

A.3.5 Statistical Methods

Initial comparison of spine parameters as a function of distance (0 to 6 μm and greater than 6 μm) from the fibrillar Aβ plaque for the 134 measured plaques used linear mixed models with a first order autoregressive covariance structure. Subject level effects were animal, with repeated measures of plaque and shell. Fixed effects were fibrillar Aβ plaque volume, mean X-34 fluorescence intensity within the plaque, total non-fibrillar Aβ intensity within the shell, immunohistochemistry run, and (to control for any possible effects of the small difference in ages between mice) age group. For analysis of the impact of plaque and non-fibrillar Aβ effects on dendritic spine density, linear mixed models with a first order autoregressive covariance structure were used to analyze each concentric shell. Plaque was a repeated measure within animal, with fixed effects of fibrillar Aβ plaque volume, mean X-34 fluorescence intensity within the plaque, total non-fibrillar Aβ intensity within the shell, immunohistochemistry run, and age group. Spine density in each shell, i.e. at each distance from the plaque, was the dependent variable. Based on the results of the preceding linear mixed models, further analyses of spine density, morphology and total f-actin content per spine were conducted for shells within 0 to 6 μm of the plaque perimeter. These analyses used mixed models, with repeated measures within animals of plaque and shell, and fixed effects of fibrillar Aβ plaque volume, mean X-34 fluorescence intensity within the plaque, total non-fibrillar Aβ intensity within each shell, immunohistochemistry run, and age group. Additional models in which final section thickness was entered to evaluate whether section shrinkage during processing might have influenced the associations did not alter the results except where indicated. All intensity measurements used in the analyses were normalized across immunohistochemistry run to account for assay variability.

A.4 RESULTS

A.4.1 Detection of Aβ-Immunoreactivity Surrounding Fibrillar Aβ Plaques

Anti-Aβ antibodies 6E10, 4G8, and anti-$A\beta_{x-40}$ revealed a similar pattern of label concentrated in the immediate surrounding area of the X-34-positive fibrillar Aβ plaque (Figure A.2.A). Three-dimensional surface renderings also demonstrated accumulation of Aβ-immunoreactivity around X-34-positive fibrillar Aβ plaques (Figure A.2.B). Figure A.3 graphically depicts the distribution of 6E10 antibody label as a function of distance from the plaque with the highest Aβ-immunoreactivity located adjacent to the plaque.

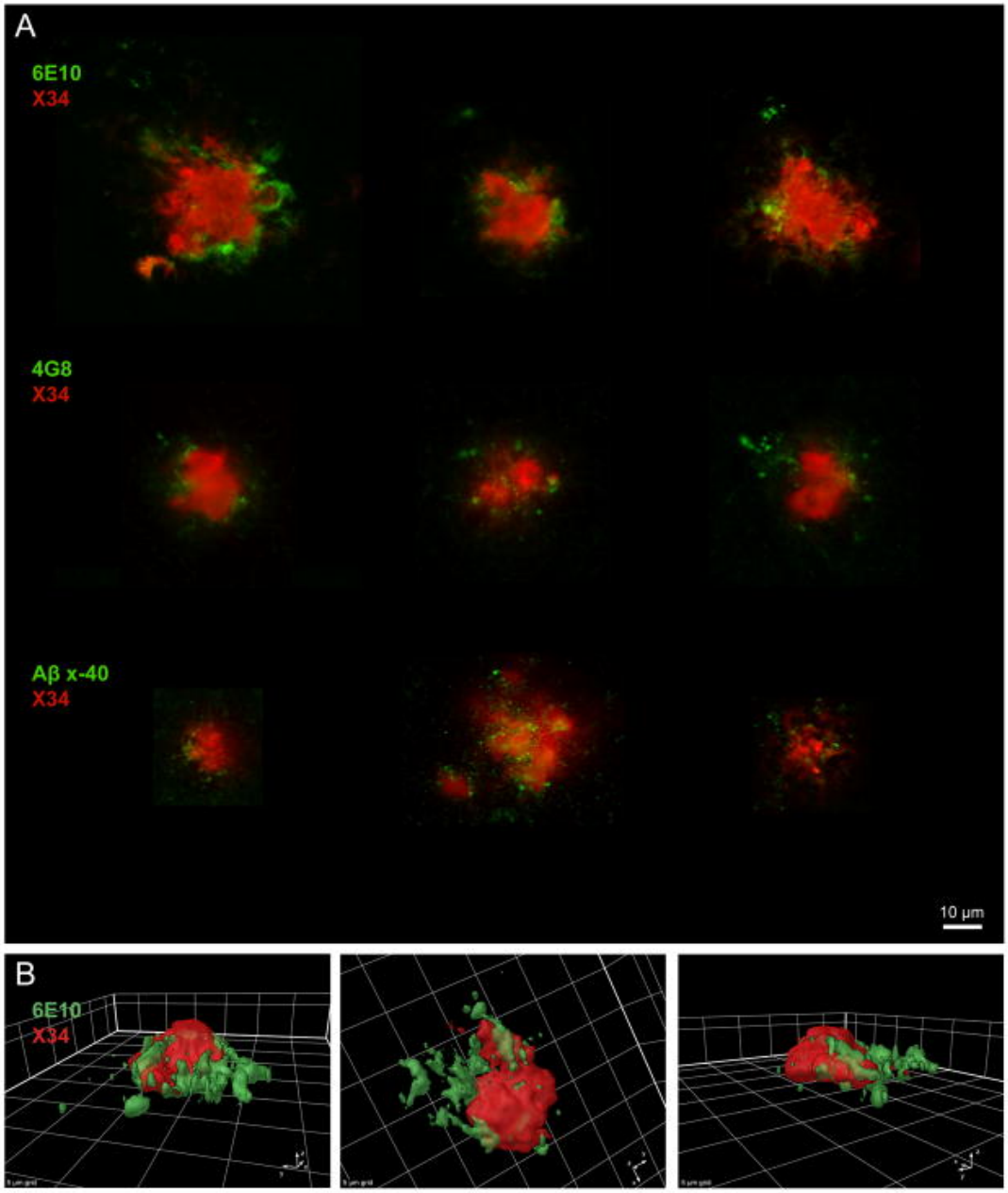

Figure A.2 Plaques dual-labeled with X-34 and anti- amyloid-β (Aβ) antibodies. (**A**) X-34 positive fibrillar Aβ plaques (red) and Aβ-Immunoreactivity detected with anti-Aβ antibodies (green). The antibodies, 6E10, 4G8, and anti-$A\beta_{x\text{-}40}$ label the N-terminus, amino acids 17–24, and the C-terminus neo-epitope of Aβ, respectively. Several examples shown for each antibody reveal a similar pattern of label external to the outside edge of the fibrillar Aβ plaque, and in the immediate surrounding areas. (**B**) Three-dimensional surface rendering of a plaque dual-labeled with X-34 and 6E10. The 3 rotated views illustrate the accumulation of Aβ-Immunoreactivity labeled with 6E10 (green) adjacent to and in the area surrounding an X-34-labeled fibrillar Aβ plaque (red).

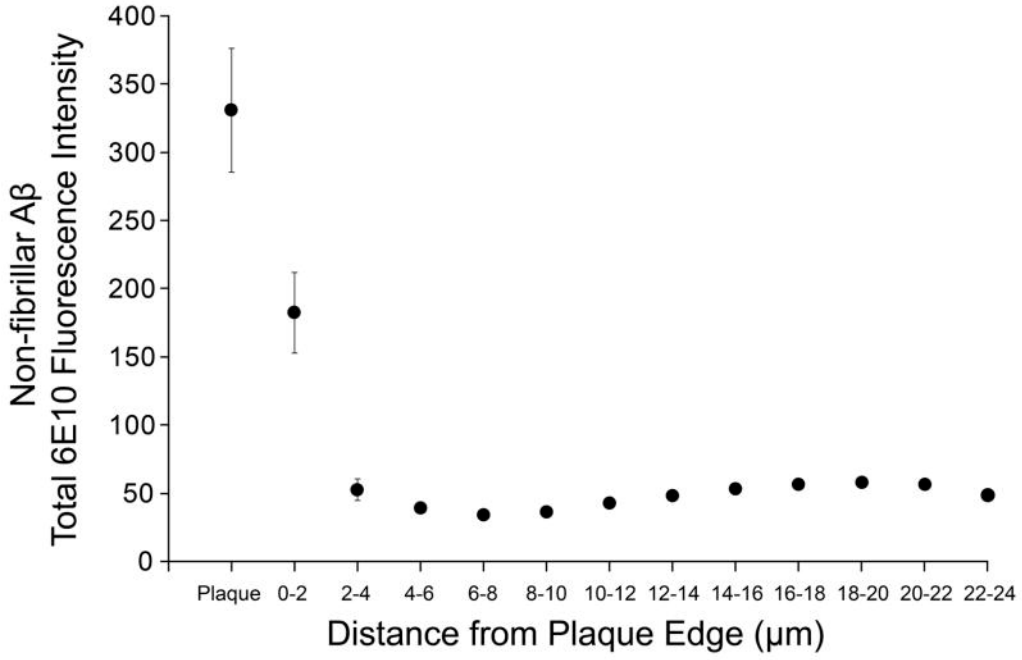

Figure A.3 Amyloid-β (Aβ) immunoreactivity (total 6E10 fluorescence intensity) within each 3-dimensional shell as a function of distance from the plaque. The means of 134 plaques analyzed are shown. The majority of the Aβ-Immunoreactivity is concentrated within the first few μm of the fibrillar Aβ plaque. Bars indicate SEM.

A.4.2 Spine Density, Spine Morphology, and Mean Phalloidin Fluorescence Intensity Per Spine Vary as a Function of Distance from Fibrillar Aβ Plaques

Decreased dendritic spine density around fibrillar Aβ plaques was qualitatively observed with near complete spine ablation in the area occupied by the X-34-positive fibrillar Aβ plaque (Figure, Supplemental Digital Content 4, http://links.lww.com/NEN/A477), with reduced spine densities apparent out to a distance of 6 μm from the perimeter of the plaque (Figure A.4). Quantitative analyses of a total of 830,634 spines in the PSAPP mouse cortex confirmed that spine density was lower within this 6-μm perimeter of the Aβ plaque (Figure A.4; Table A.1). In contrast, we analyzed spine densities in 16-week-old male C57BL6/J mice (Figure Supplemental

Digital Content 5, http://links.lww.com/NEN/A478). A phantom plaque was created in the middle of each image stack and 12 concentric shells were constructed as in the PSAPP mice and spine densities were calculated. There was no significant difference of spine density between any of the shells in the C57BL6/J mice.

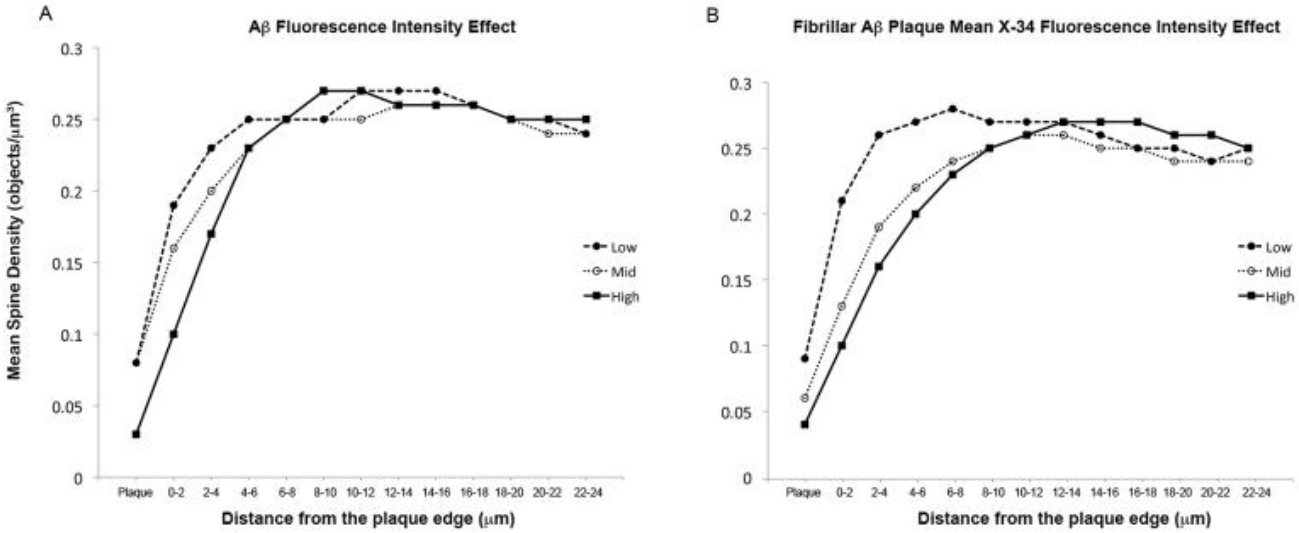

Figure A.4 Mean spine density as a function of distance from the plaque. (**A, B**) Aβ-Immunoreactivity fluorescence intensity (**A**) and fibrillar Aβ plaque mean X-34 fluorescence intensity (**B**) are shown separated into low (●), medium (O), and high (■) tertiles to demonstrate graphically the effects evaluated in Table 2.]

Table A.1 Summary of Dendritic Spine Characteristics as a Function of Distance from the Plaque (n = 134)

	Distance From Plaque			
	0–6 µm	6–24 µm		
Spine Parameter	n = 110119 Spines	n = 720515 spines	F (df)	p
Density, μm^{-3}				
Mean (SD)	0.161 (0.12)	0.2556 (0.10)	629.63	<0.001
Range	<0.01– 0.52	<0.01– 0.53	(1,1720)	
Volume, μm^3				
Mean (SD)	0.076 (0.03)	0.079 (0.03)	13.80	<0.001
Range	0.01–0.19	0.02– 0.20	(1,1492)	
Surface area, μm^2				
Mean (SD)	1.41 (0.44)	1.47 (0.44)	23.47	<0.001
Range	0.27–3.18	0.61–3.04	(1,1492)	
Shape complexity, $sphericity^{-1}$				
Mean (SD)	1.64 (0.09)	1.66 (0.08)	57.04	<0.001
Range	1.37– 2.02	1.46–1.89	(1,1508)	
Normalized total phalloidin intensity per spine, gray level				
Mean (SD)	29,443 (26,249)	24,287 (18,620)	25.08	<0.001
Range	68–279,006	1,832–223,278	(1,1558)	

In addition to reductions in spine density within the 6-µm perimeter of the Aβ plaque, spine volume was lower in this region and spine surface area was reduced, resulting in a reduction in spine shape complexity (Table 1). Despite these changes in spine morphology, there was no decrease in mean phalloidin intensity per spine. In fact there was a significant increase in these values within the 6-µm perimeter, indicating an increased concentration of f-actin within these spines.

A.4.3 Relationships of Spine Density, Spine Morphology, and Mean Phalloidin Fluorescence Intensity Per Spine with Fibrillar Aβ Plaque Volume, Aβ Plaque Mean X-34 Fluorescence Intensity, and Non-Fibrillar Aβ 6E10 Fluorescence Intensity

Linear mixed models showed that a decrease in spine density was independently associated with greater fibrillar Aβ plaque mean X-34 fluorescence intensity the first 6 µm from the plaque and with greater total Aβ-immunoreactivity (6E10 fluorescence intensity) within the first 2 µm of the

plaque edge (Table A.2; Figure A.4). No significant effect was seen due to fibrillar Aβ plaque volume.

Table A.2 Stepwise linear regressions of spine densities starting within the fibrillar Aβ plaque and extending to a distance of 24 μm from the plaque perimeter

Predictor Variable	Distance	β	T	p
Fibrillar Aβ plaque mean X-34 fluorescence intensity	Plaque	−0.029	−2.595	*0.011*
	0–2 μm	−0.051	−3.889	*<0.001*
	2–4 μm	−0.040	−3.349	*0.001*
	4–6 μm	−0.022	−2.162	*0.033*
	6–8 μm	−0.012	−1.308	0.194
	8–10 μm	−0.0002	−0.018	0.985
	10–12 μm	0.007	0.872	0.385
	12–14 μm	0.010	1.147	0.254
	14–16 μm	0.011	1.208	0.229
	16–18 μm	0.008	0.883	0.379
	18–20 μm	0.009	1.043	0.299
	20–22 μm	0.019	1.993	*0.049*
	22–24 μm	0.011	1.202	0.232
Aβ-immunoreactivity (6E10 fluorescence intensity)	Plaque	−0.005	−0.972	0.333
	0–2 μm	−0.017	−2.196	*0.030*
	2–4 μm	−0.020	−1.945	*0.054*
	4–6 μm	−0.009	−0.965	0.336
	6–8 μm	0.001	0.098	0.922
	8–10 μm	0.005	0.650	0.517
	10–12 μm	0.002	0.197	0.844
	12–14 μm	0.005	0.557	0.578
	14–16 μm	0.008	0.996	0.321
	16–18 μm	0.009	1.154	0.251
	18–20 μm	0.013	1.627	0.106
	20–22 μm	0.014	1.619	0.108
	22–24 μm	0.016	2.002	*0.047*
Fibrillar Aβ plaque volume	Plaque	$-5.546e^{-6}$	−0.678	0.499
	0–2 μm	$-7.589e^{-6}$	−0.748	0.456
	2–4 μm	$-4.450e^{-6}$	−0.469	0.640
	4–6 μm	$-5.987e^{-6}$	−0.746	0.457
	6–8 μm	$-4.120e^{-6}$	−0.570	0.570
	8–10 μm	$-3.875e^{-6}$	−0.571	0.569
	10–12 μm	$-1.388e^{-6}$	−0.202	0.840
	12–14 μm	$-1.838e^{-6}$	−0.262	0.794
	14–16 μm	$8.186e^{-7}$	0.119	0.905
	16–18 μm	$2.901e^{-6}$	0.409	0.683
	18–20 μm	$6.298e^{-6}$	0.921	0.359
	20–22 μm	$-6.737e^{-6}$	−0.912	0.364
	22–24 μm	$6.285e^{-6}$	0.981	0.329

Italics highlight $p < 0.05$.

Decreases in spine volume and surface area were significantly associated with non-fibrillar Aβ 6E10 fluorescence intensity within 6 μm of the fibrillar Aβ plaque edge (Table A.3). Interestingly, the relative amount of f-actin as indexed by phalloidin fluorescence intensity measured per spine did not change as a function of Aβ-immunoreactivity (Table A.3). There were no significant associations of fibrillar Aβ plaque mean X-34 fluorescence intensity with spine morphology or relative amount of f-actin.

Table A.3 Association of Spine Morphologic Measures with β-Amyloid and Plaque Features

Dependent Measure	Predictor Variable	F (df)	p
Spine volume, μm^3	Aβ-immunoreactivity (normalized total 6E10 fluorescence intensity)	9.313 (1,393)	*0.002*
	Fibrillar Aβ plaque volume	0.008 (1,363)	0.929
	Fibrillar Aβ plaque mean X-34 fluorescence intensity	1.527 (1,351)	0.217
Spine surface area, μm^2	Aβ-immunoreactivity (normalized total 6E10 fluorescence intensity)	8.643 (1,393)	*0.003*
	Fibrillar Aβ plaque volume	0.060 (1,356)	0.807
	Fibrillar Aβ plaque mean X-34 fluorescence intensity	1.284 (1,343)	0.258
Spine shape complexity, $sphericity^{-1}$	Aβ-immunoreactivity (normalized total 6E10 fluorescence intensity)	8.760 (1,378)	*0.003*
	Fibrillar Aβ plaque volume	1.895 (1,297)	0.170
	Fibrillar Aβ plaque mean X-34 fluorescence intensity	0.013 (1,273)	0.911
Total phalloidin/spine, gray level	Aβ-immunoreactivity (normalized total 6E10 fluorescence intensity)	0.340 (1,390)	0.560
	Fibrillar Aβ plaque volume	0.144 (1,373)	0.705
	Fibrillar Aβ plaque mean X-34 fluorescence intensity	0.648 (1,364)	0.421

Aβ, β-amyloid.

A.5 DISCUSSION

A.5.1 Spine Density and Morphology Alterations are Present Surrounding Fibrillar Aβ Plaques

We observed significant decreases in spine density within the first 6 μm beyond the perimeter of fibrillar Aβ plaque due to independent contributions of fibrillar Aβ plaque content and content of Aβ-immunoreactivity. A study by Spires et al utilizing 21- to 25-month-old Tg2576 mice similarly reported that distance from plaque perimeter correlates with deficits in spine density (Spires et al., 2005). In that study, plaque area (similar to plaque volume in the current report) was also not correlated with spine loss (Spires et al., 2005); however, the investigators found that the correlation between distance from the plaque and reduced spine density extended up to 20 μm. This discrepancy likely reflects the differences in mouse strain, in the ages and degree of plaque pathology of these animals, and/or differences in imaging methodologies between that and the current study.

In addition to reductions in spine density, we found decreases in surface area and shape complexity, and a trend towards decreased spine volume surrounding plaques. These findings suggest that spine physiology could be altered even before their disappearance. Soluble Aβ species have been shown to engage LTD and inhibit LTP pathways (Wang et al., 2002, Shankar et al., 2008), processes that typically leads to spine loss via spine f-actin depolymerization (Okamoto et al., 2004). It was therefore somewhat surprising that when investigating the relative amount of f-actin, as indexed by total phalloidin fluorescence measured per spine, we did not observe net reductions in spines close to plaques. In fact, we saw an increase in phalloidin total intensity within smaller, more spherical spines. Thus, the mechanism of spine morphology changes, at least initially, and does not appear to be through net depletion of f-actin, but through restructuring of the cytoarchitecture. Actin filaments in the spine head are very dynamic and there are several mechanisms by which actin polymerization and depolymerization are regulated to influence the spatial arrangement of f-actin in spines. For example Arp2/3 binds to existing actin filaments to nucleate new filaments and facilitate branching (Wilson et al., 2007). Another actin-regulating molecule, myosin II, binds and contracts actin filaments and is required for proper spine morphology (Korobova and Svitkina, 2010). Drebrin is an actin-binding protein localized in spines that is thought to inhibit the actin-myosin interaction and subsequently alter spine morphology (Hayashi et al., 1996). Still other proteins, such as cofilin, are responsible for proper spine head morphology, play an active role in actin dynamics (Bamburg and Bloom, 2009), and result in pathologic changes in actin in response to soluble Aβ (Davis et al., 2011). Thus, one or more of these molecular mechanisms may be acting to alter spine morphology in a manner independent of f-actin loss.

A.5.2 Relative Contributions of Fibrillar and Non-Fibrillar Aβ Species to Spine Alterations Surrounding Fibrillar Aβ Plaques

Previous in vitro studies with synthetic Aβ have reported that fibrillar Aβ forms, such as those found in Aβ plaques, are neurotoxic (Lorenzo and Yankner, 1994, Iversen et al., 1995). Other studies have implicated soluble Aβ as the primary contributor to synaptotoxicity (Lue et al., 1999, Walsh et al., 2002). Because both forms can exist in equilibrium there is some controversy regarding which is primarily responsible for pathologic effects (Zempel et al., 2010). We observed a halo of Aβ immunoreactivity in the immediate surround of the X-34 positive fibrillar Aβ plaque. We interpret this Aβ-immunoreactivity as an index enriched for the content of non-fibrillar soluble Aβ species in the plaque surround. This interpretation is based on several aspects of our approach and findings. Although the 3 antibodies used in the present study target different portions of the Aβ peptide (i.e. the N-terminus, mid portion, and C-terminus), they produced comparable patterns of Aβ immunoreactivity around the X-34 positive fibrillar Aβ plaque, which suggests that we are in fact labeling Aβ forms rather than full-length APP (which is not detected by anti-$A\beta_{x\text{-}40}$) or another related metabolic fragment. Second, there is clear evidence that at least antibodies 6E10 and 4G8 label non-fibrillar soluble species of Aβ (Kayed et al., 2010, Zempel et al., 2010). Third, soluble Aβ binds locally to synaptic structures (Koffie et al., 2009) and to various components of the extracellular matrix (Valle-Delgado et al., 2010), either of which would facilitate in situ fixation, although some non-fibrillar soluble Aβ would likely be lost by diffusion. Fourth, in the absence of formic acid pre-treatment, we saw little evidence of colocalization of anti-Aβ labeling with X-34 staining, the latter of which is highly selective for fibrillar, β-pleated sheet conformations (Ikonomovic et al., 2006). While some anti-Aβ binding

to fibrillar Aβ in plaques may still occur, our approach would have enriched the relative contribution of non-fibrillar Aβ species to the total measured Aβ-immunoreactivity. Fifth, we observed effects likely to reflect the toxicity of Aβ at distances up to 6 μm beyond the edge of the fibrillar Aβ plaque, consistent with diffusion of soluble species.

The interpretation that Aβ-immunoreactivity indexes non-fibrillar Aβ species is also consistent with the observed dissociation of Aβ-immunoreactivity and fibrillar Aβ plaque content with measures of spine morphology, in contrast to the finding that each is associated with spine loss. This dissociation suggests that fibrillar and non-fibrillar Aβ may lead to spine loss via distinct pathways. For example, dendrites passing through or in close proximity to fibrillar Aβ plaques demonstrate a number of abnormalities, including atrophy, tortuosity, varicosities, and local loss of spines in the affected segments (Spires et al., 2005, Grutzendler et al., 2007). Thus, fibrillar Aβ plaques may lead to spine loss via toxic effects on dendrites, perhaps via effects on tau, which accumulates in dendrites and can interfere with microtubule functions necessary for spine growth and maintenance (Gu and Zheng, 2009, Ittner and Gotz, 2011). In contrast, soluble Aβ species have been shown to bind directly to synaptic structures and may induce spine loss by altering post-synaptic signal transduction pathways (Shankar et al., 2008, Koffie et al., 2009).

A.5.3 Potential Limitations of this Study

Because fibrillar and non-fibrillar Aβ exist in equilibrium, there may be no in vivo (or in vitro) approach that can conclusively determine their independent effects when both are concurrently present. However, our data are consistent with a model in which Aβ fibrils in plaques are themselves toxic to spines, and serve as a reservoir for toxic soluble forms of non-fibrillar Aβ, with a concentration gradient that falls with distance from the plaque edge. Transgenic mouse

models aspire to capture some or all aspects of often uniquely human diseases, such as AD. The PSAPP mouse model demonstrates robust amyloid plaque deposition, well-characterized synaptic loss, and cognitive deficits that correlate with presence of oligomeric Aβ species (Urbanc et al., 2002), making it an excellent model to examine effects resulting from Aβ accumulation, a process that appears to correspond to the earliest stages of AD (Jack et al., 2011). However, the PSAPP model lacks the neurofibrillary tangle formation and neuronal loss that are seen as AD progresses (Urbanc et al., 2002). This discrepancy between the PSAPP model and human neuropathology enhance confidence in the interpretation that our findings are secondary to Aβ, but render uncertain whether the associations identified in the current study are ultimately present in humans. This could be addressed by extending our multiple wavelength imaging and quantification approach to human postmortem tissue but this application is not straightforward due to tissue autofluorescence and high plaque densities in AD tissue.

Another potential limitation to this study derives from our approach to spine imaging. We utilized phalloidin labeling to estimate spine volume, surface area and shape. Electron microscopy studies have shown that actin is the major cytoskeleton component in spines and plays a pivotal role in spine size and shape (Landis and Reese, 1983). Thus, phalloidin labeling presents a good overall estimate of spine shape and size; however, dendritic spines also contain other components, such as postsynaptic machinery and membrane bound organelles, that contribute to their shape and volume to some degree (Sheng and Hoogenraad, 2007). We imaged our sections via spinning disk confocal microscopy. This approach has several advantages relative to other fluorescent imaging methodologies for quantification in synaptic structures (Sweet et al., 2010). Nevertheless, our approach shares with other confocal techniques limitations in the z-axis resolution. While this limitation is mitigated by the Gaussian filter

transformation we applied during image processing, it may still have caused us to underestimate spine density by failing to discriminate spines closely apposed in the z-axis. Because we found reduced density of spines in the same region where spines were more compact, any such potential limitation would have biased against our detected effect rather than having contributed to it. Moreover, whereas alternate techniques such as array tomography may enhance z-axis resolution, they suffer from the same disadvantages for fluorescence intensity quantification (relative to spinning disk) as we have described for other laser scanning confocal techniques (Sweet et al., 2010).

Finally, our working assumption was that amyloid plaques are embedded randomly throughout all parenchymal structures, and thus sampled a large number of plaques. However, reduced spine density could be due to cell bodies around plaques if plaques preferentially form in areas of high cell body density.

A.5.4 Implications for AD

Accepting the caveats associated with the PSAPP model discussed above, our findings have significance for therapeutic strategies in AD. We found that dendritic spine degeneration and loss in cerebral cortex were independently associated with both fibrillar Aβ plaque content and with an index of non-fibrillar, presumptively soluble, Aβ species. These findings argue strongly that therapeutic strategies should consider targeting both forms of Aβ concurrently. Additionally, the novel findings that spine morphology was altered in relation to an index of non-fibrillar Aβ content, but not associated with reduced relative f-actin content per spine, suggests an effect of non-fibrillar Aβ on pathways that signal to actin-regulating molecules outside canonical LTD

pathways. The specific pathways remain to be elucidated and may represent novel targets for therapy of AD.

APPENDIX B

VSNL1 COEXPRESSION NETWORKS IN AGING INCLUDE CALCIUM SIGNALING, SYNAPTIC PLASTICITY, AND ALZHEIMER'S DISEASE PATHWAYS

Chien-Wei Lin,[1,†] Lun-Ching Chang,[1,†] George C. Tseng,[1] Caitlin M. Kirkwood,[2] Etienne L. Sibille,[2,3] and Robert A. Sweet[2,4,5,*]

[1]Department of Biostatistics, University of Pittsburgh, Pittsburgh, PA, USA [2]Department of Psychiatry, University of Pittsburgh, Pittsburgh, PA, USA [3]Campbell Family Mental Health Research Institute, Centre for Addiction and Mental Health (CAMH), Departments of Psychiatry and Pharmacology & Toxicology, University of Toronto, Toronto, ON, Canada [4]Department of Neurology, University of Pittsburgh, Pittsburgh, PA, USA [5] VISN 4 Mental Illness Research, Education and Clinical Center (MIRECC), VA Pittsburgh Healthcare System, Pittsburgh, PA, USA

Correspondence: Robert A. Sweet, Departments of Psychiatry and Neurology, University of Pittsburgh, Biomedical Science Tower, Room W-1645, 3811 O'Hara Street, Pittsburgh, PA 15213-2593, USA e-mail: sweetra@upmc.edu

Note on my contributions to this paper: *I contributed to data interpretation and helped with writing the manuscript.*

B.1 ABSTRACT

The visinin-like 1 (VSNL1) gene encodes visinin-like protein 1, a peripheral biomarker for Alzheimer disease (AD). Little is known, however, about normal VSNL1 expression in brain and the biologic networks in which it participates. Frontal cortex gray matter obtained from 209 subjects without neurodegenerative or psychiatric illness, ranging in age from 16 to 91, was processed on Affymetrix GeneChip 1.1 ST and Human SNP Array 6.0. VSNL1 expression was unaffected by age and sex, and not significantly associated with SNPs in cis or trans. VSNL1 was significantly co-expressed with genes in pathways for calcium signaling, AD, long-term potentiation, long-term depression, and trafficking of AMPA receptors. The association with AD was driven, in part, by correlation with amyloid precursor protein (APP) expression. These findings provide an unbiased link between VSNL1 and molecular mechanisms of AD, including pathways implicated in synaptic pathology in AD. Whether APP may drive increased VSNL1 expression, VSNL1 drives increased APP expression, or both are downstream of common pathogenic regulators will need to be evaluated in model systems.

B.2 INTRODUCTION

Alzheimer disease (AD) is the most prevalent form of dementia in the United States. It is characterized clinically by declining memory, progressive loss of cognitive ability, and behavioral changes. The incidence of AD increases rapidly with increasing age (Mayeux and Stern, 2012). This suggests a role of brain aging in risk for AD, although the basis of this age-dependence is not established. Neuropathologically, the hallmarks of AD are deposition of extracellular amyloid plaques that are predominantly composed of amyloid-β (Aβ) peptide and intracellular neurofibrillary tangles (NFTs) comprised of hyperphosphorylated microtubule-associated protein tau (Selkoe, 2004, Ballatore et al., 2007). Other pathologic changes include synapse and neuron loss, and reactive gliosis (Ingelsson et al., 2004).

Among these pathologies, the strongest correlate of cognitive impairment in individuals with AD is loss of synapses across neocortical regions (Terry et al., 1991, Scheff and Price, 2003), with excitatory synapses onto dendritic spines particularly affected (Baloyannis et al., 2007, Grutzendler et al., 2007). Substantial evidence now indicates that aggregation of Aβ into soluble oligomers is a primary source of synaptotoxicity in AD (Lue et al., 1999, Naslund et al., 2000, Selkoe, 2002, Walsh and Selkoe, 2007, Selkoe, 2008, Koffie et al., 2011). Although studies continue to elucidate how Aβ acts to eliminate dendritic spines, there is evidence that soluble Aβ inhibits mechanisms of long-term potentiation and/or engages mechanisms of long-term depression, including reducing NMDA receptor dependent Ca^{2+} influx, mGlutamate receptor (mGluR) activation, and low level caspase-3 activation (Selkoe, 2008, Koffie et al., 2011). The final common mechanism for these pathways converge on altered endocytotic recycling of GluR, resulting in reduced synaptic expression of GluR1 and GluR2 containing AMPA receptors and synaptic NMDA receptor (Hsieh et al., 2006).

Recently, several studies have identified visinin-like protein 1 (Vilip1), a protein encoded by the visinin-like 1 (VSNL1) gene, as a biomarker of AD. Vilip1 concentrations in cerebrospinal fluid and plasma are elevated in AD subjects relative to normal controls (Lee et al., 2008, Tarawneh et al., 2011) and to non-AD dementia subjects (Tarawneh et al., 2011). Higher levels of cerebrospinal fluid Vilip1 also predicted a faster rate of cognitive decline (Tarawneh et al., 2012). Other biomarkers for AD, such as cerebrospinal fluid measures of Aβ, tau, and phospho-tau (Jack et al., 2010), are strongly implicated in the pathogenesis of AD by genetic, post-mortem, animal model, and *in vitro* studies. To date, the evidence for Vilip1 is much more limited. We reported that genetic variations in VSNL1 were associated with risk for psychosis in AD (Hollingworth et al., 2012), a phenotype characterized by more rapid cognitive deterioration than seen in AD subjects without psychosis (Ropacki and Jeste, 2005, Murray et al., 2014b). Qualitative studies have reported that Vilip1 can be detected in association with neuritic plaques and NFTs in neocortex of AD subjects (Braunewell et al., 2001a), and may contribute to phosphorylation of tau and Ca^{2+}-mediated cell death (Schnurra et al., 2001).

Vilip1 is a highly brain expressed member of the visinin-like protein subfamily of neuronal calcium sensors (Burgoyne and Weiss, 2001). Vilip1, like other subfamily members appears to modify receptor recycling (Braunewell and Klein-Szanto, 2009). For example, the closely related subfamily member, hippocalcin, is necessary for NMDA receptor dependent long-term depression via GluR endocytosis (Palmer et al., 2005, Amici et al., 2009). Whether Vilip1 has effects on synaptic plasticity processes implicated in synapse loss in AD, such as GluR recycling, long-term potentiation, and long-term depression, is not known. However, Vilip1 has a higher affinity for Ca^{2+} than calmodulin, suggesting it may respond to the lower Ca^{2+} levels, which induce long-term depression (Burgoyne and Weiss, 2001).

The above findings are consistent with the hypothesis that VSNL1/Vilip1 may contribute to the risk for AD, possibly via age-dependent alterations in expression or by affecting processes that contribute to synapse or neuronal loss. To date, however, very little is known about normal VSNL1 expression in brain, whether it is modulated by genetic variation, and the brain-related biologic co-expression networks in which VSNL1 participates. To begin to address these questions, we assessed VSNL1 expression in two regions of frontal cortex obtained from 209 subjects spanning the adult age range, and without evidence of psychiatric or neurodegenerative illness. We found that VSNL1 expression was present throughout the adult life span and was unaffected by age, sex, and common genetic variants in cis and trans. VSNL1 co-expression networks included KEGG pathways for calcium signaling, AD, and pathways implicated in synaptic pathology in AD.

B.3 METHODS AND MATERIALS

B.3.1 Subjects

All of the brain specimens were collected during autopsies conducted at the Allegheny County Office of the Medical Examiner with permission obtained from the subjects' next-of-kin. The protocol used to obtain consent was approved by the University of Pittsburgh Institutional Review Board (IRB) and Committee for Oversight of Research Involving the Dead. An independent committee of experienced clinicians made consensus DSM-IV diagnoses for each subject, using information obtained from clinical records and structured interviews with surviving relatives. These procedures were IRB approved. Samples from a total of 212 subjects

without any DSM-IV diagnosis (i.e., including no diagnosis of a cognitive disorder) were obtained for use in this study.

B.3.2 Tissue Processing

Upon brain collection, ~2 cm coronal blocks from the right hemisphere were cut through the rostro-caudal extent of the brain and stored at −80°C. The RNA integrity (RIN) of each brain was assessed by chromatography (Agilent Bioanalyzer, Santa Clara, CA, USA). Samples were obtained from two prefrontal cortex (PFC) regions: Brodmann areas (BA) 11 and 47. These areas were selected based on prior findings showing robust age-related changes in gene expression that were highly correlated with other PFC regions (e.g., BA9) (Erraji-Benchekroun et al., 2005). Gray matter samples containing all six layers and excluding white matter were harvested from three to four consecutive 20 μm sections and stored in Trizol reagent.

B.3.3 RNA Arrays

Total RNA was extracted from frozen BA11 and BA47 samples stored in TRIZOL and were processed for microarray analysis using GeneChip Human Gene 1.1 ST from Affymetrix according to manufacturer's protocol (http://www.affymetrix.com). Gene expression data were extracted using Expression Console build 1.2.1.20. The normalization method is based on quantile normalization to eliminate batch effects. Data from arrays were processed by RMA method. Gene expression probes were processed at gene-level and taken in log2 scale for further analysis. After normalization, 33,297 gene-level probes remained. Three samples were removed

from study, one due to poor array quality, one due to outlier effect, and one due to XXY genotype, resulting in a final sample size of 209 subjects (Table B.1).

Table B.1 Demographic and technical characteristics of human subjects.

Variable	*N* (%) or mean (SD)
Age (years)	50.5 (14.6)
Range	16–91
Sex	
Male	166 (79)
Female	43 (21)
Race	
Caucasian	178 (85)
African-American	31 (15)
PMI	17.2 (5.9)
Range	4.8–37.5
pH	6.7 (0.3)
Range	5.8–7.6
RIN	8.0 (0.73)
Range	5.9–9.6

PMI, post-mortem interval; RIN, RNA integrity number.

B.3.4 Genotyping

DNA samples for 204 of the subjects were available, and processed on Affymetrix SNP 6.0 arrays, assessing genotype at 906,600 SNPs. Genotype calls were generated using Affymetrix Genotyping Console version 4.1.3. For intensity quality control (QC), we used Contrast QC,

which is the per sample QC test in the Affymetrix SNP 6.0 intensity array; two samples were removed after QC, leaving a final sample of 202 subjects for genotype measures. Birdseed v2 algorithm was used for genotyping, using the EM algorithm to drive a maximum likelihood fit of a two dimensional Gaussian mixture model.

B.3.5 Statistical Analysis

Age-dependent expression

Linear regression models were fitted to assess the association between VSNL1 expression level and demographic factors (age, sex, race). These models included as covariates the technical factors brain pH and RIN, as both were significantly associated with VSNL1 expression: $p = 7.21\text{e-}09$ (BA11) and 1.94e-04 (BA47) for pH association and $p = 3.66\text{e-}12$ (BA11) and 1.16e-08 (BA47) for RIN association. There was no significant association of VSNL1 expression with post-mortem interval (PMI, $p = 0.26$ and 0.36 in BA11 and BA47, respectively) and thus PMI was not included in the models.

eQTL mapping

eQTL analysis was performed in the 169 Caucasian subjects for whom genotype data were available. PCA analysis did not indicate population substructure within this cohort. All subjects had call rates >98%. SNPs were filtered out using the following criteria: (i) sample missing rate >10%, (ii) Minor allele frequency (MAF) <5%, and (iii) p value of Hardy–Weinberg equilibrium (HWE) test $<10^{-3}$. SNPs were defined as in cis if they were located within 50 kbp of VSNL1. All other SNPs were defined as in trans.

The eQTL model adjusted for age, pH, and RIN values (each was significantly associated with gene expression in both BA11 and BA47) since the effects of those covariates may confound eQTL findings. The eQTL model with three covariates for a given genotype was:

$$G_{ij} = \alpha_i + \gamma_i X_j + \sum_{k=1}^{3} \beta_{ik} S_{jk} + \epsilon_{ij}$$

in which: Gij: gene expression of gene i of subject j; αi: intercept term of gene i; γi: effect of the selected genotype to gene i based on additive model; Xj: genotype of subject i, 0 (homozygous major alleles), 1 (heterozygous calls), and 2 (homozygous minor alleles); βik: the effect of covariates k; k = 1 (age), 2 (pH), and 3 (RIN) in gene i; Sjk: the value of covariate k of subject j; k = 1 (age), 2 (pH), and 3 (RIN);

$$\epsilon_{ij} \sim N(0, 1)$$

We used the "Matrix eQTL" R package, a recent computationally efficient package for eQTL analysis (Shabalin, 2012), to detect the desired trans-eQTLs. We applied the adaptive weighted (AW) Fisher's method (Li and Tseng, 2011) for meta-analysis to combine eQTL *p*-values from two brain regions (BA11 and BA47). The AW Fisher's method has the advantage to distinguish study homogeneity and heterogeneity by assigning 0 or 1 study (brain region) weights for each eQTL. Detected eQTLs from the meta-analysis can have three possible resulting weights: (1,1) meaning detected eQTL in both brain regions; (1,0) showing detected eQTL in BA11 but not in BA47 and vice versa for (0,1) weight. In order to avoid heterogeneity of eQTL findings across brain regions, we selected only eQTLs that were identified in both brain regions with (1,1) weights in the AW Fisher's method.

B.3.6 Co-expression pathway analyses

To reveal the co-expression structure of VSNL1, we selected the top 400 positively and negatively correlated genes in both brain regions. The minimum observed correlation among the selected genes was 0.64, and the associated p-values suggest the corresponding false discovery rate (FDR) is <1e-04. Pathway analysis was performed via over representation analysis based on Fisher's exact test using pathway information retrieved from KEGG, BIOCARTA, and REACTOME databases. The Benjamini Hochberg procedure was used to control FDR for pathways (Benjamini and Hochberg, 1995).

B.4 RESULTS

B.4.1 VSNL1 expression

There were no significant associations of VSNL1 expression in either BA11 or BA47 with age, race, or gender (Figure B.1).

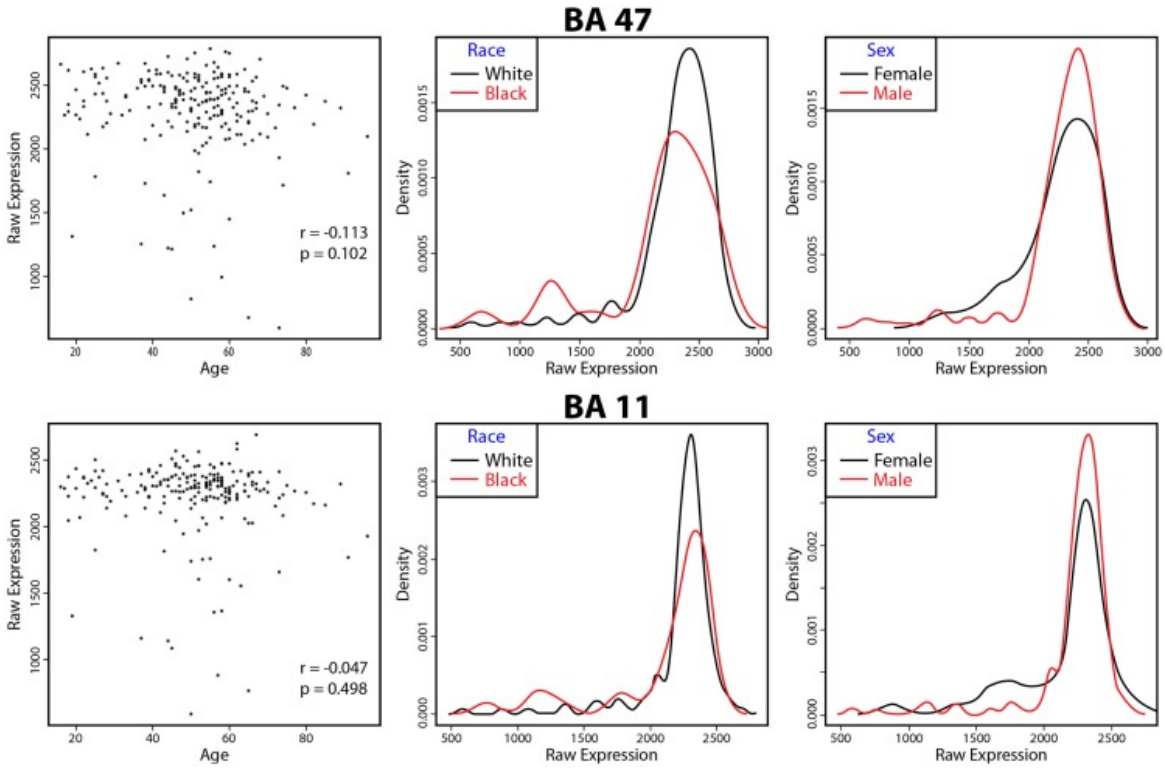

Figure B.1 VSNL1 expression as a function of age, race, and sex. The correlation of VSNL1 expression levels with age are shown in the first panels for each area. The second and third panels show the density of expression levels as a function of race and sex. No associations were significant. BA, Brodmann area.

B.4.2 VSNL1 eQTL analysis

There was no significant association of VSNL1 expression with 40 genotyped SNPs located in the cis-regulatory region (Table S1 in Supplementary Material). Examination of the association of VSNL1 expression with SNPs in trans revealed 27 SNPs with suggestive evidence of association ($p < 10-6$, Figure B.2; Table S2 in Supplementary Material). However, no SNPs reached the threshold for genome wide significance ($p < 10^{-8}$).

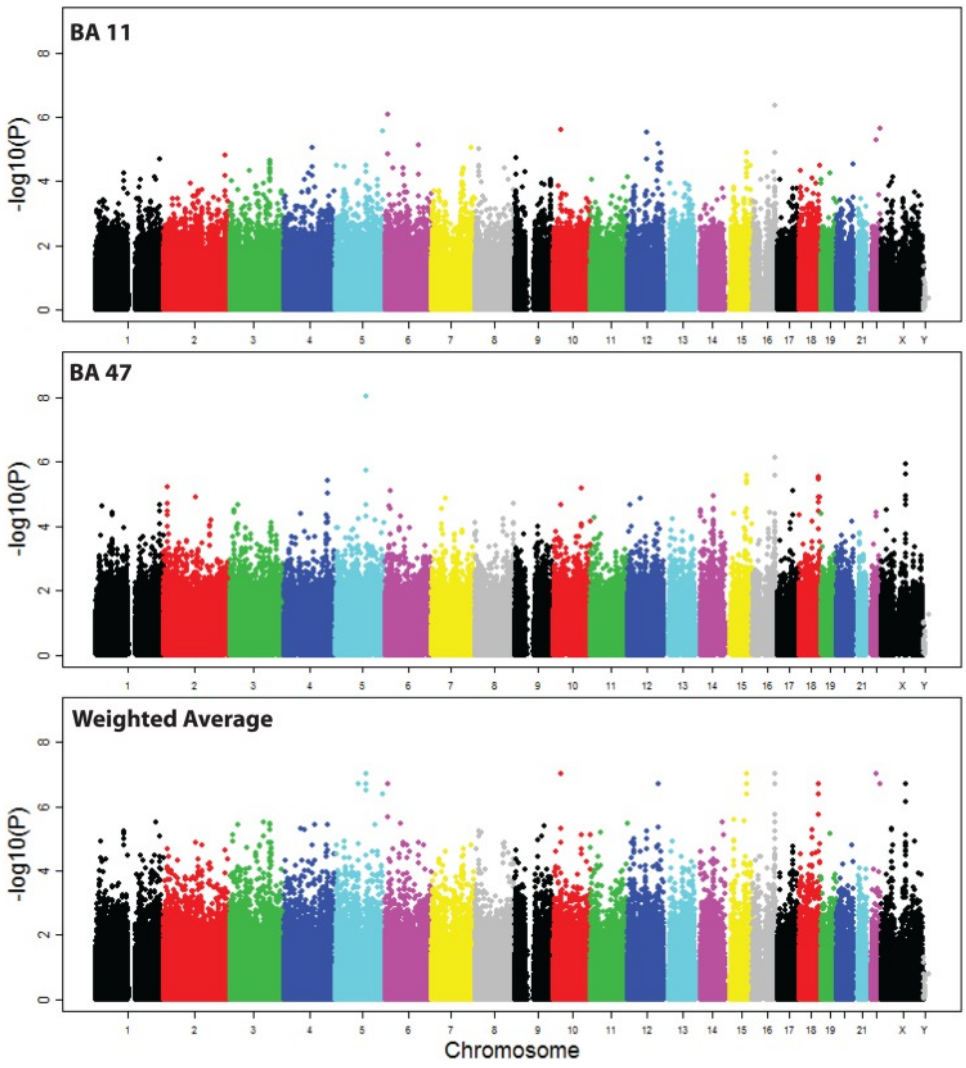

Figure B.2 Manhattan plot of SNP associations with VSNL1 expression. Associations are shown for each region, and for the weighted average of the two regions in the meta-analysis. BA, Brodmann area.

B.4.3 VSNL1 co-expression networks

We next evaluated VSNL1 co-expression. Although VSNL1 expression was itself not age dependent, many of its potential co-expression partners show age-dependent alterations in expression, including genes related to neurodegeneration (Erraji-Benchekroun et al., 2005, Glorioso et al., 2011). Therefore, we separately evaluated co-expression in subjects under and

over 50 years of age. The 400 genes with the greatest positive and negative correlations with VSNL1 expression in each age group are shown in Table S3 in Supplementary Material.

The KEGG, BIOCARTA, and REACTOME pathways showing the most significant loading for genes positively and negatively correlated with VSNL1 expression are shown in Tables B.2 and B.3, respectively (all pathways are shown in Table S4 in Supplementary Material). In subjects under 50, VSNL1 was positively correlated with genes in the KEGG pathway for AD and the BIOCARTA pathway for P35 signaling in AD (P35Alzheimers). The association with the KEGG pathway was driven by correlations with amyloid precursor protein (APP), ATP2A2, CALM1, CDK5, CHP, GSK3B, ITPR1, NDUFAB1, NDUFV2, PPP3CA, PPP3CB, and UQCRH. The association with the P35Alzheimers pathway was driven by three of the same genes (APP, CDK5, and GSK3B) as well as PPP2CA. In subjects over 50, the co-expression of VSNL1 with these AD pathways was weakened, with CDK5, CHP, and NDUFAB1 no longer among the top co-expressed genes.

Table B.2 Top pathways identified by genes showing positive correlations with VSNL1 expression.

Pathway	Age under 50			Age over 50		
	BA 47	BA 11	AVG	BA 47	BA 11	AVG
KEGG						
Aldosterone regulated sodium reabsorption	5.63E−03	5.00E−03	1.47E−05	9.00E−03	7.44E−03	1.96E−05
Alzheimers disease	1.20E−04	1.43E−03	1.47E−05	5.29E−03	6.55E−02	3.52E−04
Calcium signaling pathway	4.83E−04	1.08E−04	1.47E−05	1.10E−04	5.21E−03	1.96E−05
Cardiac muscle contraction	9.35E−04	6.19E−04	1.47E−05	8.94E−04	1.34E−03	1.96E−05
Epithelial cell signaling in *Helicobacter pylori* infection	1.96E−03	1.78E−05	1.47E−05	3.69E−04	2.02E−04	1.96E−05
Long-term potentiation	1.35E−03	1.04E−03	1.47E−05	2.92E−04	6.36E−03	1.96E−05
Oocyte meiosis	2.23E−04	9.68E−06	1.47E−05	2.76E−03	1.17E−03	1.96E−05
Oxidative phosphorylation	2.59E−04	1.59E−04	1.47E−05	7.01E−03	7.93E−03	1.96E−05
Proximal tubule bicarbonate reclamation	4.52E−03	3.60E−03	1.47E−05	5.72E−03	6.82E−03	1.96E−05
Vibrio cholerae infection	1.20E−04	2.10E−06	1.47E−05	8.76E−05	3.23E−06	1.96E−05
WNT signaling pathway	2.61E−03	1.70E−04	1.47E−05	2.88E−04	9.06E−03	1.96E−05
BIOCARTA						
AKAP centrosome pathway	1.19E−02	1.30E−02	2.58E−04	1.87E−03	1.67E−02	1.96E−05
CDC42RAC pathway	3.70E−03	2.56E−02	7.89E−05	4.59E−01	1.48E−01	1.13E−01
CHREBP2 pathway	1.17E−03	4.42E−03	1.47E−05	1.10E−03	1.64E−03	1.96E−05
CK1 pathway	5.35E−04	3.60E−03	1.47E−05	4.84E−04	3.06E−02	1.96E−05
CREB pathway	4.45E−03	4.35E−03	1.47E−05	5.62E−03	6.82E−03	1.96E−05
FCER1 pathway	7.74E−03	8.12E−03	2.74E−05	1.01E−02	1.27E−02	1.03E−04
GPCR pathway	1.20E−04	1.67E−03	1.47E−05	3.44E−04	1.27E−02	1.96E−05
HDAC pathway	3.18E−03	3.16E−03	1.47E−05	5.00E−04	4.19E−03	1.96E−05
MEF2D pathway	5.35E−04	2.56E−02	1.47E−05	3.20E−02	3.06E−02	8.39E−04
NDKDYNAMIN pathway	4.52E−03	5.83E−04	1.47E−05	3.73E−02	1.17E−03	1.96E−05
NFAT pathway	5.02E−04	1.74E−03	1.47E−05	1.88E−05	2.67E−03	1.96E−05
NOS1 pathway	3.92E−05	1.04E−03	1.47E−05	1.39E−04	1.80E−03	1.96E−05
P35Alzheimers pathway	5.30E−03	5.45E−03	1.47E−05	5.71E−02	5.43E−02	3.92E−03
PGC1A pathway	1.94E−03	1.74E−03	1.47E−05	4.36E−05	2.67E−03	1.96E−05
VIP pathway	4.04E−04	1.44E−02	1.47E−05	3.15E−03	1.78E−02	1.96E−05
REACTOME						
Acetylcholine neurotransmitter release cycle	2.67E−03	1.54E−04	1.47E−05	1.93E−04	4.13E−04	1.96E−05
DARPP32 events	3.92E−05	7.66E−05	1.47E−05	1.02E−04	1.17E−03	1.96E−05
Dopamine neurotransmitter release cycle	7.12E−03	3.91E−06	1.47E−05	8.76E−05	4.97E−06	1.96E−05
Formation of tubulin folding intermediates by CCT TRIC	1.94E−03	8.67E−03	1.47E−05	1.07E−02	1.19E−02	1.03E−04
Glucose regulation of insulin secretion	1.13E−03	6.15E−03	1.47E−05	9.88E−02	3.19E−01	4.45E−02
Glutamate neurotransmitter release cycle	2.31E−03	1.84E−04	1.47E−05	2.68E−04	4.37E−04	1.96E−05
Integration of energy metabolism	1.33E−04	3.60E−03	1.47E−05	2.34E−02	1.57E−01	4.65E−03
Neurotransmitter receptor binding and downstream transmission in the postsynaptic cell	1.94E−03	2.33E−05	1.47E−05	5.00E−04	2.67E−03	1.96E−05
Neurotransmitter release cycle	5.40E−03	9.68E−06	1.47E−05	1.02E−04	1.15E−05	1.96E−05
Norepinephrine neurotransmitter release cycle	3.89E−03	2.60E−04	1.47E−05	3.44E−04	5.25E−04	1.96E−05
Opioid signaling	1.13E−04	1.44E−04	1.47E−05	3.37E−06	1.30E−03	1.96E−05
PLC beta-mediated events	2.11E−03	4.30E−02	6.76E−05	3.44E−04	5.43E−02	1.96E−05

(Continued)

Pathway	Age under 50			Age over 50		
	BA 47	BA 11	AVG	BA 47	BA 11	AVG
PLC gamma1 signaling	4.39E−04	9.35E−03	1.47E−05	3.44E−04	1.27E−02	1.96E−05
Regulation of insulin secretion	2.74E−04	3.32E−03	1.47E−05	4.72E−03	9.62E−02	4.34E−04
Regulation of insulin secretion by acetylcholine	5.40E−03	5.66E−03	1.47E−05	1.02E−04	1.00E−02	1.96E−05
Regulation of insulin secretion by free fatty acids	3.70E−03	2.88E−03	1.47E−05	7.73E−05	6.82E−03	1.96E−05
Regulation of insulin secretion by glucagon like peptide 1	1.94E−03	6.08E−03	1.47E−05	9.99E−05	2.67E−03	1.96E−05
Regulation of ornithine decarboxylase	7.81E−04	1.38E−01	7.89E−05	1.51E−01	1.50E−02	2.74E−03
Serotonin neurotransmitter release cycle	7.12E−03	3.91E−06	1.47E−05	8.76E−05	4.97E−06	1.96E−05
Signaling by WNT	8.24E−04	1.00E−02	1.47E−05	4.25E−02	4.45E−03	1.03E−04
Signaling by NGF	2.25E−03	9.51E−04	1.47E−05	6.17E−03	1.41E−03	1.96E−05
Trafficking of AMPA receptors	3.27E−02	1.82E−04	1.47E−05	4.20E−02	2.30E−03	1.96E−05
Trafficking of GLUR2 containing AMPA receptors	1.07E−01	2.70E−04	2.74E−05	1.31E−01	4.56E−03	4.62E−04
Transmission across chemical synapses	5.94E−06	2.29E−11	1.47E−05	1.66E−08	1.53E−08	1.96E−05

Q values are shown for each region, and for the weighted average (AVG) of the two regions in the meta-analysis.
BA, Brodmann area.

Table B.3 Top pathways identified by genes showing negative correlations with VSNL1 expression.

Pathway	Age under 50			Age over 50		
	BA 47	BA 11	AVG	BA 47	BA 11	AVG
KEGG						
Allograft rejection	1.00E+00	1.00E+00	1.00E+00	1.38E−01	5.40E−01	3.37E−02
Autoimmune thyroid disease	1.00E+00	1.00E+00	1.00E+00	1.38E−01	5.40E−01	3.37E−02
Cell adhesion molecules CAMS	2.23E−01	8.54E−01	6.73E−02	4.19E−02	4.75E−01	2.78E−03
Cytokine–cytokine receptor interaction	2.23E−01	5.94E−01	4.17E−02	4.19E−02	1.68E−01	1.20E−03
Focal adhesion	6.69E−02	1.00E+00	3.85E−02	2.50E−01	1.00E+00	1.88E−01
Graft versus host disease	1.00E+00	1.00E+00	1.00E+00	1.38E−01	5.40E−01	3.37E−02
NOTCH signaling pathway	2.98E−01	1.00E+00	3.27E−01	1.38E−01	7.50E−01	4.69E−02
Pathways in cancer	8.23E−01	1.00E+00	4.25E−01	9.59E−02	6.10E−01	1.92E−02
Propanoate metabolism	3.54E−01	1.00E+00	4.30E−01	1.49E−01	4.75E−01	3.37E−02
Proximal tubule bicarbonate reclamation	1.83E−01	6.41E−01	3.85E−02	1.49E−01	2.43E−01	9.36E−03
Regulation of actin cytoskeleton	6.05E−02	8.29E−01	1.57E−02	3.32E−01	1.00E+00	2.25E−01
BIOCARTA						
MCALPAIN pathway	9.06E−02	1.00E+00	4.83E−02	1.91E−01	1.00E+00	1.61E−01
REACTOME						
Ethanol oxidation	1.00E+00	1.00E+00	1.00E+00	2.79E−01	4.19E−01	4.69E−02
GAP junction trafficking	1.59E−01	5.29E−01	1.57E−02	8.51E−01	5.35E−01	2.85E−01
Immunoregulatory interactions between a lymphoid and a non-lymphoid cell	3.51E−01	1.00E+00	2.02E−01	7.45E−02	4.67E−01	5.83E−03
Integrin cell surface interactions	9.06E−02	5.29E−01	1.00E−02	1.73E−01	9.45E−01	8.26E−02
NOTCH HLH transcription pathway	9.06E−02	1.00E+00	6.51E−02	2.78E−01	4.11E−01	4.48E−02

Q values are shown for each region, and for the weighted average (AVG) of the two regions in the meta-analysis.
BA, Brodmann area.

Other neuronal calcium sensor family members have been shown to mediate processes dependent on glutamate receptor trafficking, such as long-term potentiation and long-term depression (Palmer et al., 2005, Amici et al., 2009, Saab et al., 2009). Although the protein product of VSNL1, Vilip1, is known to alter availability of α4,β2-nicotinic acetylcholine receptors at the cell membrane via affects on endocytic trafficking (Lin et al., 2002), a similar effect on glutamate receptors has not been shown. It is of some interest, therefore, that among the top pathways identified by genes positively correlated with VSNL1 expression are the KEGG pathway for long-term potentiation and REACTOME pathways for trafficking of AMPA receptors. These associations include positive correlations with several AMPA receptor subunits: GRIA1, GRIA2, and GRIA3. Although not among the top pathways identified, there was also a significant positive correlation of VSNL1 expression with the KEGG pathway for long-term depression in both age groups (Table S4 in Supplementary Material).

B.5 DISCUSSION

We evaluated the hypothesis that VSNL1 may contribute to the development of AD by assessing whether VSNL1 demonstrated age-dependent expression and by determining the brain-related biologic co-expression networks in which VSNL1 participates. VSNL1 expression was present throughout the adult life span, but was not correlated with subject age. VSNL1 co-expression networks included AD pathways and pathways implicated in synaptic pathology in AD, including long-term potentiation, long-term depression, and trafficking of AMPA receptors. These latter findings provide an unbiased link in support of the hypothesis that VSNL1/Vilip1 may participate in molecular mechanisms of AD.

We found that VSNL1 is expressed throughout the adult lifespan in human frontal cortex and is independent of subject age. We, and others, have previously reported that there is a substantial overlap between genes demonstrating age-related changes in expression and genes involved in the pathogenesis of neurodegenerative illnesses, including AD (Glorioso and Sibille, 2011). The lack of changes in VSNL1 expression with age in our subjects suggests that any contribution of VSNL1 to the development of AD is not via this age-dependent mechanism. However, this does not preclude that VSNL1 expression could vary with age in other brain regions relevant to AD pathogenesis, such as the hippocampus. Also, it remains possible that post-transcriptional processing of VSNL1 into Vilip1 protein may vary with age. Evaluating that alternative will require future study of brain Vilip1 levels in an aging cohort.

We had previously identified an association between genetic variation in VSNL1 and the psychotic phenotype of AD (Hollingworth et al., 2012). Because one important mechanism by which genetic variants may affect risk for neurodegenerative disease is to alter the transcription of their gene products in brain (Zou et al., 2012), we evaluated whether VSNL1 expression in frontal cortex is associated within or nearby the VSNL1 locus. We did not detect an association of VSNL1 expression with any of the tested SNPs. However, the possibility that nearby SNPs, other than the ones tested, affect VSNL1 expression cannot be excluded. To assess this likelihood, we used data from the 1000 Genomes project to estimate what proportion of all common variants (minor allele frequency ≥5%) in VSNL1 were correlated with the SNPs tested in our analysis. Only 70% of the common variants were tagged by one or more of our SNPs with an $r^2 \geq 0.8$. The 30% of poorly tagged common variants includes the most strongly-associated SNP in our GWAS, rs4038131. It is also possible that genetic variants, including those evaluated in the current study, may alter VSNL1 expression only in the presence of neurodegenerative

pathology. However, it should be noted that recent tests of SNPs in the AD risk genes ABCA7, BIN1, CD2AP, CD33, CLU, CR1, EPHA1, MS4A6A, MS4A6E, and PICALM for associations with the expression of their respective genes in brain tissue from AD and healthy control subjects have been largely negative (Allen et al., 2012, Karch et al., 2012).

Although the focus of our study was on risk for AD, genetic variants in VSNL1, altered brain VSNL1 mRNA expression, and altered brain levels of Vilip1 protein have been reported in schizophrenia (Beveridge et al., 2008, Martins-de-Souza et al., 2009, Braunewell et al., 2011). Of particular relevance to the current report was the finding that microRNA miR-181b, which is elevated in schizophrenia, can downregulate VSNL1 expression in model systems and correlates with reduced VSNL1 expression in the superior temporal gyrus in subjects with schizophrenia (Beveridge et al., 2008). We were able to replicate the negative correlation between VSNL1 expression and expression of pre-miR-181b genes in our normal aging cohort in both BA11 and BA47 (Figure S1 in Supplementary Material). However, how this normative regulation of VSNL1 by miR-181b might be changed in the presence of AD pathology and/or genetic variation in VSNL1, and in particular whether they may interact to underlie the association of VSNL1 genetic variation with psychosis in AD, is not known.

VSNL1 was co-expressed with genes in several distinct pathways. This included co-expression with genes identified with AD pathways and genes involved in mediating synaptic plasticity mechanisms such as long-term potentiation, long-term depression, and trafficking of AMPA receptors. These findings support a role for Vilip1 in these processes, as co-expressed genes tend to be related functionally (Oldham et al., 2008). However, the specific nature of any functional relationship cannot be readily inferred, as co-expression can arise from many sources (Gaiteri et al., 2014). For example, gray matter homogenates are a mixture of many cell types.

Multiple genes that are specifically enriched in a single cell type, e.g. microglia, may be identified as co-expressed (Oldham et al., 2008, Hawrylycz et al., 2012). Alternatively, genes may share a mechanism regulating their transcription such as a transcription factor in common (Allocco et al., 2004), proximity within the linear sequence of DNA leading to synchronous transcription (Ebisuya et al., 2008), or colocalization within the spatial configuration of chromosomes (Homouz and Kudlicki, 2013). Similarly, epigenetic control of transcription via histone acetylation and methylation can lead to co-expression of neighboring genes (Horvath et al., 2012). Finally, mRNA degradation via microRNA binding may also lead multiple targets of a given microRNA to demonstrate correlated expression (Gennarino et al., 2012).

In summary, VSNL1 is co-expressed with functional groups and gene transcripts in AD pathways, including APP itself and pathways implicated in synaptic pathology in AD. These findings provide an unbiased link between VSNL1 and molecular mechanisms of AD. However, whether increased expression of APP may drive increased VSNL1 expression, increased VSNL1 expression drives increased APP expression, or both are concurrently altered downstream of another factor will need to be evaluated in model systems. For example, evaluation of VSNL1 expression in transgenic mouse models of AD, or evaluation of APP expression after knockdown of VSNL1 would be indicated. Similarly, whether altering VSNL1 expression modifies synaptic pathology in AD would benefit from testing within *in vitro* and/or genetic mouse models.

BIBLIOGRAPHY

(2014) 2014 Alzheimer's disease facts and figures. Alzheimers Dement 10:e47-92.

Acker CM, Forest SK, Zinkowski R, Davies P, d'Abramo C (2013) Sensitive quantitative assays for tau and phospho-tau in transgenic mouse models. Neurobiol Aging 34:338-350.

Al-Sarraf H, Philip L (2003) Increased brain uptake and CSF clearance of 14C-glutamate in spontaneously hypertensive rats. Brain Res 994:181-187.

Allen M, Zou F, Chai HS, Younkin CS, Crook J, Pankratz VS, Carrasquillo MM, Rowley CN, Nair AA, Middha S, Maharjan S, Nguyen T, Ma L, Malphrus KG, Palusak R, Lincoln S, Bisceglio G, Georgescu C, Schultz D, Rakhshan F, Kolbert CP, Jen J, Haines JL, Mayeux R, Pericak-Vance MA, Farrer LA, Schellenberg GD, Petersen RC, Graff-Radford NR, Dickson DW, Younkin SG, Ertekin-Taner N, Apostolova LG, Arnold SE, Baldwin CT, Barber R, Barmada MM, Beach T, Beecham GW, Beekly D, Bennett DA, Bigio EH, Bird TD, Blacker D, Boeve BF, Bowen JD, Boxer A, Burke JR, Buros J, Buxbaum JD, Cairns NJ, Cantwell LB, Cao C, Carlson CS, Carney RM, Carroll SL, Chui HC, Clark DG, Corneveaux J, Cotman CW, Crane PK, Cruchaga C, Cummings JL, De Jager PL, DeCarli C, DeKosky ST, Demirci FY, Diaz-Arrastia R, Dick M, Dombroski BA, Duara R, Ellis WD, Evans D, Faber KM, Fallon KB, Farlow MR, Ferris S, Foroud TM, Frosch M, Galasko DR, Gallins PJ, Ganguli M, Gearing M, Geschwind DH, Ghetti B, Gilbert JR, Gilman S, Giordani B, Glass JD, Goate AM, Green RC, Growdon JH, Hakonarson H, Hamilton RL, Hardy J, Harrell LE, Head E, Honig LS, Huentelman MJ, Hulette CM, Hyman BT, Jarvik GP, Jicha GA, Jin LW, Jun G, Kamboh MI, Karlawish J, Karydas A, Kauwe JS, Kaye JA, Kennedy N, Kim R, Koo EH, Kowall NW, Kramer P, Kukull WA, Lah JJ, Larson EB, Levey AI, Lieberman AP, Lopez OL, Lunetta KL, Mack WJ, Marson DC, Martin ER, Martiniuk F, Mash DC, Masliah E, McCormick WC, McCurry SM, McDavid AN, McKee AC, Mesulam M, Miller BL, Miller CA, Miller JW, Montine TJ, Morris JC, Myers AJ, Naj AC, Nowotny P, Parisi JE, Perl DP, Peskind E, Poon WW, Potter H, Quinn JF, Raj A, Rajbhandary RA, Raskind M, Reiman EM, Reisberg B, Reitz C, Ringman JM, Roberson ED, Rogaeva E, Rosenberg RN, Sano M, Saykin AJ, Schneider JA, Schneider LS, Seeley W, Shelanski ML, Slifer MA, Smith CD, Sonnen JA, Spina S, St George-Hyslop P, Stern RA, Tanzi RE, Trojanowski JQ, Troncoso JC, Tsuang DW, Van Deerlin VM, Vardarajan BN, Vinters HV, Vonsattel JP, Wang LS, Weintraub S, Welsh-Bohmer KA, Williamson J, Woltjer RL (2012) Novel late-onset Alzheimer disease loci variants associate with brain gene expression. Neurology 79:221-228.

Allocco DJ, Kohane IS, Butte AJ (2004) Quantifying the relationship between co-expression, co-regulation and gene function. BMC Bioinformatics 5:18.

Alzheimer A, Stelzmann RA, Schnitzlein HN, Murtagh FR (1995) An English translation of Alzheimer's 1907 paper, "Uber eine eigenartige Erkankung der Hirnrinde". Clin Anat 8:429-431.

Amici M, Doherty A, Jo J, Jane D, Cho K, Collingridge G, Dargan S (2009) Neuronal calcium sensors and synaptic plasticity. Biochem Soc Trans 37:1359-1363.

Arispe N, Rojas E, Pollard HB (1993) Alzheimer disease amyloid beta protein forms calcium channels in bilayer membranes: blockade by tromethamine and aluminum. Proc Natl Acad Sci U S A 90:567-571.

Augustinack JC, Schneider A, Mandelkow EM, Hyman BT (2002) Specific tau phosphorylation sites correlate with severity of neuronal cytopathology in Alzheimer's disease. Acta Neuropathol 103:26-35.

Bacanu SA, Devlin B, Chowdari KV, DeKosky ST, Nimgaonkar VL, Sweet RA (2005) Heritability of psychosis in Alzheimer disease. Am J Geriatr Psychiatry 13:624-627.

Ballatore C, Lee VM, Trojanowski JQ (2007) Tau-mediated neurodegeneration in Alzheimer's disease and related disorders. Nat Rev Neurosci 8:663-672.

Baloyannis SJ, Costa V, Mauroudis I, Psaroulis D, Manolides SL, Manolides LS (2007) Dendritic and spinal pathology in the acoustic cortex in Alzheimer's disease: morphological and morphometric estimation by Golgi technique and electron microscopy. Acta Otolaryngol 127:351-354.

Bamburg JR, Bloom GS (2009) Cytoskeletal pathologies of Alzheimer disease. Cell Motil Cytoskeleton 66:635-649.

Beaudoin GM, 3rd, Lee SH, Singh D, Yuan Y, Ng YG, Reichardt LF, Arikkath J (2012) Culturing pyramidal neurons from the early postnatal mouse hippocampus and cortex. Nat Protoc 7:1741-1754.

Benjamini Y, Hochberg Y (1995) Controlling the false discovery rate – a practical and powerful approach to multiple testing. J R Stat Soc Series B Stat Methodol 57:289-300.

Bernstein HG, Baumann B, Danos P, Diekmann S, Bogerts B, Gundelfinger ED, Braunewell KH (1999) Regional and cellular distribution of neural visinin-like protein immunoreactivities (VILIP-1 and VILIP-3) in human brain. J Neurocytol 28:655-662.

Beveridge NJ, Tooney PA, Carroll AP, Gardiner E, Bowden N, Scott RJ, Tran N, Dedova I, Cairns MJ (2008) Dysregulation of miRNA 181b in the temporal cortex in schizophrenia. Hum Mol Genet 17:1156-1168.

Bezprozvanny I, Mattson MP (2008) Neuronal calcium mishandling and the pathogenesis of Alzheimer's disease. Trends Neurosci 31:454-463.

Braak H, Alafuzoff I, Arzberger T, Kretzschmar H, Del Tredici K (2006) Staging of Alzheimer disease-associated neurofibrillary pathology using paraffin sections and immunocytochemistry. Acta Neuropathol 112:389-404.

Braak H, Braak E (1991) Neuropathological stageing of Alzheimer-related changes. Acta Neuropathol 82:239-259.

Brackmann M, Schuchmann S, Anand R, Braunewell KH (2005) Neuronal Ca2+ sensor protein VILIP-1 affects cGMP signalling of guanylyl cyclase B by regulating clathrin-dependent receptor recycling in hippocampal neurons. J Cell Sci 118:2495-2505.

Braunewell K, Riederer P, Spilker C, Gundelfinger ED, Bogerts B, Bernstein HG (2001a) Abnormal localization of two neuronal calcium sensor proteins, visinin-like proteins (vilips)-1 and -3, in neocortical brain areas of Alzheimer disease patients. Dement Geriatr Cogn Disord 12:110-116.

Braunewell KH, Brackmann M, Schaupp M, Spilker C, Anand R, Gundelfinger ED (2001b) Intracellular neuronal calcium sensor (NCS) protein VILIP-1 modulates cGMP signalling pathways in transfected neural cells and cerebellar granule neurones. J Neurochem 78:1277-1286.

Braunewell KH, Dwary AD, Richter F, Trappe K, Zhao C, Giegling I, Schonrath K, Rujescu D (2011) Association of VSNL1 with schizophrenia, frontal cortical function, and biological significance for its gene product as a modulator of cAMP levels and neuronal morphology. Transl Psychiatry 1:e22.

Braunewell KH, Klein-Szanto AJ (2009) Visinin-like proteins (VSNLs): interaction partners and emerging functions in signal transduction of a subfamily of neuronal Ca2+ -sensor proteins. Cell Tissue Res 335:301-316.

Burgoyne RD, Weiss JL (2001) The neuronal calcium sensor family of Ca2+-binding proteins. Biochem J 353:1-12.

Busciglio J, Lorenzo A, Yeh J, Yankner BA (1995) beta-amyloid fibrils induce tau phosphorylation and loss of microtubule binding. Neuron 14:879-888.

Bussiere T, Giannakopoulos P, Bouras C, Perl DP, Morrison JH, Hof PR (2003) Progressive degeneration of nonphosphorylated neurofilament protein-enriched pyramidal neurons predicts cognitive impairment in Alzheimer's disease: stereologic analysis of prefrontal cortex area 9. J Comp Neurol 463:281-302.

Butterfield DA (2002) Amyloid beta-peptide (1-42)-induced oxidative stress and neurotoxicity: implications for neurodegeneration in Alzheimer's disease brain. A review. Free Radic Res 36:1307-1313.

Cahill ME, Xie Z, Day M, Photowala H, Barbolina MV, Miller CA, Weiss C, Radulovic J, Sweatt JD, Disterhoft JF, Surmeier DJ, Penzes P (2009) Kalirin regulates cortical spine morphogenesis and disease-related behavioral phenotypes. Proc Natl Acad Sci U S A 106:13058-13063.

Cairns NJ, Bigio EH, Mackenzie IR, Neumann M, Lee VM, Hatanpaa KJ, White CL, 3rd, Schneider JA, Grinberg LT, Halliday G, Duyckaerts C, Lowe JS, Holm IE, Tolnay M,

Okamoto K, Yokoo H, Murayama S, Woulfe J, Munoz DG, Dickson DW, Ince PG, Trojanowski JQ, Mann DM (2007) Neuropathologic diagnostic and nosologic criteria for frontotemporal lobar degeneration: consensus of the Consortium for Frontotemporal Lobar Degeneration. Acta Neuropathol 114:5-22.

Cairns NJ, Brannstrom T, Khan MN, Rossor MN, Lantos PL (2003) Neuronal loss in familial frontotemporal dementia with ubiquitin-positive, tau-negative inclusions. Exp Neurol 181:319-326.

Capani F, Deerinck TJ, Ellisman MH, Bushong E, Bobik M, Martone ME (2001) Phalloidin-eosin followed by photo-oxidation: a novel method for localizing F-actin at the light and electron microscopic levels. J Histochem Cytochem 49:1351-1361.

Chaumont S, Compan V, Toulme E, Richler E, Housley GD, Rassendren F, Khakh BS (2008) Regulation of P2X2 receptors by the neuronal calcium sensor VILIP1. Sci Signal 1:ra8.

Chin J (2011) Selecting a mouse model of Alzheimer's disease. Methods Mol Biol 670:169-189.

Davis RC, Marsden IT, Maloney MT, Minamide LS, Podlisny M, Selkoe DJ, Bamburg JR (2011) Amyloid beta dimers/trimers potently induce cofilin-actin rods that are inhibited by maintaining cofilin-phosphorylation. Mol Neurodegener 6:10.

Dehmelt L, Halpain S (2005) The MAP2/Tau family of microtubule-associated proteins. Genome Biol 6:204.

DeKosky ST, Scheff SW (1990) Synapse loss in frontal cortex biopsies in Alzheimer's disease: correlation with cognitive severity. Ann Neurol 27:457-464.

Demuro A, Mina E, Kayed R, Milton SC, Parker I, Glabe CG (2005) Calcium dysregulation and membrane disruption as a ubiquitous neurotoxic mechanism of soluble amyloid oligomers. J Biol Chem 280:17294-17300.

Demuro A, Parker I, Stutzmann GE (2010) Calcium signaling and amyloid toxicity in Alzheimer disease. J Biol Chem 285:12463-12468.

Duff K, Eckman C, Zehr C, Yu X, Prada CM, Perez-tur J, Hutton M, Buee L, Harigaya Y, Yager D, Morgan D, Gordon MN, Holcomb L, Refolo L, Zenk B, Hardy J, Younkin S (1996) Increased amyloid-beta42(43) in brains of mice expressing mutant presenilin 1. Nature 383:710-713.

Ebisuya M, Yamamoto T, Nakajima M, Nishida E (2008) Ripples from neighbouring transcription. Nat Cell Biol 10:1106-1113.

Ekinci FJ, Linsley MD, Shea TB (2000) Beta-amyloid-induced calcium influx induces apoptosis in culture by oxidative stress rather than tau phosphorylation. Brain Res Mol Brain Res 76:389-395.

Erraji-Benchekroun L, Underwood MD, Arango V, Galfalvy H, Pavlidis P, Smyrniotopoulos P, Mann JJ, Sibille E (2005) Molecular aging in human prefrontal cortex is selective and continuous throughout adult life. Biol Psychiatry 57:549-558.

Esbjorner EK, Chan F, Rees E, Erdelyi M, Luheshi LM, Bertoncini CW, Kaminski CF, Dobson CM, Kaminski Schierle GS (2014) Direct observations of amyloid beta self-assembly in live cells provide insights into differences in the kinetics of Abeta(1-40) and Abeta(1-42) aggregation. Chem Biol 21:732-742.

Fagan AM (2014) CSF Biomarkers of Alzheimer's Disease: Impact on Disease Concept, Diagnosis, and Clinical Trial Design. Advances in Geriatrics 2014.

Fagan AM, Xiong C, Jasielec MS, Bateman RJ, Goate AM, Benzinger TL, Ghetti B, Martins RN, Masters CL, Mayeux R, Ringman JM, Rossor MN, Salloway S, Schofield PR, Sperling RA, Marcus D, Cairns NJ, Buckles VD, Ladenson JH, Morris JC, Holtzman DM (2014) Longitudinal change in CSF biomarkers in autosomal-dominant Alzheimer's disease. Sci Transl Med 6:226ra230.

Fifre A, Sponne I, Koziel V, Kriem B, Yen Potin FT, Bihain BE, Olivier JL, Oster T, Pillot T (2006) Microtubule-associated protein MAP1A, MAP1B, and MAP2 proteolysis during soluble amyloid beta-peptide-induced neuronal apoptosis. Synergistic involvement of calpain and caspase-3. J Biol Chem 281:229-240.

Fish KN, Sweet RA, Deo AJ, Lewis DA (2008) An automated segmentation methodology for quantifying immunoreactive puncta number and fluorescence intensity in tissue sections. Brain Res 1240:62-72.

Gaiteri C, Ding Y, French B, Tseng GC, Sibille E (2014) Beyond modules and hubs: the potential of gene coexpression networks for investigating molecular mechanisms of complex brain disorders. Genes Brain Behav 13:13-24.

Games D, Adams D, Alessandrini R, Barbour R, Berthelette P, Blackwell C, Carr T, Clemens J, Donaldson T, Gillespie F, et al. (1995) Alzheimer-type neuropathology in transgenic mice overexpressing V717F beta-amyloid precursor protein. Nature 373:523-527.

Garcia-Alloza M, Robbins EM, Zhang-Nunes SX, Purcell SM, Betensky RA, Raju S, Prada C, Greenberg SM, Bacskai BJ, Frosch MP (2006) Characterization of amyloid deposition in the APPswe/PS1dE9 mouse model of Alzheimer disease. Neurobiol Dis 24:516-524.

Gennarino VA, D'Angelo G, Dharmalingam G, Fernandez S, Russolillo G, Sanges R, Mutarelli M, Belcastro V, Ballabio A, Verde P, Sardiello M, Banfi S (2012) Identification of microRNA-regulated gene networks by expression analysis of target genes. Genome Res 22:1163-1172.

Geuna S, Herrera-Rincon C (2015) Update on stereology for light microscopy. Cell Tissue Res.

Gierke P, Zhao C, Brackmann M, Linke B, Heinemann U, Braunewell KH (2004) Expression analysis of members of the neuronal calcium sensor protein family: combining bioinformatics and Western blot analysis. Biochem Biophys Res Commun 323:38-43.

Gimbel DA, Nygaard HB, Coffey EE, Gunther EC, Lauren J, Gimbel ZA, Strittmatter SM (2010) Memory impairment in transgenic Alzheimer mice requires cellular prion protein. J Neurosci 30:6367-6374.

Glorioso C, Oh S, Douillard GG, Sibille E (2011) Brain molecular aging, promotion of neurological disease and modulation by sirtuin 5 longevity gene polymorphism. Neurobiol Dis 41:279-290.

Glorioso C, Sibille E (2011) Between destiny and disease: genetics and molecular pathways of human central nervous system aging. Prog Neurobiol 93:165-181.

Gomez Ravetti M, Rosso OA, Berretta R, Moscato P (2010) Uncovering molecular biomarkers that correlate cognitive decline with the changes of hippocampus' gene expression profiles in Alzheimer's disease. PLoS One 5:e10153.

Gomez-Isla T, Hollister R, West H, Mui S, Growdon JH, Petersen RC, Parisi JE, Hyman BT (1997) Neuronal loss correlates with but exceeds neurofibrillary tangles in Alzheimer's disease. Ann Neurol 41:17-24.

Gomez-Isla T, Price JL, McKeel DW, Jr., Morris JC, Growdon JH, Hyman BT (1996) Profound loss of layer II entorhinal cortex neurons occurs in very mild Alzheimer's disease. J Neurosci 16:4491-4500.

Gotz J, Deters N, Doldissen A, Bokhari L, Ke Y, Wiesner A, Schonrock N, Ittner LM (2007) A decade of tau transgenic animal models and beyond. Brain Pathol 17:91-103.

Grimmer T, Riemenschneider M, Forstl H, Henriksen G, Klunk WE, Mathis CA, Shiga T, Wester HJ, Kurz A, Drzezga A (2009) Beta amyloid in Alzheimer's disease: increased deposition in brain is reflected in reduced concentration in cerebrospinal fluid. Biol Psychiatry 65:927-934.

Grutzendler J, Helmin K, Tsai J, Gan WB (2007) Various dendritic abnormalities are associated with fibrillar amyloid deposits in Alzheimer's disease. Ann N Y Acad Sci 1097:30-39.

Gu J, Zheng JQ (2009) Microtubules in Dendritic Spine Development and Plasticity. Open Neurosci J 3:128-133.

Guo Q, Sebastian L, Sopher BL, Miller MW, Ware CB, Martin GM, Mattson MP (1999) Increased vulnerability of hippocampal neurons from presenilin-1 mutant knock-in mice to amyloid beta-peptide toxicity: central roles of superoxide production and caspase activation. J Neurochem 72:1019-1029.

Haass C, Selkoe DJ (2007) Soluble protein oligomers in neurodegeneration: lessons from the Alzheimer's amyloid beta-peptide. Nat Rev Mol Cell Biol 8:101-112.

Halpain S, Greengard P (1990) Activation of NMDA receptors induces rapid dephosphorylation of the cytoskeletal protein MAP2. Neuron 5:237-246.

Hardy J (1997) Amyloid, the presenilins and Alzheimer's disease. Trends Neurosci 20:154-159.

Hartigan JA, Johnson GV (1999) Transient increases in intracellular calcium result in prolonged site-selective increases in Tau phosphorylation through a glycogen synthase kinase 3beta-dependent pathway. J Biol Chem 274:21395-21401.

Hawrylycz MJ, Lein ES, Guillozet-Bongaarts AL, Shen EH, Ng L, Miller JA, van de Lagemaat LN, Smith KA, Ebbert A, Riley ZL, Abajian C, Beckmann CF, Bernard A, Bertagnolli D, Boe AF, Cartagena PM, Chakravarty MM, Chapin M, Chong J, Dalley RA, Daly BD, Dang C, Datta S, Dee N, Dolbeare TA, Faber V, Feng D, Fowler DR, Goldy J, Gregor BW, Haradon Z, Haynor DR, Hohmann JG, Horvath S, Howard RE, Jeromin A, Jochim JM, Kinnunen M, Lau C, Lazarz ET, Lee C, Lemon TA, Li L, Li Y, Morris JA, Overly CC, Parker PD, Parry SE, Reding M, Royall JJ, Schulkin J, Sequeira PA, Slaughterbeck CR, Smith SC, Sodt AJ, Sunkin SM, Swanson BE, Vawter MP, Williams D, Wohnoutka P, Zielke HR, Geschwind DH, Hof PR, Smith SM, Koch C, Grant SG, Jones AR (2012) An anatomically comprehensive atlas of the adult human brain transcriptome. Nature 489:391-399.

Hayashi K, Ishikawa R, Ye LH, He XL, Takata K, Kohama K, Shirao T (1996) Modulatory role of drebrin on the cytoskeleton within dendritic spines in the rat cerebral cortex. J Neurosci 16:7161-7170.

Herculano-Houzel S, von Bartheld CS, Miller DJ, Kaas JH (2015) How to count cells: the advantages and disadvantages of the isotropic fractionator compared with stereology. Cell Tissue Res.

Himmel HM, Riehle R, Stieler K, Siess M (1990) Effects of the divalent cation ionophore ionomycin on the performance of isolated guinea-pig atria. Basic Res Cardiol 85:247-256.

Hogg RC, Raggenbass M, Bertrand D (2003) Nicotinic acetylcholine receptors: from structure to brain function. Rev Physiol Biochem Pharmacol 147:1-46.

Holcomb L, Gordon MN, McGowan E, Yu X, Benkovic S, Jantzen P, Wright K, Saad I, Mueller R, Morgan D, Sanders S, Zehr C, O'Campo K, Hardy J, Prada CM, Eckman C, Younkin S, Hsiao K, Duff K (1998) Accelerated Alzheimer-type phenotype in transgenic mice carrying both mutant amyloid precursor protein and presenilin 1 transgenes. Nat Med 4:97-100.

Hollingworth P, Sweet R, Sims R, Harold D, Russo G, Abraham R, Stretton A, Jones N, Gerrish A, Chapman J, Ivanov D, Moskvina V, Lovestone S, Priotsi P, Lupton M, Brayne C, Gill M, Lawlor B, Lynch A, Craig D, McGuinness B, Johnston J, Holmes C, Livingston G, Bass NJ, Gurling H, McQuillin A, Holmans P, Jones L, Devlin B, Klei L, Barmada MM, Demirci FY, DeKosky ST, Lopez OL, Passmore P, Owen MJ, O'Donovan MC, Mayeux

R, Kamboh MI, Williams J (2012) Genome-wide association study of Alzheimer's disease with psychotic symptoms. Mol Psychiatry 17:1316-1327.

Holtzman DM, Morris JC, Goate AM (2011) Alzheimer's disease: the challenge of the second century. Sci Transl Med 3:77sr71.

Homouz D, Kudlicki AS (2013) The 3D organization of the yeast genome correlates with co-expression and reflects functional relations between genes. PLoS One 8:e54699.

Horvath S, Zhang Y, Langfelder P, Kahn RS, Boks MP, van Eijk K, van den Berg LH, Ophoff RA (2012) Aging effects on DNA methylation modules in human brain and blood tissue. Genome Biol 13:R97.

Hsiao K, Chapman P, Nilsen S, Eckman C, Harigaya Y, Younkin S, Yang F, Cole G (1996) Correlative memory deficits, Abeta elevation, and amyloid plaques in transgenic mice. Science 274:99-102.

Hsieh H, Boehm J, Sato C, Iwatsubo T, Tomita T, Sisodia S, Malinow R (2006) AMPAR removal underlies Abeta-induced synaptic depression and dendritic spine loss. Neuron 52:831-843.

Huh JW, Raghupathi R, Laurer HL, Helfaer MA, Saatman KE (2003) Transient loss of microtubule-associated protein 2 immunoreactivity after moderate brain injury in mice. J Neurotrauma 20:975-984.

Hyman BT (2011) Caspase activation without apoptosis: insight into Abeta initiation of neurodegeneration. Nat Neurosci 14:5-6.

Hyman BT, Trojanowski JQ (1997) Consensus recommendations for the postmortem diagnosis of Alzheimer disease from the National Institute on Aging and the Reagan Institute Working Group on diagnostic criteria for the neuropathological assessment of Alzheimer disease. J Neuropathol Exp Neurol 56:1095-1097.

Ikonomovic MD, Abrahamson EE, Isanski BA, Debnath ML, Mathis CA, Dekosky ST, Klunk WE (2006) X-34 labeling of abnormal protein aggregates during the progression of Alzheimer's disease. Methods Enzymol 412:123-144.

Ikonomovic MD, Klunk WE, Abrahamson EE, Mathis CA, Price JC, Tsopelas ND, Lopresti BJ, Ziolko S, Bi W, Paljug WR, Debnath ML, Hope CE, Isanski BA, Hamilton RL, DeKosky ST (2008) Post-mortem correlates of in vivo PiB-PET amyloid imaging in a typical case of Alzheimer's disease. Brain 131:1630-1645.

Ingelsson M, Fukumoto H, Newell KL, Growdon JH, Hedley-Whyte ET, Frosch MP, Albert MS, Hyman BT, Irizarry MC (2004) Early Abeta accumulation and progressive synaptic loss, gliosis, and tangle formation in AD brain. Neurology 62:925-931.

Irizarry MC, Soriano F, McNamara M, Page KJ, Schenk D, Games D, Hyman BT (1997) Abeta deposition is associated with neuropil changes, but not with overt neuronal loss in the

human amyloid precursor protein V717F (PDAPP) transgenic mouse. J Neurosci 17:7053-7059.

Ittner LM, Gotz J (2011) Amyloid-beta and tau--a toxic pas de deux in Alzheimer's disease. Nat Rev Neurosci 12:65-72.

Iversen LL, Mortishire-Smith RJ, Pollack SJ, Shearman MS (1995) The toxicity in vitro of beta-amyloid protein. Biochem J 311 (Pt 1):1-16.

Jack CR, Jr., Knopman DS, Jagust WJ, Shaw LM, Aisen PS, Weiner MW, Petersen RC, Trojanowski JQ (2010) Hypothetical model of dynamic biomarkers of the Alzheimer's pathological cascade. Lancet Neurol 9:119-128.

Jack CR, Jr., Vemuri P, Wiste HJ, Weigand SD, Aisen PS, Trojanowski JQ, Shaw LM, Bernstein MA, Petersen RC, Weiner MW, Knopman DS (2011) Evidence for ordering of Alzheimer disease biomarkers. Arch Neurol 68:1526-1535.

James BD, Leurgans SE, Hebert LE, Scherr PA, Yaffe K, Bennett DA (2014) Contribution of Alzheimer disease to mortality in the United States. Neurology 82:1045-1050.

Jankowsky JL, Fadale DJ, Anderson J, Xu GM, Gonzales V, Jenkins NA, Copeland NG, Lee MK, Younkin LH, Wagner SL, Younkin SG, Borchelt DR (2004) Mutant presenilins specifically elevate the levels of the 42 residue beta-amyloid peptide in vivo: evidence for augmentation of a 42-specific gamma secretase. Hum Mol Genet 13:159-170.

Janocko NJ, Brodersen KA, Soto-Ortolaza AI, Ross OA, Liesinger AM, Duara R, Graff-Radford NR, Dickson DW, Murray ME (2012) Neuropathologically defined subtypes of Alzheimer's disease differ significantly from neurofibrillary tangle-predominant dementia. Acta Neuropathol 124:681-692.

Jin M, Shepardson N, Yang T, Chen G, Walsh D, Selkoe DJ (2011) Soluble amyloid beta-protein dimers isolated from Alzheimer cortex directly induce Tau hyperphosphorylation and neuritic degeneration. Proc Natl Acad Sci U S A 108:5819-5824.

Johanson CE, Duncan JA, Stopa EG, Baird A (2005) Enhanced prospects for drug delivery and brain targeting by the choroid plexus-CSF route. Pharm Res 22:1011-1037.

Kamal A, Almenar-Queralt A, LeBlanc JF, Roberts EA, Goldstein LS (2001) Kinesin-mediated axonal transport of a membrane compartment containing beta-secretase and presenilin-1 requires APP. Nature 414:643-648.

Karch CM, Jeng AT, Nowotny P, Cady J, Cruchaga C, Goate AM (2012) Expression of novel Alzheimer's disease risk genes in control and Alzheimer's disease brains. PLoS One 7:e50976.

Kasai H, Fukuda M, Watanabe S, Hayashi-Takagi A, Noguchi J (2010) Structural dynamics of dendritic spines in memory and cognition. Trends Neurosci 33:121-129.

Kayed R, Canto I, Breydo L, Rasool S, Lukacsovich T, Wu J, Albay R, 3rd, Pensalfini A, Yeung S, Head E, Marsh JL, Glabe C (2010) Conformation dependent monoclonal antibodies distinguish different replicating strains or conformers of prefibrillar Abeta oligomers. Mol Neurodegener 5:57.

Kirkwood CM, Ciuchta J, Ikonomovic MD, Fish KN, Abrahamson EE, Murray PS, Klunk WE, Sweet RA (2013) Dendritic spine density, morphology, and fibrillar actin content surrounding amyloid-beta plaques in a mouse model of amyloid-beta deposition. J Neuropathol Exp Neurol 72:791-800.

Klein AM, Kowall NW, Ferrante RJ (1999) Neurotoxicity and oxidative damage of beta amyloid 1-42 versus beta amyloid 1-40 in the mouse cerebral cortex. Ann N Y Acad Sci 893:314-320.

Koffie RM, Hyman BT, Spires-Jones TL (2011) Alzheimer's disease: synapses gone cold. Mol Neurodegener 6:63.

Koffie RM, Meyer-Luehmann M, Hashimoto T, Adams KW, Mielke ML, Garcia-Alloza M, Micheva KD, Smith SJ, Kim ML, Lee VM, Hyman BT, Spires-Jones TL (2009) Oligomeric amyloid beta associates with postsynaptic densities and correlates with excitatory synapse loss near senile plaques. Proc Natl Acad Sci U S A 106:4012-4017.

Koppel J, Acker C, Davies P, Lopez OL, Jimenez H, Azose M, Greenwald BS, Murray PS, Kirkwood CM, Kofler J, Sweet RA (2014) Psychotic Alzheimer's disease is associated with gender-specific tau phosphorylation abnormalities. Neurobiol Aging 35:2021-2028.

Korobova F, Svitkina T (2010) Molecular architecture of synaptic actin cytoskeleton in hippocampal neurons reveals a mechanism of dendritic spine morphogenesis. Mol Biol Cell 21:165-176.

Kuchibhotla KV, Goldman ST, Lattarulo CR, Wu HY, Hyman BT, Bacskai BJ (2008) Abeta plaques lead to aberrant regulation of calcium homeostasis in vivo resulting in structural and functional disruption of neuronal networks. Neuron 59:214-225.

Kurt MA, Davies DC, Kidd M, Duff K, Howlett DR (2003) Hyperphosphorylated tau and paired helical filament-like structures in the brains of mice carrying mutant amyloid precursor protein and mutant presenilin-1 transgenes. Neurobiol Dis 14:89-97.

Landis DM, Reese TS (1983) Cytoplasmic organization in cerebellar dendritic spines. J Cell Biol 97:1169-1178.

Larson ME, Lesne SE (2012) Soluble Abeta oligomer production and toxicity. J Neurochem 120 Suppl 1:125-139.

Laterza OF, Modur VR, Crimmins DL, Olander JV, Landt Y, Lee JM, Ladenson JH (2006) Identification of novel brain biomarkers. Clin Chem 52:1713-1721.

Lee JM, Blennow K, Andreasen N, Laterza O, Modur V, Olander J, Gao F, Ohlendorf M, Ladenson JH (2008) The brain injury biomarker VLP-1 is increased in the cerebrospinal fluid of Alzheimer disease patients. Clin Chem 54:1617-1623.

Li C, Pan W, Braunewell KH, Ames JB (2011) Structural analysis of Mg2+ and Ca2+ binding, myristoylation, and dimerization of the neuronal calcium sensor and visinin-like protein 1 (VILIP-1). J Biol Chem 286:6354-6366.

Li J, Tseng G (2011) An adaptively weighted statistic for detecting differential gene expression when combining multiple transcriptomic studies. Ann Appl Stat 5:994.

Li S, Hong S, Shepardson NE, Walsh DM, Shankar GM, Selkoe D (2009) Soluble oligomers of amyloid Beta protein facilitate hippocampal long-term depression by disrupting neuronal glutamate uptake. Neuron 62:788-801.

Lin CW, Chang LC, Tseng GC, Kirkwood CM, Sibille EL, Sweet RA (2015) VSNL1 Co-Expression Networks in Aging Include Calcium Signaling, Synaptic Plasticity, and Alzheimer's Disease Pathways. Front Psychiatry 6:30.

Lin L, Jeanclos EM, Treuil M, Braunewell KH, Gundelfinger ED, Anand R (2002) The calcium sensor protein visinin-like protein-1 modulates the surface expression and agonist sensitivity of the alpha 4beta 2 nicotinic acetylcholine receptor. J Biol Chem 277:41872-41878.

Longa EZ, Weinstein PR, Carlson S, Cummins R (1989) Reversible middle cerebral artery occlusion without craniectomy in rats. Stroke 20:84-91.

Loo DT, Copani A, Pike CJ, Whittemore ER, Walencewicz AJ, Cotman CW (1993) Apoptosis is induced by beta-amyloid in cultured central nervous system neurons. Proc Natl Acad Sci U S A 90:7951-7955.

Lopez OL, Becker JT, Chang YF, Sweet RA, Aizenstein H, Snitz B, Saxton J, McDade E, Kamboh MI, DeKosky ST, Reynolds CF, 3rd, Klunk WE (2013) The long-term effects of conventional and atypical antipsychotics in patients with probable Alzheimer's disease. Am J Psychiatry 170:1051-1058.

Lorenzo A, Yankner BA (1994) Beta-amyloid neurotoxicity requires fibril formation and is inhibited by congo red. Proc Natl Acad Sci U S A 91:12243-12247.

Loring JF, Wen X, Lee JM, Seilhamer J, Somogyi R (2001) A gene expression profile of Alzheimer's disease. DNA Cell Biol 20:683-695.

Lue LF, Kuo YM, Roher AE, Brachova L, Shen Y, Sue L, Beach T, Kurth JH, Rydel RE, Rogers J (1999) Soluble amyloid beta peptide concentration as a predictor of synaptic change in Alzheimer's disease. Am J Pathol 155:853-862.

Luo X, Hou L, Shi H, Zhong X, Zhang Y, Zheng D, Tan Y, Hu G, Mu N, Chan J, Chen X, Fang Y, Wu F, He H, Ning Y (2013) CSF levels of the neuronal injury biomarker visinin-like

protein-1 in Alzheimer's disease and dementia with Lewy bodies. J Neurochem 127:681-690.

Luther E, Kamentsky L, Henriksen M, Holden E (2004) Next-generation laser scanning cytometry. Methods Cell Biol 75:185-218.

MacDonald ML, Ciccimaro E, Prakash A, Banerjee A, Seeholzer SH, Blair IA, Hahn CG (2012) Biochemical fractionation and stable isotope dilution liquid chromatography-mass spectrometry for targeted and microdomain-specific protein quantification in human postmortem brain tissue. Mol Cell Proteomics 11:1670-1681.

Mackenzie IR, Neumann M, Baborie A, Sampathu DM, Du Plessis D, Jaros E, Perry RH, Trojanowski JQ, Mann DM, Lee VM (2011) A harmonized classification system for FTLD-TDP pathology. Acta Neuropathol 122:111-113.

Mackenzie IR, Neumann M, Bigio EH, Cairns NJ, Alafuzoff I, Kril J, Kovacs GG, Ghetti B, Halliday G, Holm IE, Ince PG, Kamphorst W, Revesz T, Rozemuller AJ, Kumar-Singh S, Akiyama H, Baborie A, Spina S, Dickson DW, Trojanowski JQ, Mann DM (2009) Nomenclature for neuropathologic subtypes of frontotemporal lobar degeneration: consensus recommendations. Acta Neuropathol 117:15-18.

Mackenzie IR, Neumann M, Bigio EH, Cairns NJ, Alafuzoff I, Kril J, Kovacs GG, Ghetti B, Halliday G, Holm IE, Ince PG, Kamphorst W, Revesz T, Rozemuller AJ, Kumar-Singh S, Akiyama H, Baborie A, Spina S, Dickson DW, Trojanowski JQ, Mann DM (2010) Nomenclature and nosology for neuropathologic subtypes of frontotemporal lobar degeneration: an update. Acta Neuropathol 119:1-4.

Mann DM, Iwatsubo T, Ihara Y, Cairns NJ, Lantos PL, Bogdanovic N, Lannfelt L, Winblad B, Maat-Schieman ML, Rossor MN (1996) Predominant deposition of amyloid-beta 42(43) in plaques in cases of Alzheimer's disease and hereditary cerebral hemorrhage associated with mutations in the amyloid precursor protein gene. Am J Pathol 148:1257-1266.

Mark RJ, Hensley K, Butterfield DA, Mattson MP (1995) Amyloid beta-peptide impairs ion-motive ATPase activities: evidence for a role in loss of neuronal Ca2+ homeostasis and cell death. J Neurosci 15:6239-6249.

Martins-de-Souza D, Gattaz WF, Schmitt A, Rewerts C, Marangoni S, Novello JC, Maccarrone G, Turck CW, Dias-Neto E (2009) Alterations in oligodendrocyte proteins, calcium homeostasis and new potential markers in schizophrenia anterior temporal lobe are revealed by shotgun proteome analysis. J Neural Transm 116:275-289.

Matsuzaki M, Honkura N, Ellis-Davies GC, Kasai H (2004) Structural basis of long-term potentiation in single dendritic spines. Nature 429:761-766.

Mattson MP, Cheng B, Davis D, Bryant K, Lieberburg I, Rydel RE (1992) beta-Amyloid peptides destabilize calcium homeostasis and render human cortical neurons vulnerable to excitotoxicity. J Neurosci 12:376-389.

Mayeux R, Stern Y (2012) Epidemiology of Alzheimer disease. Cold Spring Harb Perspect Med 2.

McKeith IG, Dickson DW, Lowe J, Emre M, O'Brien JT, Feldman H, Cummings J, Duda JE, Lippa C, Perry EK, Aarsland D, Arai H, Ballard CG, Boeve B, Burn DJ, Costa D, Del Ser T, Dubois B, Galasko D, Gauthier S, Goetz CG, Gomez-Tortosa E, Halliday G, Hansen LA, Hardy J, Iwatsubo T, Kalaria RN, Kaufer D, Kenny RA, Korczyn A, Kosaka K, Lee VM, Lees A, Litvan I, Londos E, Lopez OL, Minoshima S, Mizuno Y, Molina JA, Mukaetova-Ladinska EB, Pasquier F, Perry RH, Schulz JB, Trojanowski JQ, Yamada M (2005) Diagnosis and management of dementia with Lewy bodies: third report of the DLB Consortium. Neurology 65:1863-1872.

McKhann G, Drachman D, Folstein M, Katzman R, Price D, Stadlan EM (1984) Clinical diagnosis of Alzheimer's disease: report of the NINCDS-ADRDA Work Group under the auspices of Department of Health and Human Services Task Force on Alzheimer's Disease. Neurology 34:939-944.

Mercer EA, Korhonen L, Skoglosa Y, Olsson PA, Kukkonen JP, Lindholm D (2000) NAIP interacts with hippocalcin and protects neurons against calcium-induced cell death through caspase-3-dependent and -independent pathways. EMBO J 19:3597-3607.

Miller JA, Oldham MC, Geschwind DH (2008) A systems level analysis of transcriptional changes in Alzheimer's disease and normal aging. J Neurosci 28:1410-1420.

Millet LJ, Gillette MU (2012) Over a century of neuron culture: from the hanging drop to microfluidic devices. Yale J Biol Med 85:501-521.

Mirra SS, Heyman A, McKeel D, Sumi SM, Crain BJ, Brownlee LM, Vogel FS, Hughes JP, van Belle G, Berg L (1991) The Consortium to Establish a Registry for Alzheimer's Disease (CERAD). Part II. Standardization of the neuropathologic assessment of Alzheimer's disease. Neurology 41:479-486.

Mondragon-Rodriguez S, Perry G, Luna-Munoz J, Acevedo-Aquino MC, Williams S (2014) Phosphorylation of tau protein at sites Ser(396-404) is one of the earliest events in Alzheimer's disease and Down syndrome. Neuropathol Appl Neurobiol 40:121-135.

Montagne A, Barnes SR, Sweeney MD, Halliday MR, Sagare AP, Zhao Z, Toga AW, Jacobs RE, Liu CY, Amezcua L, Harrington MG, Chui HC, Law M, Zlokovic BV (2015) Blood-brain barrier breakdown in the aging human hippocampus. Neuron 85:296-302.

Morgan AJ, Jacob R (1994) Ionomycin enhances Ca2+ influx by stimulating store-regulated cation entry and not by a direct action at the plasma membrane. Biochem J 300 (Pt 3):665-672.

Mroczko B, Groblewska M, Zboch M, Muszynski P, Zajkowska A, Borawska R, Szmitkowski M, Kornhuber J, Lewczuk P (2015) Evaluation of visinin-like protein 1 concentrations in the cerebrospinal fluid of patients with mild cognitive impairment as a dynamic biomarker of Alzheimer's disease. J Alzheimers Dis 43:1031-1037.

Mucke L, Selkoe DJ (2012) Neurotoxicity of amyloid beta-protein: synaptic and network dysfunction. Cold Spring Harb Perspect Med 2:a006338.

Mullen RJ, Buck CR, Smith AM (1992) NeuN, a neuronal specific nuclear protein in vertebrates. Development 116:201-211.

Murray PS, Kirkwood CM, Gray MC, Fish KN, Ikonomovic MD, Hamilton RL, Kofler JK, Klunk WE, Lopez OL, Sweet RA (2014a) Hyperphosphorylated tau is elevated in Alzheimer's disease with psychosis. J Alzheimers Dis 39:759-773.

Murray PS, Kirkwood CM, Gray MC, Ikonomovic MD, Paljug WR, Abrahamson EE, Henteleff RA, Hamilton RL, Kofler JK, Klunk WE, Lopez OL, Penzes P, Sweet RA (2012) beta-Amyloid 42/40 ratio and kalirin expression in Alzheimer disease with psychosis. Neurobiol Aging 33:2807-2816.

Murray PS, Kumar S, Demichele-Sweet MA, Sweet RA (2014b) Psychosis in Alzheimer's disease. Biol Psychiatry 75:542-552.

Nagerl UV, Eberhorn N, Cambridge SB, Bonhoeffer T (2004) Bidirectional activity-dependent morphological plasticity in hippocampal neurons. Neuron 44:759-767.

Naslund J, Haroutunian V, Mohs R, Davis KL, Davies P, Greengard P, Buxbaum JD (2000) Correlation between elevated levels of amyloid beta-peptide in the brain and cognitive decline. JAMA 283:1571-1577.

O'Nuallain B, Freir DB, Nicoll AJ, Risse E, Ferguson N, Herron CE, Collinge J, Walsh DM (2010) Amyloid beta-protein dimers rapidly form stable synaptotoxic protofibrils. J Neurosci 30:14411-14419.

Okamoto K, Nagai T, Miyawaki A, Hayashi Y (2004) Rapid and persistent modulation of actin dynamics regulates postsynaptic reorganization underlying bidirectional plasticity. Nat Neurosci 7:1104-1112.

Oldham MC, Konopka G, Iwamoto K, Langfelder P, Kato T, Horvath S, Geschwind DH (2008) Functional organization of the transcriptome in human brain. Nat Neurosci 11:1271-1282.

Oliveira JM, Henriques AG, Martins F, Rebelo S, da Cruz ESOA (2015) Amyloid-beta Modulates Both AbetaPP and Tau Phosphorylation. J Alzheimers Dis.

Ono K, Condron MM, Teplow DB (2009) Structure-neurotoxicity relationships of amyloid beta-protein oligomers. Proc Natl Acad Sci U S A 106:14745-14750.

Palmer CL, Lim W, Hastie PG, Toward M, Korolchuk VI, Burbidge SA, Banting G, Collingridge GL, Isaac JT, Henley JM (2005) Hippocalcin functions as a calcium sensor in hippocampal LTD. Neuron 47:487-494.

Paterlini M, Revilla V, Grant AL, Wisden W (2000) Expression of the neuronal calcium sensor protein family in the rat brain. Neuroscience 99:205-216.

Pauwels K, Williams TL, Morris KL, Jonckheere W, Vandersteen A, Kelly G, Schymkowitz J, Rousseau F, Pastore A, Serpell LC, Broersen K (2012) Structural basis for increased toxicity of pathological abeta42:abeta40 ratios in Alzheimer disease. J Biol Chem 287:5650-5660.

Paxinos G FK (2004) The Mouse Brain in Stereotaxic Coordinates: Compact Second Edition. Compact Second Edition:1-120.

Phillips M, Boman E, Osterman H, Willhite D, Laska M (2011) Olfactory and visuospatial learning and memory performance in two strains of Alzheimer's disease model mice--a longitudinal study. PLoS One 6:e19567.

Rabinovici GD, Miller BL (2010) Frontotemporal lobar degeneration: epidemiology, pathophysiology, diagnosis and management. CNS Drugs 24:375-398.

Rapoport M, Dawson HN, Binder LI, Vitek MP, Ferreira A (2002) Tau is essential to beta -amyloid-induced neurotoxicity. Proc Natl Acad Sci U S A 99:6364-6369.

Regeur L, Jensen GB, Pakkenberg H, Evans SM, Pakkenberg B (1994) No global neocortical nerve cell loss in brains from patients with senile dementia of Alzheimer's type. Neurobiol Aging 15:347-352.

Resnick SM, Sojkova J, Zhou Y, An Y, Ye W, Holt DP, Dannals RF, Mathis CA, Klunk WE, Ferrucci L, Kraut MA, Wong DF (2010) Longitudinal cognitive decline is associated with fibrillar amyloid-beta measured by [11C]PiB. Neurology 74:807-815.

Roberson ED, Scearce-Levie K, Palop JJ, Yan F, Cheng IH, Wu T, Gerstein H, Yu GQ, Mucke L (2007) Reducing endogenous tau ameliorates amyloid beta-induced deficits in an Alzheimer's disease mouse model. Science 316:750-754.

Ropacki SA, Jeste DV (2005) Epidemiology of and risk factors for psychosis of Alzheimer's disease: a review of 55 studies published from 1990 to 2003. Am J Psychiatry 162:2022-2030.

Rossler M, Zarski R, Bohl J, Ohm TG (2002) Stage-dependent and sector-specific neuronal loss in hippocampus during Alzheimer's disease. Acta Neuropathol 103:363-369.

Saab BJ, Georgiou J, Nath A, Lee FJ, Wang M, Michalon A, Liu F, Mansuy IM, Roder JC (2009) NCS-1 in the dentate gyrus promotes exploration, synaptic plasticity, and rapid acquisition of spatial memory. Neuron 63:643-656.

Sanchez L, Madurga S, Pukala T, Vilaseca M, Lopez-Iglesias C, Robinson CV, Giralt E, Carulla N (2011) Abeta40 and Abeta42 amyloid fibrils exhibit distinct molecular recycling properties. J Am Chem Soc 133:6505-6508.

Scheff SW, Price DA (1993) Synapse loss in the temporal lobe in Alzheimer's disease. Ann Neurol 33:190-199.

Scheff SW, Price DA (2003) Synaptic pathology in Alzheimer's disease: a review of ultrastructural studies. Neurobiol Aging 24:1029-1046.

Scheff SW, Price DA, Schmitt FA, DeKosky ST, Mufson EJ (2007) Synaptic alterations in CA1 in mild Alzheimer disease and mild cognitive impairment. Neurology 68:1501-1508.

Scheltens P, Barkhof F, Leys D, Wolters EC, Ravid R, Kamphorst W (1995) Histopathologic correlates of white matter changes on MRI in Alzheimer's disease and normal aging. Neurology 45:883-888.

Schnurra I, Bernstein HG, Riederer P, Braunewell KH (2001) The neuronal calcium sensor protein VILIP-1 is associated with amyloid plaques and extracellular tangles in Alzheimer's disease and promotes cell death and tau phosphorylation in vitro: a link between calcium sensors and Alzheimer's disease? Neurobiol Dis 8:900-909.

Selkoe DJ (2002) Alzheimer's disease is a synaptic failure. Science 298:789-791.

Selkoe DJ (2004) Alzheimer disease: mechanistic understanding predicts novel therapies. Ann Intern Med 140:627-638.

Selkoe DJ (2008) Soluble oligomers of the amyloid beta-protein impair synaptic plasticity and behavior. Behav Brain Res 192:106-113.

Serrano-Pozo A, Frosch MP, Masliah E, Hyman BT (2011) Neuropathological alterations in Alzheimer disease. Cold Spring Harb Perspect Med 1:a006189.

Shabalin AA (2012) Matrix eQTL: ultra fast eQTL analysis via large matrix operations. Bioinformatics 28:1353-1358.

Shankar GM, Bloodgood BL, Townsend M, Walsh DM, Selkoe DJ, Sabatini BL (2007) Natural oligomers of the Alzheimer amyloid-beta protein induce reversible synapse loss by modulating an NMDA-type glutamate receptor-dependent signaling pathway. J Neurosci 27:2866-2875.

Shankar GM, Li S, Mehta TH, Garcia-Munoz A, Shepardson NE, Smith I, Brett FM, Farrell MA, Rowan MJ, Lemere CA, Regan CM, Walsh DM, Sabatini BL, Selkoe DJ (2008) Amyloid-beta protein dimers isolated directly from Alzheimer's brains impair synaptic plasticity and memory. Nat Med 14:837-842.

Sharma AK, Rohrer B (2004) Calcium-induced calpain mediates apoptosis via caspase-3 in a mouse photoreceptor cell line. J Biol Chem 279:35564-35572.

Shelton MA, Newman JT, Gu H, Sampson AR, Fish KN, MacDonald ML, Moyer CE, DiBitetto JV, Dorph-Petersen KA, Penzes P, Lewis DA, Sweet RA (2015) Loss of Microtubule-

Associated Protein 2 Immunoreactivity Linked to Dendritic Spine Loss in Schizophrenia. Biol Psychiatry.

Sheng M, Hoogenraad CC (2007) The postsynaptic architecture of excitatory synapses: a more quantitative view. Annu Rev Biochem 76:823-847.

Shimizu S, Abt A, Meucci O (2011) Bilaminar co-culture of primary rat cortical neurons and glia. J Vis Exp.

Shipton OA, Leitz JR, Dworzak J, Acton CE, Tunbridge EM, Denk F, Dawson HN, Vitek MP, Wade-Martins R, Paulsen O, Vargas-Caballero M (2011) Tau protein is required for amyloid {beta}-induced impairment of hippocampal long-term potentiation. J Neurosci 31:1688-1692.

Simic G, Kostovic I, Winblad B, Bogdanovic N (1997) Volume and number of neurons of the human hippocampal formation in normal aging and Alzheimer's disease. J Comp Neurol 379:482-494.

Spilker C, Braunewell KH (2003) Calcium-myristoyl switch, subcellular localization, and calcium-dependent translocation of the neuronal calcium sensor protein VILIP-3, and comparison with VILIP-1 in hippocampal neurons. Mol Cell Neurosci 24:766-778.

Spilker C, Dresbach T, Braunewell KH (2002) Reversible translocation and activity-dependent localization of the calcium-myristoyl switch protein VILIP-1 to different membrane compartments in living hippocampal neurons. J Neurosci 22:7331-7339.

Spires TL, Meyer-Luehmann M, Stern EA, McLean PJ, Skoch J, Nguyen PT, Bacskai BJ, Hyman BT (2005) Dendritic spine abnormalities in amyloid precursor protein transgenic mice demonstrated by gene transfer and intravital multiphoton microscopy. J Neurosci 25:7278-7287.

Stancu IC, Vasconcelos B, Terwel D, Dewachter I (2014) Models of beta-amyloid induced Tau-pathology: the long and "folded" road to understand the mechanism. Mol Neurodegener 9:51.

Stejskal D, Sporova L, Svestak M, Karpisek M (2011) Determination of serum visinin like protein-1 and its potential for the diagnosis of brain injury due to the stroke: a pilot study. Biomed Pap Med Fac Univ Palacky Olomouc Czech Repub 155:263-268.

Stutzmann GE, Caccamo A, LaFerla FM, Parker I (2004) Dysregulated IP3 signaling in cortical neurons of knock-in mice expressing an Alzheimer's-linked mutation in presenilin1 results in exaggerated Ca2+ signals and altered membrane excitability. J Neurosci 24:508-513.

Sugiyama Y, Kawabata I, Sobue K, Okabe S (2005) Determination of absolute protein numbers in single synapses by a GFP-based calibration technique. Nat Methods 2:677-684.

Sweet RA, Fish KN, Lewis DA (2010) Mapping Synaptic Pathology within Cerebral Cortical Circuits in Subjects with Schizophrenia. Front Hum Neurosci 4:44.

Sweet RA, Hamilton RL, Lopez OL, Klunk WE, Wisniewski SR, Kaufer DI, Healy MT, DeKosky ST (2000) Psychotic symptoms in Alzheimer's disease are not associated with more severe neuropathologic features. Int Psychogeriatr 12:547-558.

Takeuchi A, Irizarry MC, Duff K, Saido TC, Hsiao Ashe K, Hasegawa M, Mann DM, Hyman BT, Iwatsubo T (2000) Age-related amyloid beta deposition in transgenic mice overexpressing both Alzheimer mutant presenilin 1 and amyloid beta precursor protein Swedish mutant is not associated with global neuronal loss. Am J Pathol 157:331-339.

Takuma H, Tomiyama T, Kuida K, Mori H (2004) Amyloid beta peptide-induced cerebral neuronal loss is mediated by caspase-3 in vivo. J Neuropathol Exp Neurol 63:255-261.

Tantral L, Malathi K, Kohyama S, Silane M, Berenstein A, Jayaraman T (2004) Intracellular calcium release is required for caspase-3 and -9 activation. Cell Biochem Funct 22:35-40.

Tarawneh R, D'Angelo G, Macy E, Xiong C, Carter D, Cairns NJ, Fagan AM, Head D, Mintun MA, Ladenson JH, Lee JM, Morris JC, Holtzman DM (2011) Visinin-like protein-1: diagnostic and prognostic biomarker in Alzheimer disease. Ann Neurol 70:274-285.

Tarawneh R, Lee JM, Ladenson JH, Morris JC, Holtzman DM (2012) CSF VILIP-1 predicts rates of cognitive decline in early Alzheimer disease. Neurology 78:709-719.

Terry RD, Masliah E, Salmon DP, Butters N, DeTeresa R, Hill R, Hansen LA, Katzman R (1991) Physical basis of cognitive alterations in Alzheimer's disease: synapse loss is the major correlate of cognitive impairment. Ann Neurol 30:572-580.

Thal DR, Walter J, Saido TC, Fandrich M (2015) Neuropathology and biochemistry of Abeta and its aggregates in Alzheimer's disease. Acta Neuropathol 129:167-182.

Tosun D, Joshi S, Weiner MW (2013) Neuroimaging predictors of brain amyloidosis in mild cognitive impairment. Ann Neurol 74:188-198.

Tsai J, Grutzendler J, Duff K, Gan WB (2004) Fibrillar amyloid deposition leads to local synaptic abnormalities and breakage of neuronal branches. Nat Neurosci 7:1181-1183.

Urbanc B, Cruz L, Le R, Sanders J, Ashe KH, Duff K, Stanley HE, Irizarry MC, Hyman BT (2002) Neurotoxic effects of thioflavin S-positive amyloid deposits in transgenic mice and Alzheimer's disease. Proc Natl Acad Sci U S A 99:13990-13995.

Valerio M, Porcelli F, Zbilut JP, Giuliani A, Manetti C, Conti F (2008) pH effects on the conformational preferences of amyloid beta-peptide (1-40) in HFIP aqueous solution by NMR spectroscopy. ChemMedChem 3:833-843.

Valle-Delgado JJ, Alfonso-Prieto M, de Groot NS, Ventura S, Samitier J, Rovira C, Fernandez-Busquets X (2010) Modulation of Abeta42 fibrillogenesis by glycosaminoglycan structure. FASEB J 24:4250-4261.

Vatsavayi AV, Kofler J, Demichele-Sweet MA, Murray PS, Lopez OL, Sweet RA (2014) TAR DNA-binding protein 43 pathology in Alzheimer's disease with psychosis. Int Psychogeriatr 26:987-994.

Walsh DM, Klyubin I, Fadeeva JV, Rowan MJ, Selkoe DJ (2002) Amyloid-beta oligomers: their production, toxicity and therapeutic inhibition. Biochem Soc Trans 30:552-557.

Walsh DM, Klyubin I, Shankar GM, Townsend M, Fadeeva JV, Betts V, Podlisny MB, Cleary JP, Ashe KH, Rowan MJ, Selkoe DJ (2005) The role of cell-derived oligomers of Abeta in Alzheimer's disease and avenues for therapeutic intervention. Biochem Soc Trans 33:1087-1090.

Walsh DM, Selkoe DJ (2007) A beta oligomers - a decade of discovery. J Neurochem 101:1172-1184.

Wang HW, Pasternak JF, Kuo H, Ristic H, Lambert MP, Chromy B, Viola KL, Klein WL, Stine WB, Krafft GA, Trommer BL (2002) Soluble oligomers of beta amyloid (1-42) inhibit long-term potentiation but not long-term depression in rat dentate gyrus. Brain Res 924:133-140.

Watson RE, Jr., Wiegand SJ, Clough RW, Hoffman GE (1986) Use of cryoprotectant to maintain long-term peptide immunoreactivity and tissue morphology. Peptides 7:155-159.

West MJ, Coleman PD, Flood DG, Troncoso JC (1994) Differences in the pattern of hippocampal neuronal loss in normal ageing and Alzheimer's disease. Lancet 344:769-772.

West MJ, Kawas CH, Stewart WF, Rudow GL, Troncoso JC (2004) Hippocampal neurons in pre-clinical Alzheimer's disease. Neurobiol Aging 25:1205-1212.

Wilmot B, McWeeney SK, Nixon RR, Montine TJ, Laut J, Harrington CA, Kaye JA, Kramer PL (2008) Translational gene mapping of cognitive decline. Neurobiol Aging 29:524-541.

Wilson LM, Mok YF, Binger KJ, Griffin MD, Mertens HD, Lin F, Wade JD, Gooley PR, Howlett GJ (2007) A structural core within apolipoprotein C-II amyloid fibrils identified using hydrogen exchange and proteolysis. J Mol Biol 366:1639-1651.

Wu HY, Hudry E, Hashimoto T, Kuchibhotla K, Rozkalne A, Fan Z, Spires-Jones T, Xie H, Arbel-Ornath M, Grosskreutz CL, Bacskai BJ, Hyman BT (2010) Amyloid beta induces the morphological neurodegenerative triad of spine loss, dendritic simplification, and neuritic dystrophies through calcineurin activation. J Neurosci 30:2636-2649.

Yang Y, Wang XB, Frerking M, Zhou Q (2008) Spine expansion and stabilization associated with long-term potentiation. J Neurosci 28:5740-5751.

Zempel H, Thies E, Mandelkow E, Mandelkow EM (2010) Abeta oligomers cause localized Ca(2+) elevation, missorting of endogenous Tau into dendrites, Tau phosphorylation, and destruction of microtubules and spines. J Neurosci 30:11938-11950.

Zhang Y, Rempel DL, Zhang J, Sharma AK, Mirica LM, Gross ML (2013) Pulsed hydrogen-deuterium exchange mass spectrometry probes conformational changes in amyloid beta (Abeta) peptide aggregation. Proc Natl Acad Sci U S A 110:14604-14609.

Zhao CJ, Noack C, Brackmann M, Gloveli T, Maelicke A, Heinemann U, Anand R, Braunewell KH (2009) Neuronal Ca2+ sensor VILIP-1 leads to the upregulation of functional alpha4beta2 nicotinic acetylcholine receptors in hippocampal neurons. Mol Cell Neurosci 40:280-292.

Zheng WH, Bastianetto S, Mennicken F, Ma W, Kar S (2002) Amyloid beta peptide induces tau phosphorylation and loss of cholinergic neurons in rat primary septal cultures. Neuroscience 115:201-211.

Zhou Q, Homma KJ, Poo MM (2004) Shrinkage of dendritic spines associated with long-term depression of hippocampal synapses. Neuron 44:749-757.

Zou F, Chai HS, Younkin CS, Allen M, Crook J, Pankratz VS, Carrasquillo MM, Rowley CN, Nair AA, Middha S, Maharjan S, Nguyen T, Ma L, Malphrus KG, Palusak R, Lincoln S, Bisceglio G, Georgescu C, Kouri N, Kolbert CP, Jen J, Haines JL, Mayeux R, Pericak-Vance MA, Farrer LA, Schellenberg GD, Petersen RC, Graff-Radford NR, Dickson DW, Younkin SG, Ertekin-Taner N (2012) Brain expression genome-wide association study (eGWAS) identifies human disease-associated variants. PLoS Genet 8:e1002707.